Deltares

Enabling Delta Life

Environmental impact of tidal power in the Eastern Scheldt Storm Surge Barrier

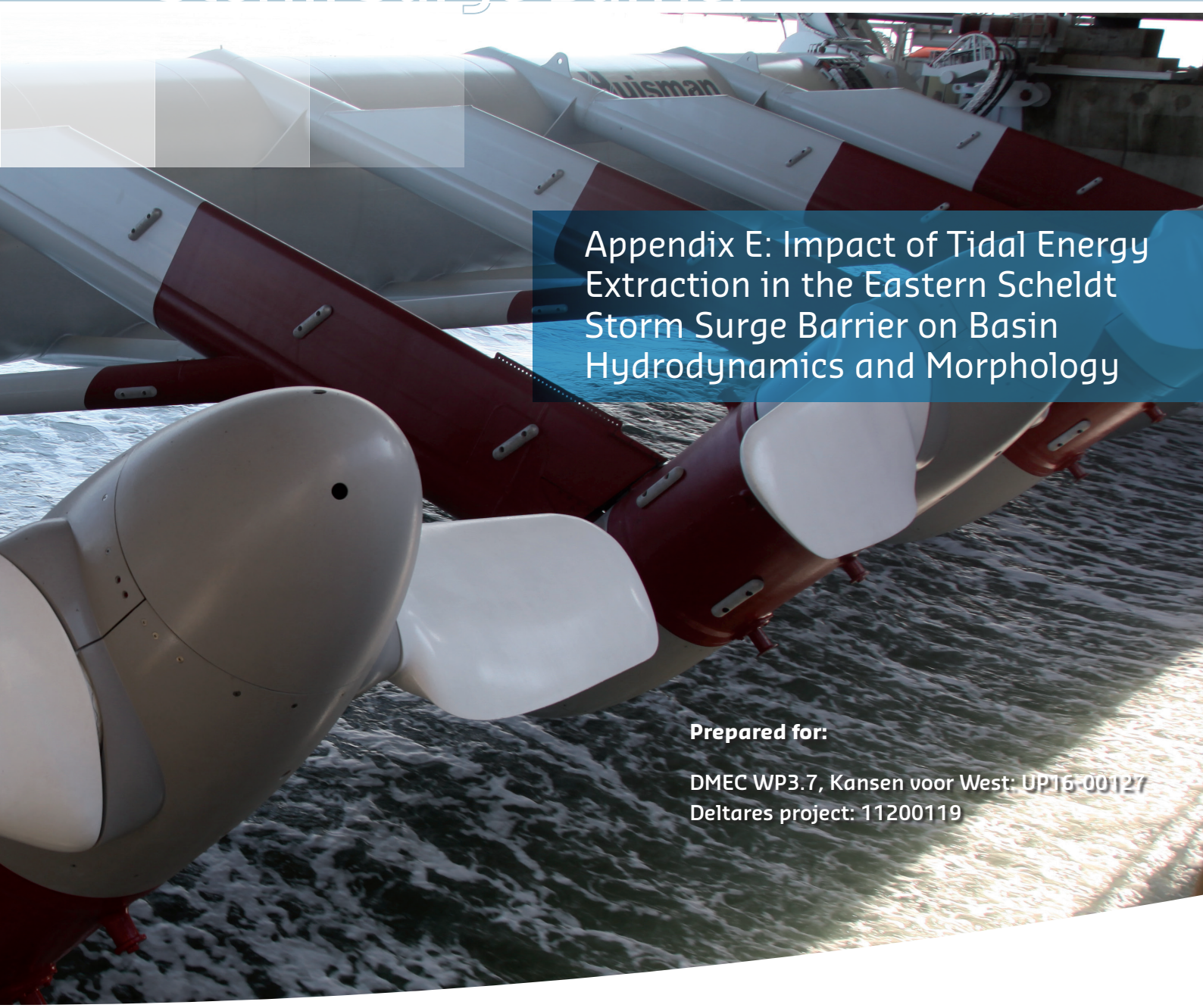

Appendix E: Impact of Tidal Energy Extraction in the Eastern Scheldt Storm Surge Barrier on Basin Hydrodynamics and Morphology

Prepared for:

DMEC WP3.7, Kansen voor West: UP16-00127
Deltares project: 11200119

Impact of Tidal Energy Extraction in the Eastern Scheldt Storm Surge Barrier on Basin Hydrodynamics and Morphology

Kamilla Guijt

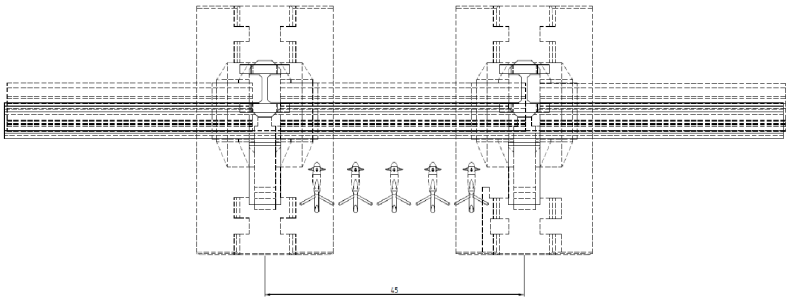

Impact of Tidal Energy Extraction in the Eastern Scheldt Storm Surge Barrier on Basin Hydrodynamics and Morphology

by

Kamilla Guijt

in partial fulfillment of the requirements for the degree of Master of Science
in Hydraulic Engineering
at the Delft University of Technology,
to be defended publicly on January 16th, 2018

Student number:	4149475	
Project duration:	March 6th, 2017 - January 16th, 2018	
Thesis committee:	Prof. dr. ir. Z. B. Wang,	TU Delft
	Dr. ir. B. C. van Prooijen,	TU Delft
	Dr. ir. R. J. Labeur,	TU Delft
	Ir. A. C. Bijlsma,	Deltares
	Ir. V. M. Gatto	TU Delft

An electronic version of this thesis is available at `http://repository.tudelft.nl/`.

Cover image by J.W.G. Ooms, Deltares, 2017

TU Delft

Deltares
Enabling Delta Life

Abstract

The Eastern Scheldt basin is protected by a semi-open storm surge barrier that was completed in 1986. This barrier includes 62 openings with gates between piers, which are only closed during extreme storm surges. In 2015 a set of five turbines was installed in one of the openings as a pilot for tidal energy extraction. The construction of the barrier significantly changed the basin hydrodynamics (tidal volume, range and velocities) and associated basin morphodynamics (sedimentation and erosion patterns of tidal flats and channels). This thesis investigates the incremental impact of tidal energy extraction in the barrier on the hydrodynamics and morphology of the basin, covering both scenarios with turbines installed currently and potential upscaling of tidal energy extraction.

Due to the construction of the barrier, the average tidal range and velocities have significantly decreased throughout the basin (Louters et al., 1998), and therefore tidal and meteorological (wind and waves) processes driving sediment transport over tidal flats are no longer in equilibrium with the bathymetry. Working towards a new equilibrium, tidal flats erode and channels fill up. This is expected to continue over a long period of time. Turbines installed in barrier openings block and shear local flow and increase turbulence levels (Verbeek et al., 2017). As the flow passes through the blades, it will lose momentum due to the thrust force exerted by the blades. This will lead to an increase in effective resistance at a barrier opening and therefore a further drop in tidal range and velocities throughout the basin.

An available two-dimensional Delft3D model (Pezij, 2015) covers relevant hydrodynamics and morphodynamics of the basin with barrier, openings, channels and tidal flats. This model was modified to account for tidal energy extraction. The tidal turbines were parameterized through a momentum sink that increases the flow resistance locally. This sink term was calibrated using a state-of-the-art three-dimensional model of one opening with five turbines. To evaluate variations in resistance, a sensitivity range was defined as input to the numerical simulations. Upscaling scenarios were specified, in which different sets of the barrier openings are equipped with tidal turbines (varying between 2 to 17 openings with turbines out of the 62 gate openings of the barrier).

Numerical simulations over one spring-neap cycle were performed for these scenarios. Results show small deviations in tidal range, volume and discharges throughout the basin due to tidal energy extraction, compared to changes that have occurred due to the construction of the barrier. Reductions in tidal range and volume appear to be near-linearly increasing with the number of turbines installed. Deviations in tidal range increase in landward direction. Between the barrier and mid-basin, peak discharges decrease in channels directly behind the barrier section with turbines and increase in channels behind sections with no turbines. From mid- to end-basin, discharges are not affected by positioning of turbines, only the amount of energy extraction.

Simulation results indicate that the emergence time of tidal flats decreases due to tidal energy extraction as a result of an increase in mean low water level throughout the basin. The increase in low water level due to tidal energy extraction would only be a fraction of the increase in water level due to sea-level rise in coming years. Additionally, the reduction in acreage was estimated based on hypsometric curves of the three largest individual tidal flats. The reduction in acreage of these flats due to the rise in mean low water level resulting from tidal energy extraction is relatively small compared to the ongoing loss in acreage due to both sea-level rise and erosion resulting from the barrier construction.

Further work is required to improve basin and turbine modeling and evaluate long-term morphodynamics (sediment transport). Separately a comprehensive socio-environmental evaluation is required to compare benefits from (renewable) tidal energy extraction to the (incremental) ecological impact resulting from further reduction in acreage of tidal flats that support animal and bird life.

Acknowledgments

This thesis completes the master Hydraulic Engineering at Delft University of Technology. The research has been carried out in collaboration with the research institute Deltares.

I would like to thank my thesis committee, Zheng Bing Wang, Robert Jan Labeur, Bram van Prooijen, Arnout Bijlsma and Marco Gatto for their guidance during this thesis. Zheng Bing, thank you for being the chair of my committee and for your useful advice during the committee meetings. Robert Jan, thanks for guiding me through the structuring of this report and always being ready to help out. Bram, thank you for your input and ideas during committee meetings. Arnout, I would like to thank you for your guidance and for always paying attention to every detail, it made my work better. Marco, thanks for helping me formulate the research topic and all your input throughout the process.

Besides my thesis committee, I would like to thank all the people involved with the Eastern Scheldt tidal power project from Deltares, Delft University of Technology and Tocardo; Anton, Tom, Wilbert, Thieu, Merel, Pieter, Magnus and Ronald. I appreciate the opportunity to be a part of the project and enjoyed working weekly in the project room and the monthly meetings. A special thanks to Anton for always being prepared to help and give advise. Tom, thanks for helping out with the STAR-CCM+ model data. Merel, your enthusiasm and dedication is inspiring.

Moreover, I would like to thank Antonio for introducing this thesis topic to me, Lodewijk for always answering my questions and providing me with the necessary model and data of the Eastern Scheldt and Qinghua for helping me with the cluster.

Lastly, I would like to thank my parents for all their support.

K. Guijt
Delft, January 2018

Contents

List of Symbols and Abbreviations

Symbols

a	-	Constant
A_b	m^2	Basin surface area
A_c	m^2	Channel surface area
A_e	m^2	Inlet entrance wet cross-sectional area
A_f	m^2	Tidal flat surface area
A_g	m^2	Cross-sectional area gate
A_r	m^2	Swept area tidal turbine
$A(z)$	m^2	Surface area w.r.t certain water level
C_{2D}	$m^{1/2}/s$	2D Chézy coefficient
b	-	Constant
C_d	–	Drag coefficient
c	kg/m^3	Sediment concentration
c_p	–	Power coefficient
c_{loss}	–	Loss coefficient
c_t	–	Thrust coefficient
C_W	–	Coefficient for wind shear stress
d	m	Depth below a horizontal plane of reference (datum)
f	$1/s$	Coriolis parameter (inertial frequency)
F	kN	Thrust force
g	m/s^2	Gravitational acceleration
h	m	Water depth ($d+\zeta$)
j	–	Coefficient
m,n		Grid indices Delft3D
M_x	m/s^2	Source or sink of momentum in x-direction
M_ξ	m/s^2	Source or sink of momentum in ξ-direction
N_v	–	Number of values
P	m^3	Tidal prism
P_a	W	Available power
P_t	W	Power extracted by turbines
Q_e	m^3/s	Discharge through inlet basin
Q_g	m^3/s	Discharge through gate
R	m	Turbine radius
S	$m^3/year$	Sediment transport
t	s	Time
u	m/s	Fluid velocity in the x-direction
u_r	m/s	Undisturbed upstream velocity
U	m/s	Depth averaged velocity in x- or ξ-direction
U_2	m/s	Velocity outside stream-tube (of the wake of a turbine)
U_r	m/s	Flow speed across turbine
U_w	m/s	Downstream velocity (from turbine wake)
v	m/s	Fluid velocity in the y-direction
V	m/s	Depth averaged velocity in y- or η direction
V_c	m^3	Volume channel
V_f	m^3	Volume tidal flat
W	m/s	Wind speed

x, y	m	Horizontal Cartesian coordinates
X	m	Multiplication factor for resistance
X_i	m	Predicted value
Y_i	m	Observed value
z	m	Water level w.r.t. NAP
Δ_x	m	Width of cell
λ	$-$	Tip speed ratio
μ	$-$	Discharge coefficient
μ_b	$-$	Barrier opening discharge coefficient
μ_{b+t}	$-$	Barrier opening with turbines discharge coefficient
ω	rad/s	Rotational speed
ρ_a	kg/m^3	Density of air
ρ_w	kg/m^3	Density of water
θ	rad	Angle between the wind direction and x-direction
ξ, η	$-$	Horizontal curvilinear coordinates
υ_t	Pas	Eddy-viscosity coefficient for horizontal momentum exchange
ζ	m	Water level above a horizontal plane of reference (datum)
ζ_u	m	Upstream water level
ζ_d	m	Downstream water level

Abbreviations

2DH	Two-dimensional Horizontal (depth averaged)
ADCP	Acoustic Current Doppler Profiler
ANT	Autonomous Negative Trend
ES	Eastern Scheldt
HAM	Hammen
HATT	Horizontal-axis Tidal Turbine
MHW	Mean High Water
MLW	Mean Low Water
MRO	Maximum Roll-out
MTR	Mean Tidal Range
NAP	Normaal Amsterdams Peil (Dutch Ordnance Datum)
NF	Near-future
NJ	Neeltje Jans
NS	North Sea
PRO	Partial Roll-out
RGP	Roggenplaat
RMSE	Root Mean Square Error
RO	Roll-out
RP	Roompot
SCH	Schaar
SLR	Sea-level Rise
TSR	Tip Speed Ratio
WL	Water Level

1 Introduction

1.1. Background

Tidal energy is a promising contributor for the future renewable energy mix. Currently, several tidal energy pilot projects are operational in the Netherlands. One of these is a set of five turbines installed in 2015 in one of the openings of the Eastern Scheldt storm surge barrier, where tidal velocities are locally enhanced due to the semi-open nature of the barrier.

1.1.1. Area Description

Figure 1.1 shows an overview of the Eastern Scheldt basin. The barrier is located at the western edge of the basin, where the basin meets the North Sea. The inter-tidal areas (yellow) distributed along the basin are formed by channels surrounding them (blue) and locally generated waves. The ES is closed off from the original river discharge, through a number of dams. Therefore it is no longer classified as an estuary and is referred to as a tidal basin.

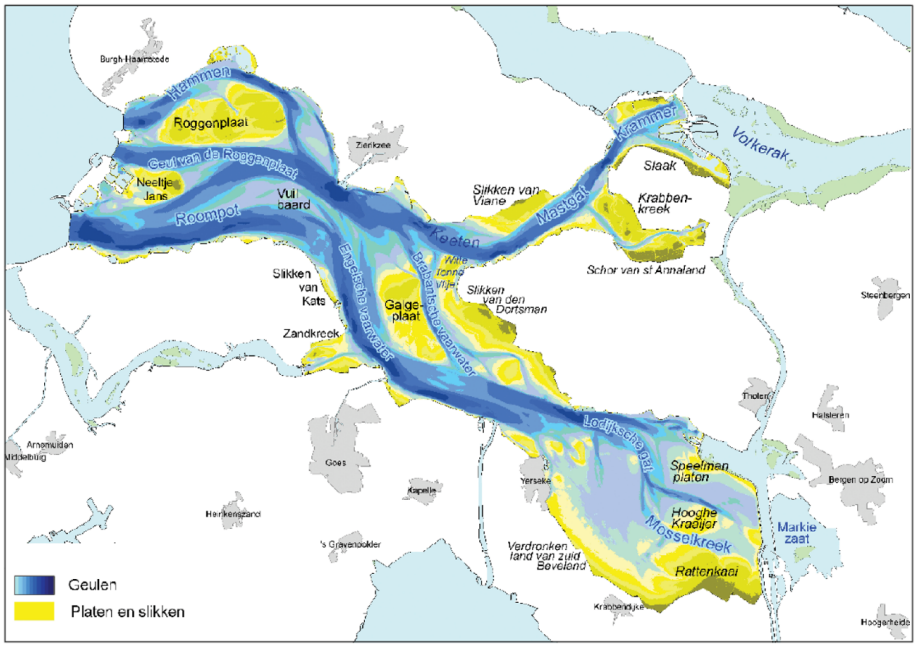

Figure 1.1: Overview of Eastern Scheldt basin. Geulen = Channels (blue), Platen en slikken = Inter-tidal areas (yellow) (E-Overheid)

Figure 1.2 shows a close-up of the barrier (seen from the west). The barrier consists of three main sections, named after the channels at those locations, namely Hammen, Schaar and Roompot. The barrier has 62 gate openings, each with a width of 45 meters.

Figure 1.2: Aerial picture of Eastern Scheldt barrier, seen from the west (Biesboer, 2011)

The pilot array is situated in the Roompot section (gate opening 8). The turbines are connected to a 50 m long support structure. The five turbines have a combined capacity of about 1.2 MW, which can provide electricity for approximately 1000 households (Tocardo). Figure 1.3 shows how the turbines and support structure are installed in the barrier.

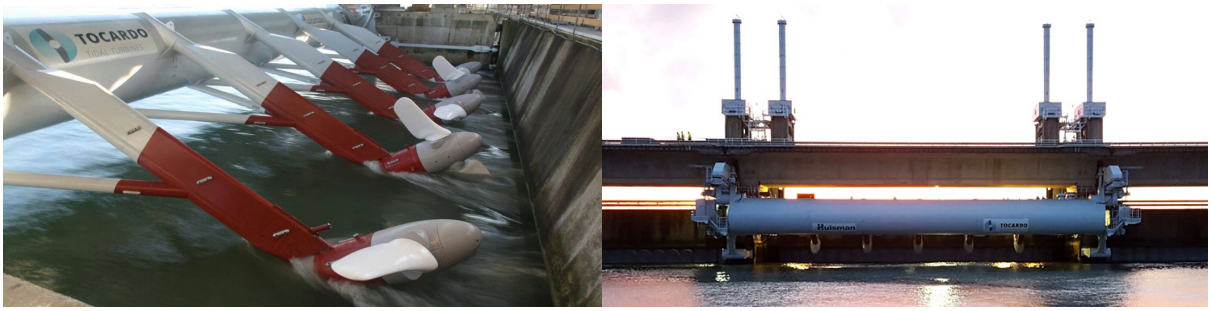

(a) Turbines (RVO) (b) Support Structure (DMEC)

Figure 1.3: Tidal turbines and their support structure in the ES storm surge barrier

1.1.2. Problem Description

The barrier was built in 1986 as one of the measures in the Delta Plan. This plan comprised many protective measures in response to extensive flooding in the low-lying lands in the southwest of the Netherlands during a storm surge in 1953. Between the fixed piers, the barrier has 62 openings (and corresponding gates) that are normally open. To protect the Eastern Scheldt (ES) basin, the gates are closed when water levels in the North Sea exceed a critical level.

The ES basin consists of channels and inter-tidal areas (hereafter referred to as 'tidal flats'), which are alternately inundated and exposed by the tide (Bosboom and Stive, 2015). These tidal flats are essential for local ecology as they form habitats for animals such as cockles and mussels, which in turn are food for local birds. Moreover, the tidal flats are important to coastal protection, as they dissipate wave energy before it reaches the basin's shores and dikes (Van Zanten and Adriaanse, 2008).

After the construction of the barrier, the reduced discharge through the opening resulted in a decrease in tidal volume entering and leaving the basin during a tidal cycle, and thus an overall decrease in tidal range and tidal velocities throughout the basin. The consequence of this change in basin hydrodynamics is that the relatively deep channels are no longer in morphological equilibrium with the decreased tidal volume and are filling with sediment. This is known as the sediment deficit of the Eastern Scheldt basin.

The sediment filling the channels is provided by the tidal flats. Erosion due to locally wind-generated waves (which are largely unaffected by the barrier construction) now exceeds the sediment deposition resulting from the, now reduced, tidal currents (Eelkema, 2013). Sea-level rise has led to increased submergence time of the tidal flats, which together with the loss in acreage due to erosion is undesirable from an ecological

point of view, as firstly less food is available for birds and secondly less time is available for feeding (De Ronde et al., 2013).

Little to no sediment enters the basin anymore since the completion of the barrier, and therefore the tidal flats are currently the only sediment source. Without any interventions it is expected that 400-600 million m^3 of sediment will ultimately be transported from the tidal flats into the channels before a new equilibrium is reached (Kohsiek et al., 1987). This morphological change to the tidal flats in the ES basin and its consequent impact on ecology is denoted as an autonomous negative trend (De Ronde et al., 2013). It results from erosion of the tidal flats induced by the sediment deficit and is aggravated by sea-level rise.

Tidal turbines in barrier openings extract energy from the in- and outflowing water, resulting in a further drop in tidal volume, range and velocities. This is expected to enhance the autonomous negative trend, which is undesirable. The current placement of turbines in one opening is not expected to have significant impact on the basin hydrodynamics. For a potential future upscaling, with turbines installed in more barrier openings, it is uncertain whether the hydro- and morphodynamical (and ultimately environmental) effects are outweighed by the increased energy production. To be able to assess the incremental impact of possible upscaling of tidal energy extraction, the changes in hydro- and morphodynamics need further investigation.

1.1.3. Problem Definition

The ideal situation would be extracting a substantial amount of renewable energy from the barrier without significantly enhancing the autonomous negative trend of the basin. However, it is likely that tidal energy extraction will influence the hydrodynamics in such a way as to increase the rate of erosion of the tidal flats. There is currently little knowledge on the effects of tidal energy extraction in a storm surge barrier on hydro- and morphodynamics in a tidal basin. The impact of tidal energy extraction on the ES basin to the ongoing autonomous negative trend has not been quantified for the current installation nor for possible upscaling.

1.2. Research Approach

1.2.1. Research Questions

The problem definition leads to the following research question:

How are basin hydrodynamics and tidal flat morphology affected by tidal energy extraction in the Eastern Scheldt barrier?

This question is split up in different sub-questions:

1. How can relevant hydro- and morphodynamic processes of a tidal basin in combination with tidal energy extraction in a storm surge barrier at its inlet be modeled?
2. How are basin hydrodynamics affected by upscaling of tidal energy extraction?
3. How does upscaling of tidal energy extraction contribute to the ongoing morphological changes of tidal flats?

1.2.2. Methodology

Firstly, relevant literature is reviewed and reported. Based on requirements following from the literature review, a model is set-up to include both relevant processes for tidal basin hydrodynamics and tidal energy extraction. Simulations are performed for various upscaling scenarios. The model results are used to formulate conclusions on the hydrodynamic impact as a result of upscaling of tidal energy extraction in the ES barrier. Moreover, the possible impact on tidal flat morphology is evaluated based on the hydrodynamic model results.

1.2.3. Scope

This thesis includes an analysis of the changes in large-scale hydrodynamics within the ES basin due to local tidal energy extraction. The aim is to make predictions on the changes in hydrodynamics with a model, and speculate on morphodynamic impact as a result of these changes. The focus of the morphodynamic analysis is on tidal flats surrounded by channels. This thesis does not aim to gain an understanding of the complex local flow changes due to tidal turbines, but rather to gain sufficient knowledge in order to make a parameterization of the energy extraction induced by them. Moreover, full morphological modeling is not part of this work. This thesis is a contribution to a research project about the impact of the ES pilot installation

on basin hydro- and morphodynamics. This research project will continue after the completion of this thesis, and will evaluate the morphodynamics in more detail.

1.2.4. Structure of Report

This thesis comprises of the following chapters:

Chapter 2 reports a literature review.
Chapter 3 formulates the modeling concept.
Chapter 4 describes the method.
Chapter 5 shows hydrodynamic simulation results.
Chapter 6 reflects on tidal flat morphology.
Chapter 7 discusses the results.
Chapter 8 provides the conclusions and recommendations of this thesis.

2

Literature Review

In this chapter, relevant literature is reviewed and reported. Firstly, general background information on tidal basin hydro- and morphodynamics is described. Hereafter, a description of the hydrodynamics and morphology in the Eastern Scheldt basin is provided, including the governing processes of tidal flat morphodynamics. This is followed by a review of tidal turbines and their effect on local flow. After this, the unique placement of tidal turbines in a barrier is discussed. Furthermore, approaches to modeling of tidal basins, a barrier and tidal turbines are reported. At the end of this chapter the key points of the literature review are stated, research gaps are evaluated and the work approach is formulated.

2.1. Tidal Basin Theory

This section provides background information on tidal propagation, the general hydrodynamic and morphological processes of a tidal basin and tidal flat morphodynamics within such a basin. This theoretical knowledge is necessary for understanding the ES system.

2.1.1. Tidal Propagation

Tides are caused by the gravitational forces between moon, sun and earth (Bosboom and Stive, 2015). The combination of these attraction forces and the rotation of the earth results in a predictable variation between mean low water (MLW) and mean high water (MHW), referred to as a tidal range. Every 12 hours and 25 minutes this pattern repeats itself, which results in two flood periods and two ebb periods per day. Furthermore, the alignment of the earth, sun and moon results in spring-neap tidal cycles. When the sun, moon and earth are completely aligned the tidal amplitude is larger because the solar and lunar forces reinforce each other, this is called a spring tide. When they are not aligned, the tidal amplitude is lower because the forces cancel each other and this is called a neap tide. A spring-neap cycle lasts about 15 days (Bosboom and Stive, 2015).

2.1.2. Hydrodynamic and Morphological Elements of a Tidal Basin

A tidal basin has three main elements: the ebb-tidal delta (outside of basin entrance), channels and tidal flats (inside basin). Figure 2.1 shows the definitions of these elements and corresponding characteristics. The tidal prism is the volume of water between mean high water and mean low water. Tidal flats are the total volume of sediment above mean low water. Channels are the volume of water in channels below mean low water. A tidal basin may theoretically reach a morphological equilibrium (Wang et al., 2014), with corresponding equilibrium sizes of the ebb-tidal delta, channels and tidal flats. This equilibrium depends on the hydrodynamic forcing that the tidal basin is exposed to over a certain time period.

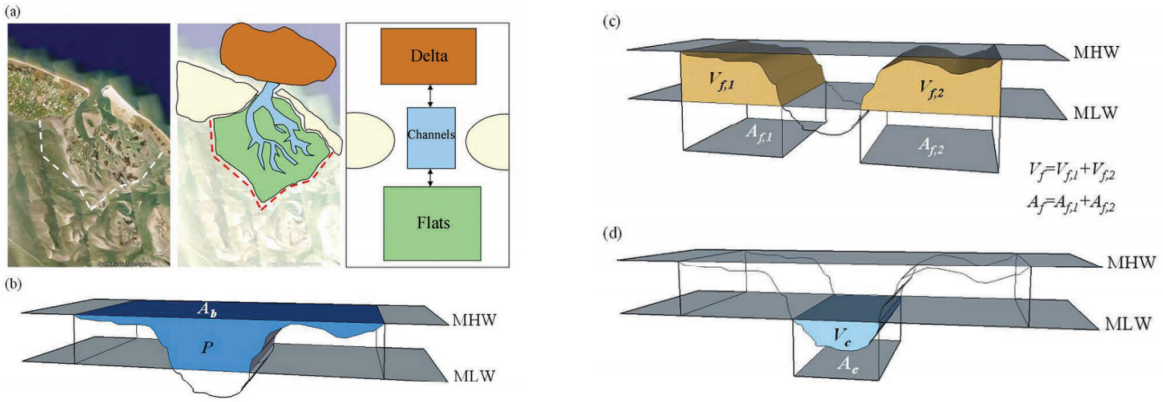

Figure 2.1: (a) Morphological elements of a tidal basin (ebb-tidal delta, channels, tidal flats), (b) definition of the hydrodynamic parameter tidal prism, (c) definition of the morphodynamic parameters tidal flat area and volume and (d) definition of the hydrodynamic parameters channel area and volume (Wang et al., 2014)

2.1.3. Tidal Flat Morphodynamics

The evolution of tidal flats is an important element of this work, and depends on the forcing mechanisms that they are exposed to.

Definition

Morphodynamics is the feedback mechanism by which hydrodynamic forcing determines the evolution of morphology which in turn influences hydrodynamic behavior (Friedrichs, 2012), as schematically shown in Figure 2.2.

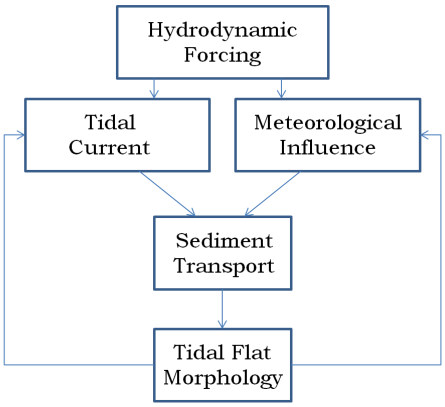

Figure 2.2: Schematization of processes governing tidal flat morphodynamics, adapted from Friedrichs (2012)

A tidal flat which is in equilibrium has the same shape within a certain duration (tidal cycle, spring-neap cycle etc) of natural forcing (Friedrichs, 2012). The morphodynamic equilibrium of a tidal flat depends on the processes governing sediment transport during such a period.

Tidal Current

A tidal basin fills when the water level in the adjoining sea rises during the flood-phase of a tidal cycle. While the water moves in a landward direction, the current carries stirred sediment with it through the channels and onto the tidal flats, where it can settle. When the water level at sea falls, the flow direction reverses causing a current in seaward direction and a corresponding transport of sediment in the opposite direction. The residual sediment transport gradient over tidal flats resulting from the tide depends on the magnitude and shape of the current velocity in both directions, local depth and grain size in the basin (Gatto et al., 2017) (Bosboom and Stive, 2015). Within the basin, a tidal range between high and low waters exists. This range influences the morphodynamic behavior due to inundation period of different height zones of tidal flats in

combination with meteorological forcing.

Meteorological Influence
Meteorological influences can significantly alter the sediment transport gradient over a tidal flat (Green and Coco, 2013). These meteorological contributors are wind induced currents, surges and waves. The currents and bed shear stresses resulting from these processes can be highly effective in altering the flow direction and the stirring of sediment on a tidal flat. The effects depend on the fetch, wind speed, bathymetry and the tide (water level).

Other mechanisms such as aeolian transport, density driven currents can also contribute to sediment transport over a tidal flat (Gatto et al., 2017) (Das, 2010).

2.2. Hydrodynamics and Morphology of the Eastern Scheldt Basin

This section explains the characteristics of the ES basin. Additionally, an overview is provided of the hydrodynamic changes and resulting morphological changes that have occurred, and are still occurring, due to the various construction works in the ES basin since 1958. Moreover, the governing processes of tidal flat morphodynamics in the ES are reviewed. It is necessary to understand these changes in order to understand how tidal turbines will affect the ES basin.

2.2.1. Basin Characteristics

The Eastern Scheldt basin contains channels and tidal flats. There are four tidal flats which are completely surrounded by channels; Roggenplaat, Neeltje Jans, Galgenplaat and Hoogekraaier, see Figure 2.3. The ebb-tidal delta is no longer in connection with the basin, as the barrier blocks sediment transport from outside.

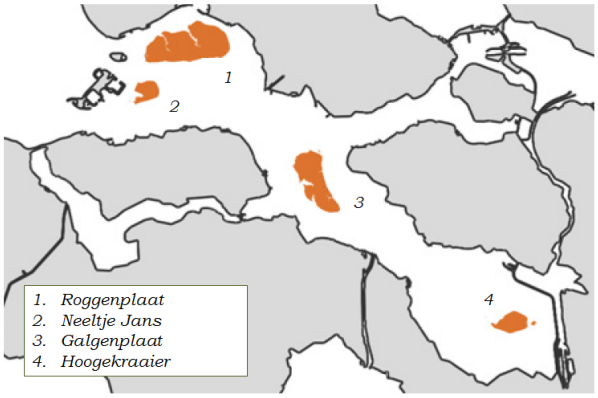

Figure 2.3: Overview of tidal flats in the Eastern Scheldt basin, adapted from De Vet et al. (2017b)

The tidal range in the ES is not constant throughout the basin due to resonance of the tidal wave. The range increases from west to east (2.5m near the barrier up to 3.4m in the southeast branch). Moreover, the predominant wind direction is from the southwest and it is assumed that the barrier blocks the waves coming from offshore, and therefore only locally generated wind waves are present.

2.2.2. Consequences of the Barrier Construction

A brief overview is provided of the changes in hydrodynamics and morphology, a more detailed description of the Delta Works and their consequences is found in Appendix A. Moreover, articles by Louters et al. (1998), Vroon (1994) and Mulder and Louters (1994) give extensive descriptions on this topic.

Changes in Hydrodynamics
The construction works (barrier and various dams) have resulted in a reduction of the tidal range, volume and velocities within the basin. The tidal volume has decreased by approximately 30%, the current velocities have decreased 20-40% in the western and central parts of the basin. The average tidal range has decreased by 12% (Louters et al., 1998). Figure 2.4 shows the reduction in flood volume at the mouth of the basin as a result of the construction of the barrier between 1980 and 1986.

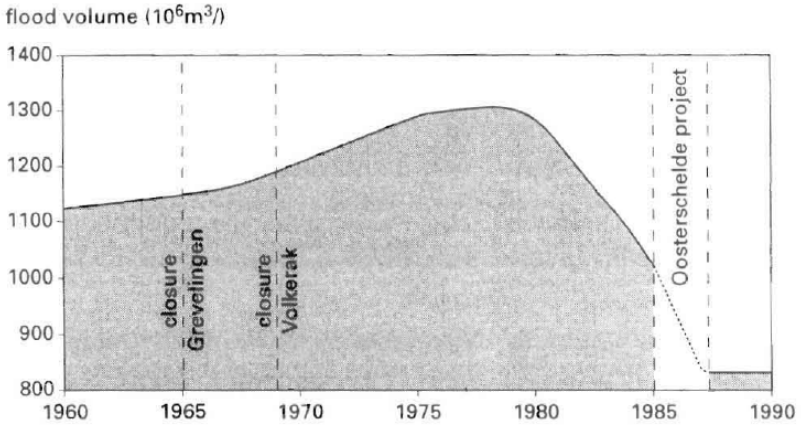

Figure 2.4: Evolution of flood tidal volume at the mouth of the ES basin since 1960 (Louters et al., 1998)

Morphological Development

The consequence of this change in basin hydrodynamics is that the relatively deep channels are no longer in morphological equilibrium with the decreased tidal volume and are filling with sediment. This is known as the sediment deficit of the Eastern Scheldt basin. The sources of sediment filling the channels are tidal flats, as the barrier blocks import of sediment. The tidal flats will continue to erode until a new equilibrium is reached.

According to De Vet et al. (2017b) and Eelkema (2013), tidal flats in the ES basin were in dynamic equilibrium, or even slightly increasing in height, before the construction of the storm surge barrier. After the construction works, tidal flats have been eroding strongly. This change in trend is most likely due to the change in hydrodynamics imposed by the barrier (De Vet et al., 2017b). Figure 2.5 shows the decline in height, area and volume of tidal flats in the ES.

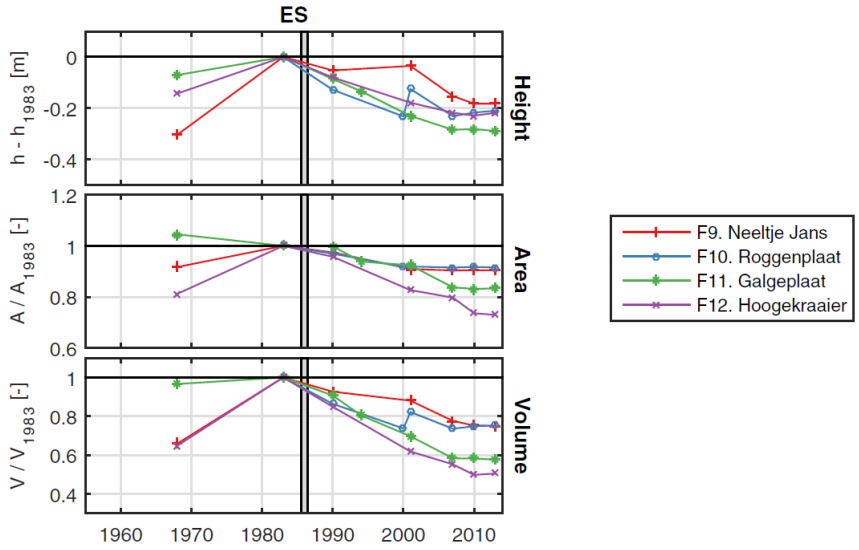

Figure 2.5: Long term changes of the average height, area and volume of flats in the ES. The vertical gray box indicates the completion of the storm surge barrierDe Vet et al. (2017b)

The sediment deficit of the channels is causing erosion of tidal flats, and sea-level rise (SLR) is causing decreased emergence of these areas. Due to the combination of these effects, all tidal flats combined are decreasing in area by approximately 60 ha per year (De Ronde et al., 2013). The tidal flats surrounded by channels comprise of about 25% of this area and are thus eroding by approximately 15 ha per year. Since the construction of the barrier, about 1300 hectares (10%) have been lost due to erosion and sea-level rise. In Figure 2.6 a prediction of the reduction in emerged area between 2010-2100 is shown for all tidal flats combined, and for different emergence time intervals (i.e. 80-100% indicates the total area which is emerged

for 9.80-12.25 hours during a tidal cycle).

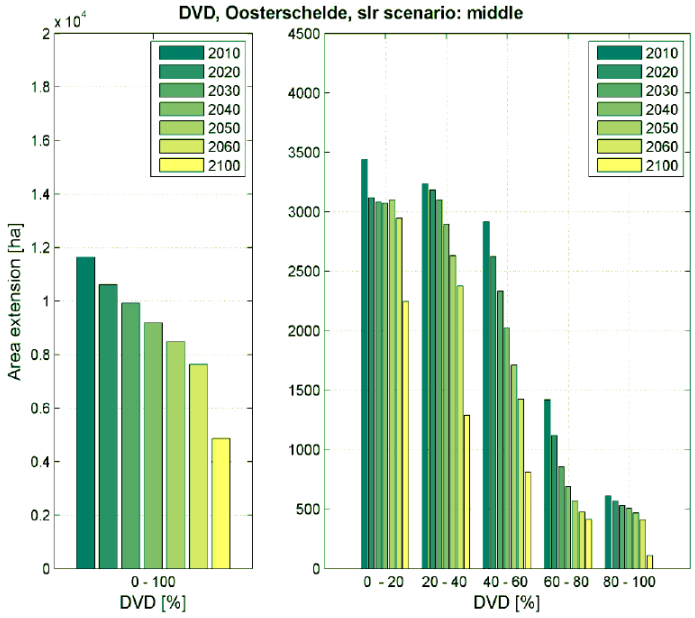

Figure 2.6: (a) decrease in emerging area for all tidal flats in the ES over time and (b) decrease in emerging area per emergence time interval for the scenario 'middle' (De Ronde et al., 2013)

This prediction indicates that the tidal flats will continue to erode for a long period of time, until they are completely diminished, if no interventions are taken.

2.2.3. Governing Processes of Tidal Flat Morphodynamics in the Eastern Scheldt

Sediment transport over tidal flats in the ES basin is governed by the combination of tidal asymmetry, the tidal range and wind induced currents and waves.

Sediment Transport due to Tidal Asymmetry

Asymmetries in peak velocities and lag effects determine sediment transport within the basin due to the tide (Dronkers, 1986) (Gatto et al., 2017). It is assumed in this thesis that asymmetries in velocities are governing in sediment transport gradients over the tidal flats in the ES. This is because lag effects become important when the settling velocity is small enough with respect to the water depth to assume that the response of sediment concentrations in the water column to variations in velocities is not instantaneous (which is not the case in the ES).

Sediment in the ES is therefore sensitive to variations in local asymmetry of maximum velocities. When maximum flood velocities are higher than ebb velocities, there is flood dominance, which favors landward sediment transport. Sediment responds instantaneously to the flow velocity u. The transport (S) is described by equation 2.1. The coefficient j lies in the range between 3-5 depending on the situation, c is the concentration of sediment (Bosboom and Stive, 2015).

$$S \approx c|u^{j-1}|u \tag{2.1}$$

The velocities in the ES basin have decreased between 20-40% (depending on the location in the basin) compared to before construction of the barrier, according to Louters et al. (1998). Das (2010) concluded in her research that tidal flow velocities at present, are not strong enough to bring sediment onto the areas above low water at all for the Galgenplaat tidal flat. Moreover, De Vet et al. (2017a) states that under calm weather conditions, flow velocities (due to both tide and wind) on the Roggenplaat are too small to induce substantial sediment transport rates. Besides, De Vet et al. (2017a) states that without inclusion of meteorological influences, the flow over the Roggenplaat is driven by water level gradients due to differences in tidal propagation of channels surrounding the tidal flat. Therefore, it is uncertain whether tidal asymmetry plays a role in the

erosion and sedimentation of the tidal flats at present.

Tidal Range

Both De Vet et al. (2017b) and Louters et al. (1998) state that the profile of tidal flats is directly related to the tidal range in which it is situated. Flats situated in areas with a large tidal range (like the Western Scheldt) are higher and have steeper slopes than flats with smaller tidal ranges (such as the ES).

The reduction in tidal range in the ES drastically reduced the frequency of flooding in different height zones of tidal flats (Louters et al., 1998), and consequently the influence of wind and wave induced shear stresses. The reduction in tidal range in the ES has led to a decreased inundation frequency of the higher parts of the tidal flats and increased frequency in the lower parts (Mulder and Louters, 1994). Higher erosion rates are observed in the higher parts; above mean low water, surface areas have decreased. Below this level, surface areas have increased, see Figure 2.7.

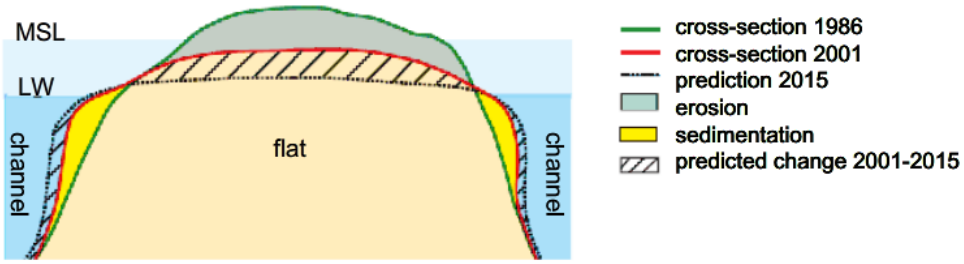

Figure 2.7: Morphological development of tidal flats in the ES basin between 1986 and 2015 (Bosboom and Stive, 2015)

Wind Driven Current

Moving air (i.e. wind) exerts a shear stress on the water surface. This shear stress causes the water in the upper part of the water column to move in the direction of the wind. The resulting current depends on the wind speed, fetch length and water depth (Bosboom and Stive, 2015). In shallow areas, the effect of this current becomes stronger, as high velocities are present near the bed which induces a bed shear stress.

De Vet et al. (2017a) states that with the inclusion of a substantial wind event, the main flow on the Roggenplaat flat is well in line with the governing wind direction. Wind is capable of fully altering the direction of the main flow. For simulations performed by De Vet et al. (2017a) including all processes, the main sediment transport is in NE direction, in line with prevailing wind direction.

Wind Induced Waves

Waves can be created by the wind depending on the fetch within a basin (Green and Coco, 2013). When the depth becomes too small compared to the wave length, the wave exerts a shear stress on the bed. Wave induced shear stresses are highly efficient in stirring of sediment (De Vet et al., 2017a). The influence of waves on tidal flats depends on the tide (water level) and the local bathymetry.

Das (2010) found in her research on the Galgenplaat that both storm events and calm conditions induce erosion, although storm conditions more significantly so. De Vet et al. (2017a) states that the net sediment transport rates on the Roggenplaat are significantly smaller if waves are not included in the simulation, implying that waves are crucial for sediment transport rates over tidal flat in the ES basin.

2.3. Tidal Turbine Theory

In this section tidal turbines are described and their effect on local flow. In order to understand the effect of tidal energy extraction on large scale basin hydrodynamics, it is necessary to understand how tidal turbines affect local flow.

2.3.1. Horizontal-axis Tidal Turbine

Various designs for tidal turbines exist, but in this research horizontal-axis tidal turbines (HATTs) are considered since these are installed in the ES barrier. The principle of power extraction by a HATT is that linear momentum of moving water is converted to angular momentum by the rotor blades. The power produced by the rotation of the blades is converted into usable power for the grid (Baston et al., 2015). The flow past a tidal

turbine is sketched in Figure 2.8 (Whelan et al., 2009). In the figure, U is the undisturbed upstream velocity, U_t is the flow speed at the turbine. U_2 is the velocity outside the stream-tube of the turbine (bypass flow) and U_w is the downstream velocity. As the flow passes through the swept area of the blades, a horizontal thrust force (F) is applied on the fluid, thereby losing momentum. A pressure drop is seen in the form of a water level drop at that location.

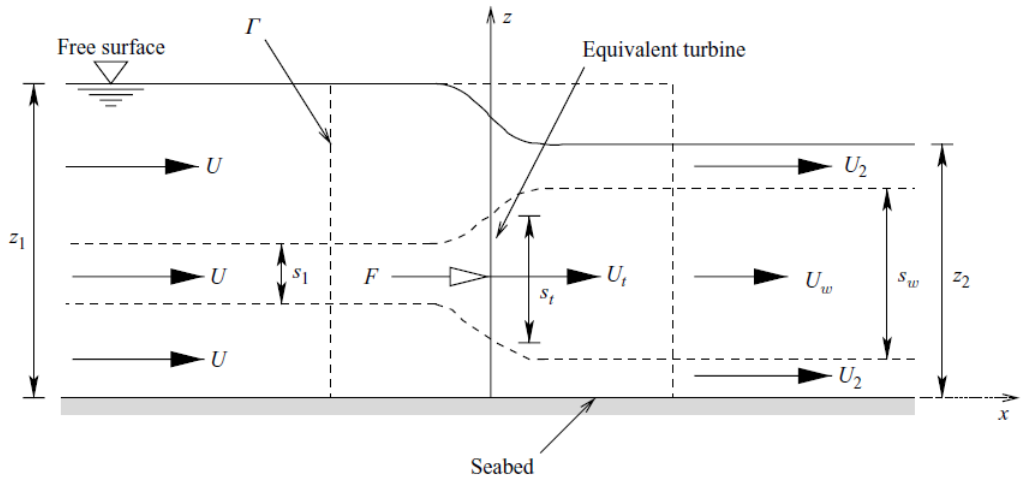

Figure 2.8: two-dimensional sketch of flow past a tidal turbine (Whelan et al., 2009)

Tidal turbines block and shear local flow and increase turbulence levels (Verbeek et al., 2017), see Figure 2.9. In free surface flow, the wake of a turbine has increased turbulence intensities up to a distance of 20 rotor diameters and vortices formed at the back of blades are present 2-5 rotor diameters downstream (Verbeek et al., 2017).

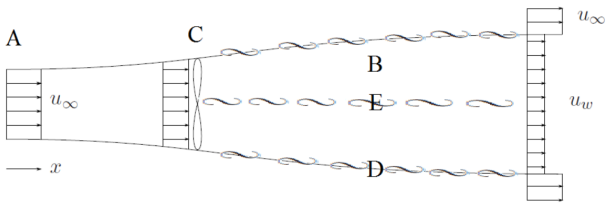

Figure 2.9: A conceptual picture of the wake of a HATT, A) is the free stream, B) is the wake, C) is the rotor position, D) is the shear layer at the wake edge with fluctuations induced by tip vortices, E) is the center line of the wake with hub vortices (Verbeek et al., 2017)

2.3.2. Power and Thrust

Power

The HATT converts energy from the flow into usable power. The available power (P_a) is shown in equation 2.2. In this Equation, A_r is the swept area of the turbine and u_r is the undisturbed upstream velocity.

$$P_a = \frac{1}{2}\rho_w A_r u_r^3 \tag{2.2}$$

The turbine cannot convert all the available power into usable power; the power that the turbine produces (P_t) is determined by equation 2.3. In this formulation c_p is a power coefficient, defined in equation 2.4. The maximum value of this coefficient is 0.59, according to the theory of Betz (Betz, 1966).

$$P_t = \frac{1}{2}c_p\rho_w A_r u_r^3 \tag{2.3}$$

$$c_p = \frac{P_t}{P_a} \tag{2.4}$$

A HATT has a rated capacity, which is the maximum power it can produce during the highest flow velocities. However, these maximums only occur for short periods during maximum ebb and flood. Figure 2.10 shows the power coefficient of a tidal turbine as a function of the tip speed ratio (TSR) λ. This dimensionless tip speed ratio gives the rotational speed of the turbines as a function of the flow velocity, see Equation 2.5 (Val et al., 2014). ω is rotor rotational speed, R is the rotor diameter and U is the speed of flow.

$$\lambda = \frac{\omega R}{U} \tag{2.5}$$

The figure shows that turbines have a maximum power coefficient when the TSR is around 6, however at lower and higher tip speed ratios (and therefore flow velocities) the power coefficient is smaller.

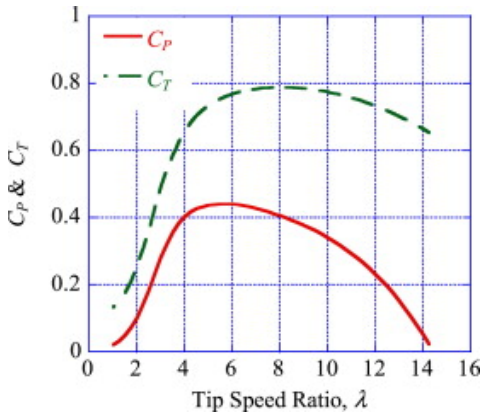

Figure 2.10: Thrust and power curves of a tidal turbine (Val et al., 2014)

The produced power is a function of flow velocity, which changes throughout the tidal cycle and the spring-neap cycle. This is demonstrated in Figure 2.11 for a hypothetical tidal turbine in the Wadden Sea (Mungar, 2014). The Figure shows the average power produced per day in the month of June in A) and the instantaneous power on one day in B).

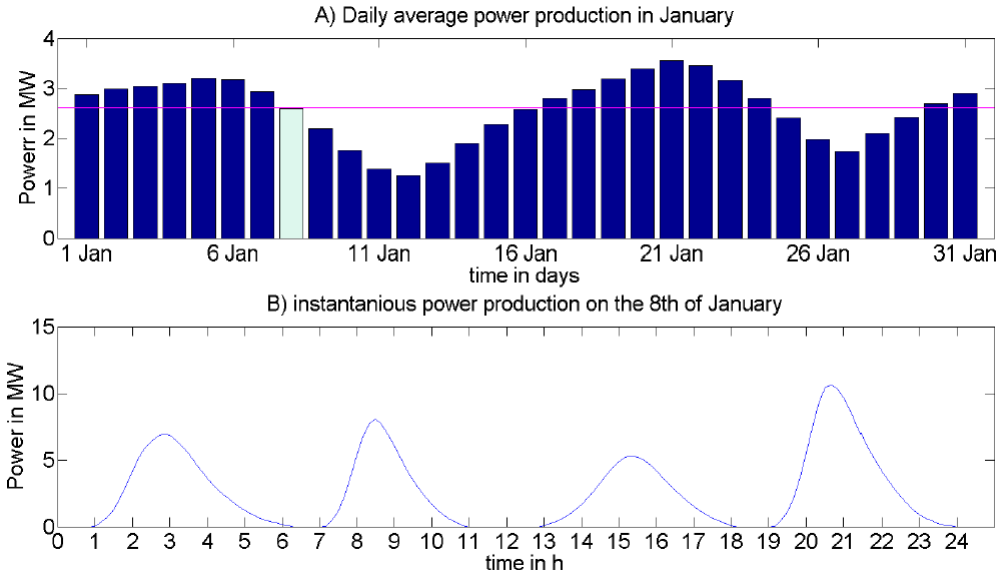

Figure 2.11: A) Average power production per day and B) instantaneous power in one day for a hypothetical tidal turbine in the Wadden Sea (Mungar, 2014)

Thrust

The thrust force felt by the flow is defined in Equation 2.6 (Baston et al., 2015). In this Equation c_t is the thrust

coefficient.

$$F = \frac{1}{2} c_t \rho_w A_r u_r^2 \tag{2.6}$$

The corresponding thrust curve is shown in Figure 2.10 for a tidal turbine as a function of the TSR. Maximum thrust is felt by the incoming flow when the TSR is around 8, and is much lower at lower TSR and slightly lower at higher TSR. The thrust force is directly linked to extracted momentum of the flow. Therefore the momentum extraction varies as a function of flow velocity.

2.4. Tidal Turbines in a Barrier

This section discusses the unique placement of tidal turbines in a barrier. The resistance to the flow caused by the barrier is explained. Moreover, the interaction between the barrier and turbines is discussed. Lastly, the impact of tidal turbines of large scale flow is evaluated. These considerations are important for the modeling of the whole system.

2.4.1. Barrier Resistance

The ES barrier causes resistance to the incoming and outgoing flow (Delft Hydraulics and Rijkswaterstaat, 1989). This resistance is caused by frictional losses of the bottom and sides of gate openings and form losses caused by flow deceleration downstream of the structure, flow separation, energy conversion by turbulence, momentum transfer and generation of eddies. The wakes caused by the resistance of the openings are seen in Figure 2.12 during a flood situation.

Figure 2.12: Aerial photograph of flow through the Eastern Scheldt barrier during flood (Biesboer, 2011)

2.4.2. Barrier and Turbine Interaction

The configuration of turbines in a gate opening of a semi-open barrier is a unique situation, with no known comparable configurations. The turbines are not located in a free-stream situation, but in the contracted flow of the barrier. Figure 2.13 shows a picture taken at the barrier during ebb while the turbines are operational. In the opening with turbines, smaller wakes are distinguished in the bigger wake of the barrier opening itself.

Figure 2.13: Photograph taken from above Roompot 8. Eastern Scheldt barrier and turbine wake interaction during ebb, photograph taken by M. Verbeek (2017)

The turbines are located at the basin side of the sill in the barrier opening. This means that the turbines are located in the already contracted flow in the flood situation, but before the contraction in the ebb situation. This could lead to different resistances for flood and ebb. It should be noted that the ES turbines are not aways operational. When the head difference over the barrier exceeds a certain value, the turbines are lifted from the water.

2.4.3. Impact on Large Scale Flow

The increased turbulence intensities of the wake of a tidal turbine are noticeable at a distance of 20 rotor diameters from the turbine, which is smaller than the wake of the barrier itself. The complex nature of the wake is not essential for the large scale hydrodynamics of the basin. Therefore, the flow disturbance of the tidal turbines can be regarded as an increase in effective resistance at a barrier opening.

2.5. Modeling of a Tidal Basin, Barrier and Turbines

In order to make predictions, a model is necessary which includes the relevant aspects of tidal basin as well as the barrier and turbines. In this section modeling tidal flow through a barrier with tidal turbines is discussed. First, the principle of hydrodynamic flow modeling is explained. Secondly, the implementation of a barrier in such a model is described. Thirdly, the implementation of turbines in a flow model is explored.

2.5.1. Modeling Tidal Flow

Various tools can be used to model tidal flow:

- Hydraulic scale models
- One-dimensional numerical models
- Two-dimensional numerical models
- Three-dimensional numerical models

Each of these tools has a different way of computing the flow. The choice of model depends on the purpose of the research and, the desired level of detail and computational effort. Hydraulic scale models use the same physical principles as those occurring in reality. The numerical models solve the Navier-Stokes equations in different ways.

In the numerical modeling of tidal flow, flow computations are based on the Navier-Stokes equations (hydrodynamic equations for incompressible fluid with a constant density). Three-dimensional models solve the equations fully. For two-dimensional models, assumptions are made that vertical velocities and accelerations are negligible. This results in a hydrostatic pressure distribution leading to the depth-averaged continuity and momentum equations (Delft Hydraulics and Rijkswaterstaat, 1989). For one-dimensional flow, the equations are reduced by integrating them in a lateral direction as well.

Each model has its advantages and disadvantages. A hydraulic scale model has the most accurate representation of reality, but it expensive and complex to make. A three dimensional model has the largest level of

detail, but is most computationally expensive. A one-dimensional model has the lowest level of detail, but is fastest computational wise.

2.5.2. Modeling the Eastern Scheldt Basin

The Eastern Scheldt basin covers an area of 370 km^2. Due to it's size, a hydraulic scale model is unfeasible and for a numerical model, the resolution of a model covering the entire basin will always be relatively large and the dimension small. Many modeling tools have been used and are being used for the ES basin at present for design, safety and research purposes.

Barrier Resistance

The ES barrier causes resistance to the ingoing and outgoing flow (Delft Hydraulics and Rijkswaterstaat, 1989). Resistance is a result of frictional and form losses felt by the flow as it passes through the barrier. Since the dimension and resolution of models representing the ES basin generally do not allow for a representation of the barrier nor these losses, they have to be schematized.

The steady state sub-critical flow rate through the barrier (Q_e) is formulated in equation 2.7. In this equation μ is the discharge coefficient, A_e is the wet cross sectional area of the opening, g is the gravitational acceleration, ζ_u is the upstream water level and ζ_d is the downstream water level.

$$Q_e = \mu A_e \sqrt{2g|\zeta_u - \zeta_d|} \tag{2.7}$$

For the impact of the barrier on large scale flow, the discharge characteristics of the barrier are expressed as μA, the effective flow opening of the barrier. The sum of effective flow openings determines the tidal range in the basin (Delft Hydraulics and Rijkswaterstaat, 1989). Such discharge coefficient has been used in models to represent the flow through the barrier.

In a one-dimensional model, one single quantity of the discharge coefficient describes all effects (Delft Hydraulics and Rijkswaterstaat, 1989). In a two-dimensional model, the lateral variation of the discharge characteristics has to be included in this coefficient. In three dimensions all these losses should be included without an additional term.

Initial Implementation

During the design stages of the ES barrier various models were used by Delft Hydraulics and Rijkswaterstaat. Scale models and two-dimensional numerical models (WAQUA) were used for detailed design purposes and a one-dimensional model (IMPLIC) was used for operational forecasts. Governing hydraulic parameters were derived from flume tests (Delft Hydraulics and Rijkswaterstaat, 1989). The hydraulic characteristics of the barrier could be simulated correctly in two-dimensional numerical models by using the same discharge coefficients determined from flume tests. For the one-dimensional model, an overall discharge coefficient for the entire channel was used, this was determined from a scale model or through a two dimensional model.

Further Implementation

The construction of the ES barrier caused significant changes to hydrodynamics and morphology within the basin. Many studies have been performed to understand the effects, and to come up with solutions to counter-act the autonomous negative trend. Recent studies used the Delft3D software: Pezij (2015), Eelkema (2013), De Bruijn (2012), De Pater (2012), Das (2010) and Hoogduin (2009). This software can be used in two and three dimensions; the aforementioned models used the two-dimensional depth averaged version. The benefit of this software is the possibility to include waves and sediment transport.

2.5.3. Modeling Tidal Turbines

Common practice for modeling a tidal basin is to use a one- or two- dimensional model. For one and two-dimensional implementations of turbines, a parameterization is necessary, as the complex nature of turbines cannot be represented by the resolution and dimension of the model.

Options for Turbine Parameterization

Options for parametrization of tidal turbines are summarized below, for more information on implementations of these options, see Baston et al. (2015).

- Adding **bottom friction** to the model to represent the loss due to the turbines. The bottom friction is enhanced at the location of the turbine.

- Adding a **momentum sink** term to the momentum equations, to represent the loss of momentum due to tidal energy extraction. This sink term could be either time- or velocity dependent. The momentum extraction of the turbines is not constant in time, but varies with the speed of the flow. A velocity-dependent momentum sink term, which varies as a function of velocity, is most representative for tidal energy extraction.

Moreover, a modification to turbulent closure models could be added. A modification to the turbulent closure models accounts for momentum and turbulent hydrodynamic effects (Baston et al., 2015). However, turbulent effects of turbines are not of importance for large-scale flow.

Eastern Scheldt Implementations

Previous Implementation

Deltares investigated the impact of tidal energy extraction in two gate openings on water levels in the basin (De Kleermaeker, 2013). This investigation used the one-dimensional IMPLIC model. The turbines were included through a momentum sink term which was theoretically derived.

The research showed that the tidal range reduces in the ES basin if turbines are implemented in the model as a momentum sink. The conclusions were that on average during high water, there was a lower water level (between 0.4 to 0.5 cm lower) and that during low water, there was a higher water level (0.3 cm higher) if two barrier openings had turbines. This was around 0.1 to 0.2 % deviation of the maximum tidal range for the situation without turbines. There was a bigger deviation further away from the barrier, due to tidal resonance within the basin, therefore these are average values which occur about mid-basin; closer to the barrier there was a smaller deviation, and landward there was a bigger deviation.

Current Implementation

At the time of writing this thesis, Deltares was developing a three-dimensional model in Star-CCM+ for the barrier including turbines in order to understand the effects on local flow in more detail. This model represented the installed turbines in Roompot 8. Only two gate openings (one with and one without turbines) were included and 200 meters in both upstream and downstream directions. This model was still under development and was not yet completely validated. However, this model could be useful as input for an estimate for the increased resistance in a gate opening due to turbines.

2.6. Research Definition

This section states the key points from the literature review. Knowledge gaps are identified and the work approach is described.

2.6.1. Key Points of Literature

The key points of the reviewed literature for the hydrodynamics and morphology of the ES basin, tidal turbine theory, tidal turbines in a barrier and modeling of basin, barrier and turbines are summarized.

Hydrodynamics and Morphology of the Eastern Scheldt Basin

The construction of the barrier led to changes in tidal volume, tidal range and velocities throughout the basin. The consequence of this change in basin hydrodynamics is that the channels are no longer in morphological equilibrium with the decreased tidal volume and are filling with sediment, while tidal flats are eroding.

Morphological development of tidal flats in the ES basin is determined by tidal and meteorological forcing; tidal range, tidal velocities and wind induced waves and currents. Interaction between these processes and the bathymetry determines sediment transport gradients over tidal flats in the ES. Before the construction of the barrier, the combination of these processes resulted in a natural equilibrium. With the completion of the barrier, the tidal range and velocities decreased significantly. These reductions in velocities caused a decrease in sediment deposition on tidal flats. Reductions in tidal range caused wind and wave induced shear stresses to have a larger impact at different height zones of the tidal flat. As a result, tidal flats erode and channels fill with sediment. The deterioration of the tidal flats is aggravated by sea-level rise which causes a decreased emergence of tidal flats.

Summarizing, the deterioration of tidal flats in the ES is caused by two main factors; sea-level rise and erosion induced by the sediment deficit of channels, see Figure 2.14.

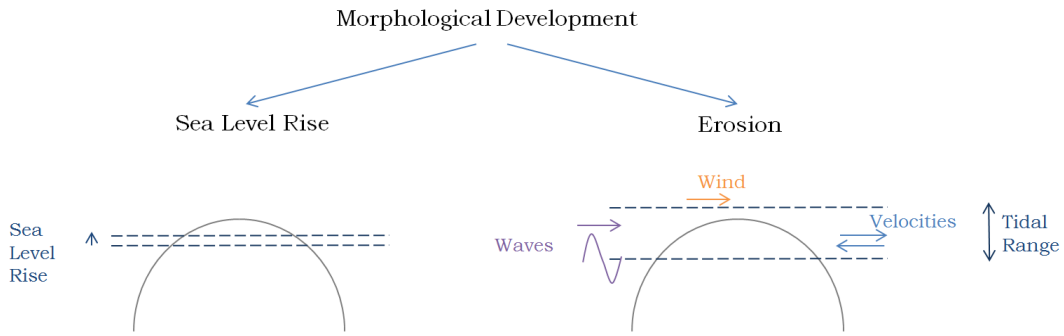

Figure 2.14: Processes causing morphological changes to tidal flats in the ES basin

Tidal Turbine Theory
A HATT changes the hydrodynamics of local flow by the blockage of the turbine, sheared flow and increased turbulence levels. As the flow passes through the swept area of the blades, they exerts a thrust force on the flow, thereby losing momentum. The power produced by the turbines and the thrust force encountered by the flow are a function of the undisturbed upstream flow velocity.

Tidal Turbines in a Barrier
The Eastern Scheldt barrier causes a resistance to the flow. The wakes produced by contraction of the flow through gate openings continue for a large distance downstream. The tidal turbines each produce a wake, which is much smaller than the wakes of the barrier itself and are therefore not important for large-scale hydrodynamics. The local flow disturbance of the turbines will lead to an increase in effective resistance at a barrier opening, and thus a decrease in tidal volume entering and leaving the basin. The expected hydrodynamic effects are reductions in the tidal range and tidal velocities throughout the basin, indicated in red in Figure 2.15

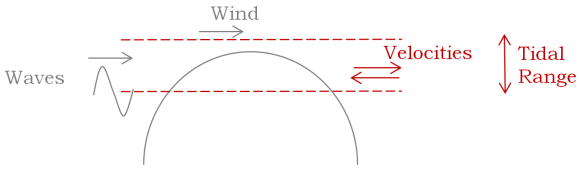

Figure 2.15: Affected hydrodynamic processes (indicated in red) due to tidal energy extraction in the ES

Modeling of a Tidal Basin, Barrier and Turbines
Numerical and scale models are available for the purpose of hydrodynamic modeling. In numerical modeling, a trade-off always exists between level of detail and computational effort.

The ES basin covers a large area and thus a representative model will have a large resolution and small dimension in order to have a feasible computational time. When modeling flow through a barrier, the frictional and form losses caused by the barrier cannot be physically replicated in such a model and therefore the total resistance to the flow is included through a discharge coefficient. The definition of this coefficient changes depending on the dimension of the model.

Modeling tidal turbines in such a numerical model poses a similar problem, their effects on local flow cannot be physically represented. Turbine parameterization can be therefore be included by adding additional bottom friction or by adding a momentum sink term to momentum equations. In previous research of tidal energy extraction in the ES barrier, additional resistance due to turbines was implemented in a one-dimensional model of the basin through a momentum sink term. The results showed small reductions in water levels if two barrier openings were equipped with turbines. Currently, a three-dimensional model of one gate opening is being developed, which could provide data for this work.

2.6.2. Knowledge Gaps

Following the literature review, some knowledge gaps are identified.

Impact of Tidal Energy Extraction on Tidal Flats

Previous research (De Kleermaeker, 2013) shows the influence of two gate openings with turbines on water levels in the ES basin. However, no link has been made between the reduction in tidal range and the influence on the deterioration of tidal flats. The important processes for the tidal flat morphology have been identified as the tidal range, tidal velocities, wind and wave induced influences. In order to evaluate the contribution of tidal energy extraction to the ongoing erosion of the tidal flats, the interaction of all these processes must be investigated.

Turbine Implementation in a Relevant Model

The relevant processes for tidal flat morphodynamics must be included in a model covering such processes in order to make meaningful predictions. Tidal turbines in the ES storm surge barrier have not previously been implemented in such a model.

Impact of Upscaling of Tidal Energy Extraction

Effects of upscaling scenarios have not yet been investigated. If the pilot has positive outcomes, in terms of power production, environmental impact and safety, the possibility would exist for a larger deployment of tidal turbine arrays. A study of the changes in hydrodynamics and morphology in the basin is necessary before such a decision can be made.

Summarizing, in order to answer the research questions, a relevant model must be set-up including the channels and flats in the basin, barrier and turbines as well as sediment transport and relevant tidal and meteorological processes. This model should be used to test the hydro- and morphodynamic impact due to different upscaling scenarios of tidal energy extraction.

2.6.3. Work Approach

The focus of this work and the steps to be taken to answer the research questions are formulated.

Focus

This thesis focuses on the hydrodynamic changes caused by tidal energy extraction, see Figure 2.16. Wind, waves and sediment transport are not yet investigated in this work due to time constraints. Hydrodynamic behavior provides a good first indication on the magnitude of changes that may occur to the morphodynamics. This thesis provides a basis for the larger hydro- and morphological research project that will continue after completion of this thesis. It is therefore important that such processes are taken into consideration for continuation of the research, even though they are not treated in this work. These processes are expected to be treated in the continuation of this work.

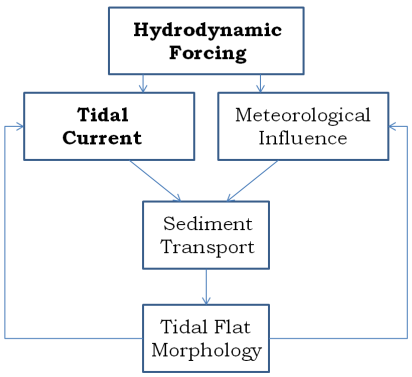

Figure 2.16: Schematization of processes governing tidal flat morphodynamics, adapted from Friedrichs (2012), focus of this work indicated in bold

Approach
Firstly, the requirements of the model in terms of basin hydro- and morphodynamics, turbine inclusion and computational effort are evaluated. Hypotheses are formulated for the effects of upscaling of tidal energy on the flow throughout the basin which should be tested with the chosen model.

The chosen numerical model is set up to make predictions of the flow, meteorological forcing and sediment dynamics, although only flow is analyzed. Different upscaling scenarios are defined based on the hypotheses. To gain a better understanding on the effects on the hydrodynamics within the basin due to tidal energy extraction, simulations for the different upscaling scenarios are performed. The effects on the hydrodynamics in the basin are analyzed.

The knowledge gained from the model results are used to formulate conclusions on the hydrodynamic impact of upscaling of tidal energy extraction in the ES and the possible impact on the morphology of tidal flats.

3

Modeling Concept

This chapter evaluates the necessary modeling approach to answer the research questions. Firstly, the requirements following from the literature review for the model are discussed. Hereafter, the chosen model and the turbine parameterization and calibration in the model are described. After this, simulation considerations are explored; hypotheses for upscaling tidal energy extraction are formulated, hydrodynamic indicators for monitoring during simulations are defined and an appropriate simulation period is chosen. Lastly, the modeling approach is explained.

3.1. Model Requirements

The requirements for the software used in this research follow from the knowledge gaps; the impact of tidal energy extraction on tidal flats and the implementation of tidal energy extraction in a relevant model. The requirements are:

- **Tidal basin hydro- and morphodynamics**: The model should include all relevant aspects of the tidal basin including the barrier, tidal flats and channels. Moreover, the tidal and meteorological forcing should be included in the model. Lastly, sediment transport is necessary to evaluate the impact of turbines on the morphology of tidal flats.
- **Turbine parameterization**: The local flow disturbance of tidal turbines will lead to an increase in effective resistance at a barrier opening. Therefore, the overall momentum loss due to the increased resistance should be represented.
- **Computational effort**: For this research, it was desirable to have short computational effort, such that simulations could be analyzed and re-run relatively quickly. It was therefore desirable that simulations would not last longer than 12 hours.

A two- or three-dimensional model is necessary to cover relevant hydro- and morphodynamic processes; a one-dimensional model would not provide enough information in lateral directions and would not be able to include sediment transport. A two-dimensional model would be more beneficial computational effort wise, compared to a three-dimensional model. Although a three-dimensional model would have a higher level of detail, it would unrealistic to use for the entire ES basin in terms of computational effort considering the size of the basin. For the parameterization of turbines, bottom friction or a momentum sink in a two-dimensional model could be implemented to represent tidal energy extraction, whereas a three-dimensional model would not need any parameterization. Complex flow disturbance due to turbines can only be included in a three-dimensional model, but that level of detail was not required for this research. Therefore, a two-dimensional model would be the most appropriate in terms of basin hydro-and morphodynamics, turbine parameterization and computational effort.

Wind, waves and sediment transport options were required, which are all possible to include in the Delft3D software. This software had the added benefit that it was already used in the most recent research and ready-to-use models were available. The drawbacks of the existing Delft3D models were that their water level representation were not as accurate as those of the existing WAQUA (two-dimensional) models of the ES basin. However, the inclusion of wind, waves and sediment transport favors Delft3D over WAQUA. Moreover,

for this thesis it was of importance to identify relative changes of a situation with turbines compared to a reference case without turbines. Therefore, the precise representation of water levels was not of primary importance, but the relative change. The inclusion of the aforementioned options was more essential to answer the research questions than the accuracy of water levels. Therefore Delft3D is the most appropriate software in terms of basin hydrodynamic and morphodynamic analysis.

The easiest option for turbine parameterization in such a two-dimensional Delft3D model would be to increase bottom friction locally. However, since the barrier is located at the same location, this may bring unwanted effects. It would be best if the turbines could be a separate function within the model. A time-dependent momentum sink is possible through the porous plate function in Delft3D.

The work performed for this thesis does not use the wind, wave and sediment transport options in the software. They are mentioned, because it was important that they were included for the purpose of further research for the larger research project on the basin hydro- and morphodynamics.

3.2. Model Choice

The software that met the requirements best was Delft3D in two dimensions (depth averaged). This section explains the software and the turbine parameterization and calibration.

3.2.1. Software

Hydrodynamic Equations
Delft3D solves the (depth-averaged) non-linear shallow water equations derived from the three-dimensional Navier-Stokes equations for incompressible free surface flow. The assumption is that the basin in this case, is much longer than it is deep and that vertical velocities and accelerations are therefore small. This assumption results in a hydrostatic pressure distribution. The momentum equation in horizontal x direction is given in Equation 3.1 (Delft Hydraulics and Rijkswaterstaat, 1989). The equations (in both x and y directions) account for convection and diffusion, pressure forces, bottom friction, wind stress and any other momentum sinks or sources. The equations are numerically solved in Delft3D.

$$\frac{\partial U}{\partial t} + U\frac{\partial U}{\partial x} + V\frac{\partial U}{\partial y} = fV + \upsilon_t\left(\frac{\partial^2 U}{\partial x^2} + \frac{\partial^2 U}{\partial y^2}\right) - g\frac{\partial \zeta}{\partial x} - \frac{gU\sqrt{U^2+V^2}}{C_{2D}^2 h} + \frac{\rho_a C_W W^2 sin\theta}{h\rho_w} + M_x \tag{3.1}$$

In these Equations x and y are are coordinates, U and V are the depth averaged velocities in x and y directions, ζ is the water level above some horizontal plane of reference, h is the water depth, f is the Coriolis parameter, υ_t is the eddy-viscosity coefficient for horizontal momentum exchange, C_{2D} is a 2D Chezy coefficient for bottom friction, g is the gravitational acceleration, C_W is the coefficient for wind shear stress, W is the wind speed, θ is the angle between the wind direction and x-direction, ρ_w is the density of water, ρ_a is the density of air, and M_x is any other momentum sink/source.

Numerical Aspects
The momentum equations are solved using a finite difference method in combination with a staggered grid. This is a grid in which water level, velocity components and depth points are defined at different locations, see Figure 3.1.

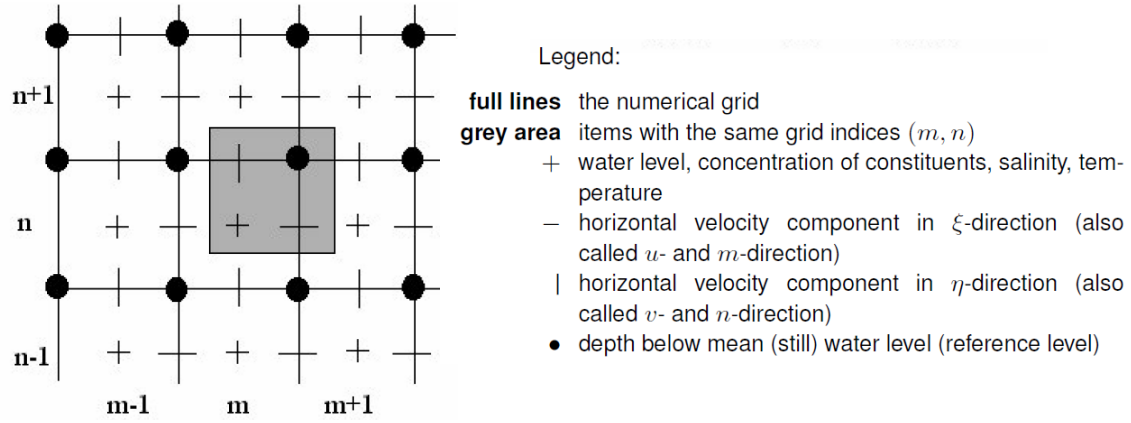

Figure 3.1: Staggered grid Delft3D (Deltares Systems, 2014)

Modules
Delft3D-FLOW is the central module which calculates non-steady flow and sediment transport. Moreover, the WAVE module can be used in parallel which uses SWAN (Simulating WAves Near-shore) to generate the waves. These modules are coupled such that after a certain amount of specified time there is a feedback of information.

3.2.2. Parameterization through Porous Plates

The additional resistance due to tidal energy extraction can be modeled by porous plates. Porous plates are partly permeable structures which increase flow resistance. Porous plates add a quadratic sink term to the local momentum balance, see Equation 3.2 (Deltares Systems, 2014). In this equation M_ξ is the momentum loss in ξ direction, Δx is the width of the cell, U is the velocity in ξ direction and V the velocity in η direction. The user may specify the $c_{loss,u}$ coefficient.

$$M_\xi = -\frac{c_{loss,u}}{\Delta x} U \sqrt{U^2 + V^2} \tag{3.2}$$

A number of limitations are present for this choice of parameterization of turbines. The first limitation is that that the momentum sink represented by porous plates is time-dependent. The thrust force (and therefore momentum extraction) is velocity-dependent in reality, since the efficiency of turbines varies depending on the upstream flow velocity. However, it is assumed that using a time-dependent momentum loss is expected to lead to only a small overall over-estimation of the resistance. Another shortcoming of the porous plate function, is that different c_{loss} values cannot be implemented for flood and ebb. The positioning of the turbines at the basin side of the sill might result in differences in resistance. Lastly, the porous plates cannot be excluded from computations when the head difference over the barrier exceeds a certain limit, while the turbines are lifted from the water when this happens in reality.

Although there are a number of shortcomings to this parameterization, it is considered representative enough for a first estimation of tidal energy extraction on large-scale hydrodynamics.

3.2.3. Calibration of Tidal Turbines

Since a state-of-the-art three-dimensional model is available, results from these model simulations are used as input for the increased resistance in gate openings with turbines. The porous plates in the Delft3D model will be calibrated such that the desired resistance is reached for gate openings with turbines.

Some limitations to using this data are present. The results of the three-dimensional model were not completely validated yet at the time that this research was performed. Moreover, only limited simulations were performed with the model.

Other approaches to the calibration of the porous plates were considered, but could not be used for various reasons. Deltares attempted to derive discharge coefficients from water level measurements, but there was too much uncertainty in these measurements to draw conclusions. Moreover, due to the unique configuration of the turbines, free-stream formulations are not representative. Therefore, the only option was to use the three-dimensional model data as input for the increased resistance.

3.3. Simulation Considerations

In this section, considerations for the simulations with the chosen model are discussed. The effects of upscaling of tidal energy is considered and hypotheses are made about the positioning of turbines in barrier sections and the length-scale of their effects in the basin. Moreover, hydrodynamic indicators are stated, which should be monitored during simulations. Lastly, the simulation period is discussed.

3.3.1. Upscaling of Tidal Energy Extraction

The last knowledge gap identified in Chapter 2 was the effects of upscaling of tidal energy extraction. In order to formulate scenarios for testing the effect of upscaling of tidal energy with the chosen model, the effects of different configurations must be evaluated. For this reason, hypotheses are made. The hypotheses are not based on reviewed literature, but on expert judgment.

It is unknown what the roll-out of turbine arrays will be in the future. Hydrodynamic effects of tidal energy extraction may be significantly influenced by positioning of turbine arrays in the barrier. Three fields are defined for the formulation of hypotheses on upscaling of tidal energy extraction, see Figure 3.2, namely the near-field, mid-field and far-field. The reasoning behind the separation of the basin in this way is explained per field.

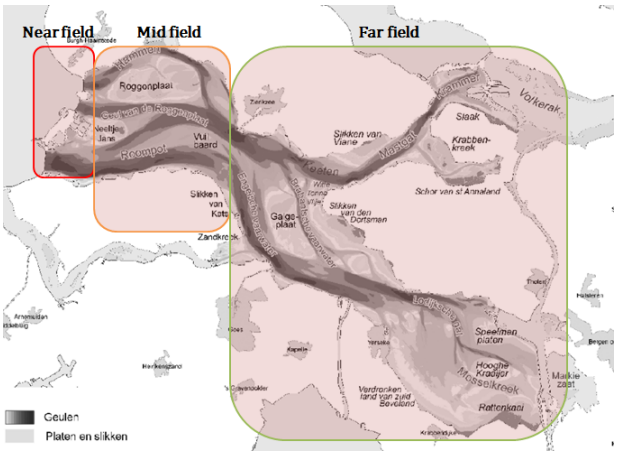

Figure 3.2: Overview of basin with separation of of near-, mid- and far-field

Near-field - The near-field is 50 rotor diameters from the barrier in both east and west directions. This is the area where turbulence caused by turbines occurs. This thesis does not focus on the local flow effects due to tidal turbines.

Mid-field - The mid-field spans between the near-field and the Zeelandbrug (mid-basin). In the mid-field, discharges through different barrier sections directly influence the behavior of flow in those channels. Implementation of turbines in different sections of the barrier would change the flow through channels behind those sections. If the implementation is asymmetric (i.e. Hammen section equipped with turbines, but not the other two sections of the barrier), this could induce a phase shift between two channels surrounding tidal flats in this area and a resulting change in water level gradient over tidal flats.

Far-field - The far-field spans between the mid-field and the end of the basin. The channels braid and meander before reaching this part of the basin. The amount of extraction is expected to influence the hydrodynamic behavior in this field, however the positioning within the barrier is not expected to have an impact.

The hypotheses for the positioning of the turbines are:

1. The current installation will not have a major impact on the hydro- and morphodynamics in the mid- or far-field compared to the impact of the barrier.
2. Increasing tidal energy extraction will have an increasing impact on the hydro- and morphodynamics in the mid- and far-field.

3. The positioning of the tidal energy extraction stations, and potential asymmetries in the positioning, will affect the hydro- and morphodynamic development in the mid-field. Only the amount of tidal energy extraction will affect the hydro- and morphodynamics in the far-field, but the positioning will not.

3.3.2. Hydrodynamic Indicators

In order to test these hypotheses, an analysis must be performed on the simulations. Three hydrodynamic indicators have been defined, which should be monitored during simulations. The hydrodynamic indicators are:

- **Tidal volume** throughout the basin. The reduction in tidal volume entering and leaving the basin due to the construction of the barrier led to the decrease in tidal range and velocities throughout the basin. Tidal volume relates to the morphological equilibrium for the basin. Therefore, changes in the tidal volume indicate how much the sediment deficit of the channels is enhanced.
- **Tidal range** throughout the basin. The decrease in tidal range led to increased impact of wave and wind shear stresses on the tidal flats. By examining the change in tidal range, a comparison can be made between the reduced tidal range due to tidal energy extraction and the construction of the barrier.
- **Discharges** in the channels. The discharges in the channels can be seen as being proportional the velocities. The decreased velocities in the channels decreased the sedimentation on the flats. Moreover, asymmetries in the positioning of tidal turbines in barrier sections could induce a phase shift between two channels surrounding tidal flats in the mid-field. By examining discharges in the channels at various places, this effect can be examined.

3.3.3. Simulation Period

One simulation period lasting one spring-neap cycle is chosen for this research, which is considered to cover sufficient variability in hydrodynamic behavior to be representative for longer time-scales and be realistic computational wise. This spring-neap cycle should be chosen based on average wind conditions (for both speed and direction) in combination with a representative spring neap cycle for yearly variations. The wind conditions are taken into account with in mind further research including wind in the simulations.

3.4. Modeling Approach

A model is set-up including channels, tidal flats and the barrier as well as the required tidal and meteorological processes and sediment transport. A representative spring-neap cycle is chosen for the simulations. This model is calibrated and validated with measured data at various measuring stations in the basin for the situation without turbines.

The increased resistance of gate openings with turbines is implemented in the model by porous plates in those openings. The resistance is determined using output of the three-dimensional STAR-CCM+ model. The loss coefficient of the porous plates is adapted such that the desired resistance is reached. A sensitivity range is taken around this resistance to take into account uncertainties of the parametrization and calibration.

Simulation scenarios are formulated based on the hypotheses, where scenarios comprise of variations in combinations of gate openings equipped with turbines. Relevant monitoring locations within the model, to be monitored during the simulations, are implemented for relevant hydrodynamic indicators.

3.5. Key Points

The Delft3D software in two-dimensions was chosen as most suitable considering the representation of relevant tidal basin hydro- and morphodynamic processes, the parameterization of turbines in the model and computational effort. Tidal energy extraction can be included as an additional resistance term in this model, using porous plates, thereby using a momentum sink approach. The resistance of the porous plates will be calibrated using output data from a three-dimensional STAR-CCM+ model of one gate opening with turbines.

Hypotheses were formulated, which should be verified by the model. They considered hydrodynamic effects of upscaling scenarios of tidal energy extraction in near-field (close to barrier), mid-field (barrier to mid-basin) and far-field (mid- to end-basin). Moreover, hydrodynamic indicators (tidal volume, range and discharges), to be monitored during simulations were defined and a spring-neap cycle was chosen as an appropriate simulation period.

A modeling approach was described which will be implemented in the next chapter.

4

Method

This chapter reports the method of this research. The model set-up is described including an explanation of the barrier schematization. This model is validated with measured water levels in the basin. Hereafter, an explanation is provided regarding the parameterization of turbines using the three-dimensional model data. Following this, the scenarios that are simulated are explained. Hereafter, the motoring locations during simulations are described.

4.1. Model Set-up

In this section an explanation is provided of the model set-up, including the grid and bathymetry, boundary conditions, model parameters and settings, simulation period and barrier schematization in the model. An existing model is used, which was created by Pezij (2015) to investigate nourishments in the eastern part of the basin. An schematization of the model-set-up is shown in Figure 4.1. The grid/bathymetry, barrier schematization and boundary conditions are input for the model which is calibrated with water level measurements. The model can run for a specified simulation period, in which it will calculate flow and waves (not in this work) for each time step within the simulation period and provide the hydrodynamic behavior in the ES basin during this period.

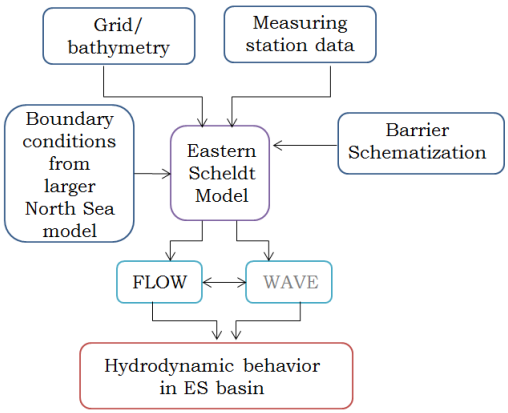

Figure 4.1: Model set-up of the Eastern Scheldt basin in Delft3D shown schematically

4.1.1. Grid and Bathymetry

An illustration of the bathymetry of the ES model in Delft3D is shown in Figure 4.2. The grid covers this same area. The domain includes the ES basin as well as a large offshore section. This part of the model, which extended about 30 km offshore, was necessary to ensure model stability (Pezij, 2015). The resolution of the grid varies between 30m in the basin to 450 meters in the offshore area.

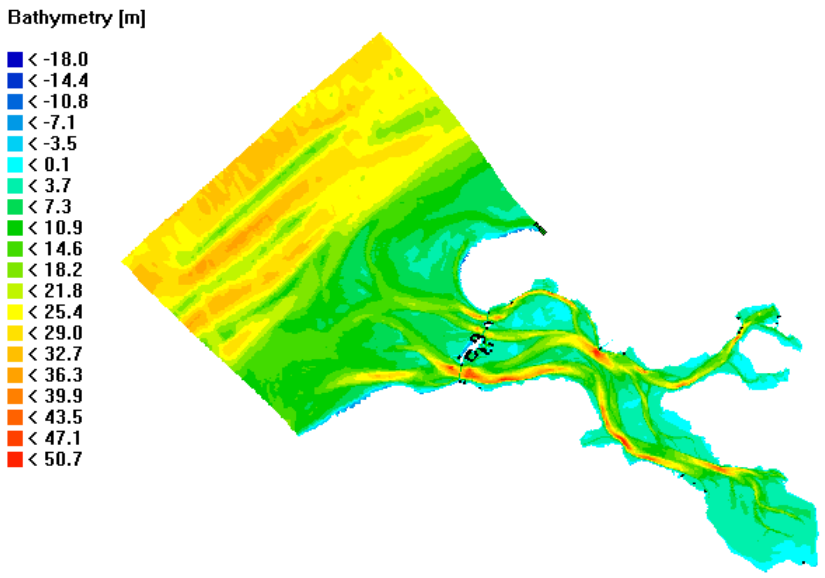

Figure 4.2: Bathymetry of the ES basin in the Delf3D model

4.1.2. Boundary Conditions

The boundary conditions for the model originated from the North sea model DCSMv6-ZUNOv4. This data was provided by Rijkswaterstaat.

4.1.3. Model Parameters and Settings

The parameters and setting are presented in table 4.1.

Table 4.1: Model Parameters

Parameter	Value	Unit
Grid points m direction	244	
Grid points n direction	579	
Total grid points	141,276	
Time step	0.125	$minute$
Bed roughness (Manning)	0.029	$s/m^{1/3}$
Gravity	9.813	m/s^2
Water density	1025	kg/m^3

4.1.4. Simulation Period

The model of Pezij (2015) was calibrated and validated for the period of 1st of September 2013 until the 31st of December 2014, since the boundary conditions were from this period. The simulation period for this work was therefore within this time-frame. One simulation period lasting one spring-neap cycle was chosen for this research, which was considered a long enough time period. The chosen spring-neap cycle was from 15th of June 2014 until the 30th of June 2014. This spring-neap cycle was chosen based on average wind conditions (for both speed and direction) in combination with a representative spring neap cycle. All spring-neap cycles in the period of September 2013 until December 2014 were tested on these criteria (with in mind further research including wind in the simulations). The spring-neap cycle 15-30 June was most representative.

4.1.5. Barrier Schematization

Original Schematization

The barrier schematization of the model created by Pezij (2015) consisted of porous plates and a barrier structure, representing te energy loss and flow constriction respectively. These were necessary as the actual barrier structure (with sill and upper beams, bed protection, pillars) cannot be included in Delft3D due to the model

resolution and dimension. Therefore, porous plates and a barrier structure were implemented to represent frictional and form losses felt by the flow as it passes through the barrier.

Updated Schematization

The turbine parameterization was closely linked to the barrier schematization in the Delft3D model. The purpose of the model in the research of Pezij (2015) was to generate boundary conditions for the southern part of the basin. Implementation of the barrier was not the focus of his study, as long as water levels at the end of the basin represented measurements well. For this thesis, the barrier was a crucial element (since tidal energy extraction needed to be included). For the inclusion of a turbine parameterization, it was desirable that the barrier and the turbine parameterization represented by different structures in the model. Moreover, a more realistic flow through the barrier would be beneficial overall. For these reasons, the barrier schematization was updated.

In the updated schematization, actual sill heights for each gate opening were implemented in the model bathymetry and the barrier structure was removed, see Figure 4.3. The sill heights are not the same for each opening, the sill heights per opening are found in Appendix B. As an example, the depth of Roompot 8 in the original model was 50 m, in the updated model it is 9.5 m. This change was made such that the porous plates representing the barrier could be removed (and implemented later for turbine parameterization). Unfortunately, this change did not result in the desired water levels, and the porous plates were still necessary to take into account some loss. However, the loss was much smaller. The porous plates account for approximately 20% of the resistance and bottom friction for 80% (determined by comparing discharges through the barrier for simulations with (1) the original bathymetry, (2) simulations with updated bathymetry and (3) simulations with updated bathymetry and porous plates).

(a) Original barrier schematization

(b) Updated barrier schematization

Figure 4.3: Barrier Schematizations. red line is barrier structure, broken green lines are porous plates, brown is bathymetry, blue is water level

Figure 4.4 and 4.5 show depth averaged velocities through the Roompot section of the barrier for simulations of both original and updated models. In the original model, velocities increase slightly through the Roompot barrier section. In the updated model, a clear increase in velocities is seen over the now included sill.

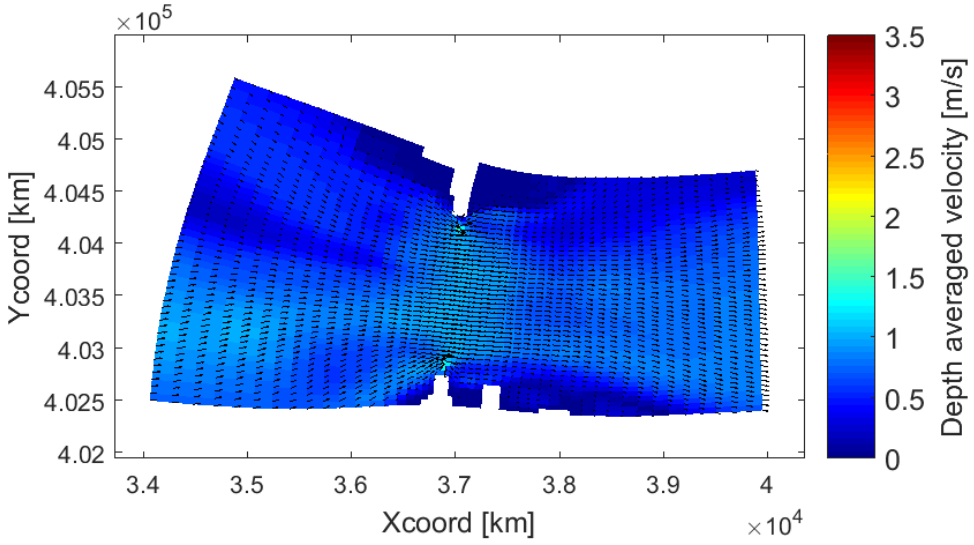

Figure 4.4: Velocity during flood through Roompot section in the original barrier schematization

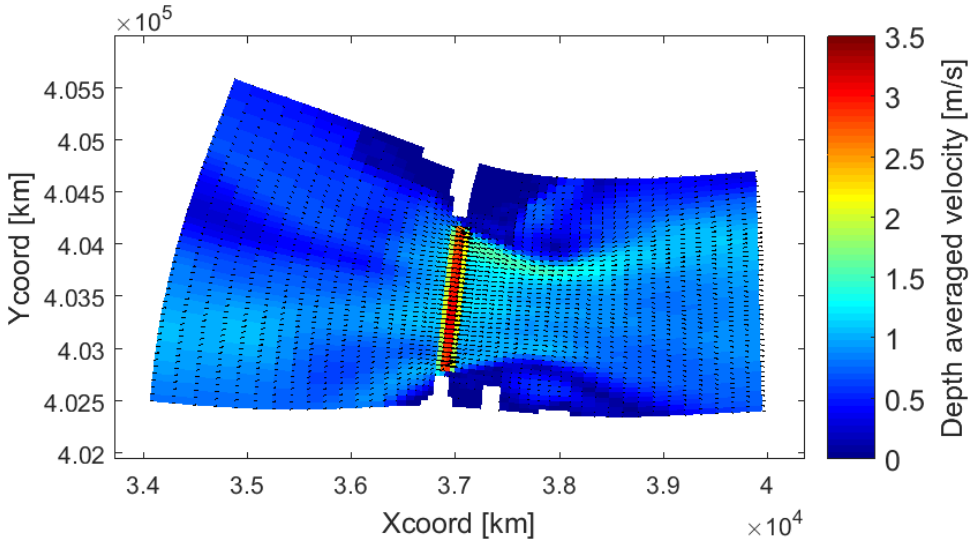

Figure 4.5: Velocity during flood through Roompot section in updated barrier schematization

Flow resistance (frictional and form losses) in the updated schematization is covered by:

- Bottom friction of the two grid cells with increased bed level
- Flow deceleration caused by the abrupt increase in depth
- Additional resistance of porous plates

The bottom friction is likely over-estimated, as the increased bed level spans over two computational cells (approximately 100 meters), see Figure 4.6, while the actual sill width is around 5 meters. The velocity increases over these computational cells (bottom friction is a function of the velocity) and the increased bottom friction is therefore included in multiple momentum computations. The pillars and top sill are not included in the model, and neither are losses due to energy conversion of turbulence (3D effects). The over-estimated bottom friction and the porous plates account for these losses.

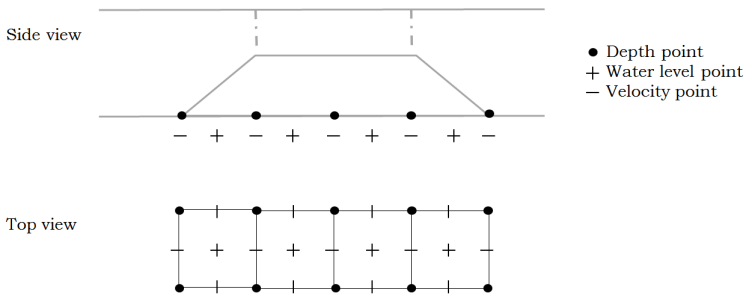

Figure 4.6: Grid schematization of barrier in Delft3D including depth points, water level points and velocity points, side and top view

An attempt was made at implementing increased sill heights in the bathymetry in combination with a barrier structure for the barrier schematization. Numerical instability was noticed in the model. Therefore, it was necessary to use porous plates to account for the small additional loss. This barrier schematization is not optimal, especially in combination with tidal energy extraction. However, considering the limitations of the model and time-span of this work, it was decided to continue with this formulation.

4.2. Validation Model with Barrier

This section shows the calibration and validation of the Eastern Scheld model without turbines.

4.2.1. Calibration

The porous plates in the updated situation had to be re-calibrated, such that water levels in the model matched measurements well again throughout the basin. This calibration period was for simulations lasting a few days in December 2013. Measurement locations for both model simulations and actual measuring stations are indicated in Figure 4.7, measurement data from the actual measuring stations was provided by Rijkswaterstaat. The porous plate calibration resulted in a loss coefficient of 0.01 per porous plate. One porous plate was implemented per gate opening, instead of previously per section.

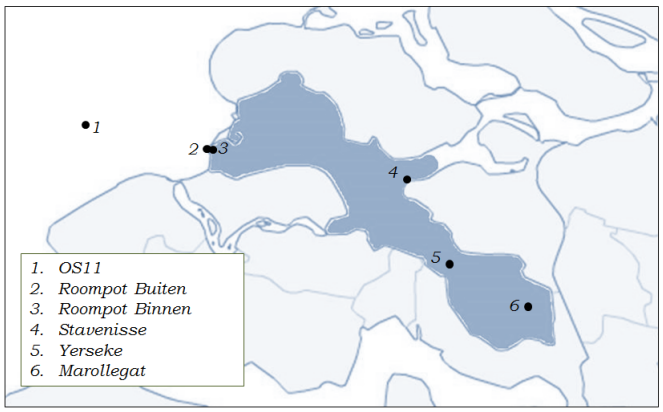

Figure 4.7: Measurement locations in the ES used for calibration and validation of Delft3D model

4.2.2. Validation

The updated model was validated by comparing a simulation lasting one month (June 2014) with measurements. Water levels obtained from model simulations are presented in Figure 4.8 for Yerseke station. In the figure, measured data is also included, at the Yerseke measuring station (Rijkswaterstaat). Some data is missing from the measurement data. The figure shows that low water levels are underestimated by the model, but generally the model representation is quite similar to measured data.

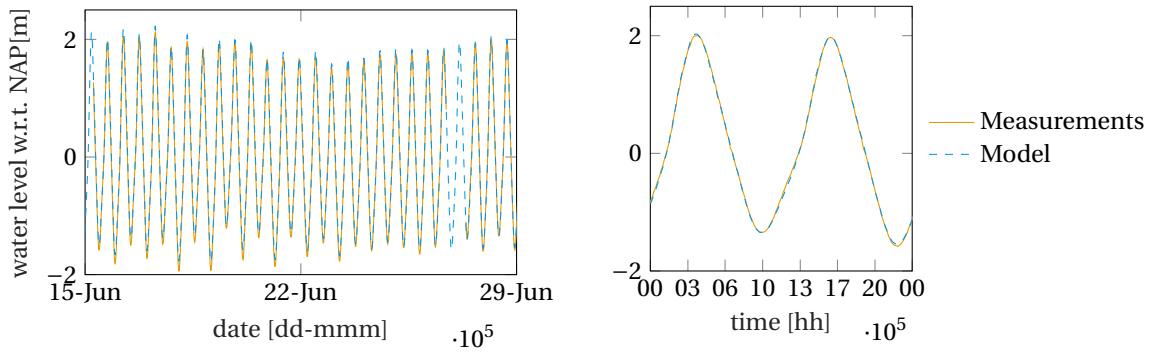

(a) WL 15-30 June 2014

(b) Zoomed in water levels

Figure 4.8: Measured and modeled water levels at Yerseke station for June 2014

The model accuracy was determined using root mean square error (RMSE). The RMSE, Equation 4.1 (Walstra, 2017), shows the average error made between observed values and predicted values. In this Equation N_v is the number of values, Y_i is observation and X_i is prediction, observation is measured data and prediction the simulation results of water levels in this case. In research about water level forecasting of the North Sea, Zijl et al. (2013) find a RMSE between 5-10 cm to be acceptable.

$$RMSE = \sqrt{\frac{1}{N_v}\sum(Y_i - X_i)^2} \tag{4.1}$$

The root mean square errors of the model are found in table 4.2 for the measuring stations OS11, Roompot Binnen, Roompot Buiten, Stavenisse, Yerseke and Marollegat. This model was considered to be accurate for the purpose of this study since the tidal range was much larger than the RMSE at the various locations.

Table 4.2: Comparison RMSE of model for various measuring stations and tidal range at those locations

	RMSE [cm]	Tidal range [cm]
OS11	6.6	301
Roompot Buiten	7.5	298
Roompot Binnen	7.3	261
Stavenisse	7.2	273
Yerseke	7.7	298
Marollegat	8.6	348

4.3. Turbine Parameterization

This section describes the turbine parameterization in the ES model. Firstly, the approach of the implementation of increased resistance due to the turbines the ES model is explained. This increased resistance is based on model output from a three-dimensional model of one gate opening with turbines. An explanation is provided how the models are coupled and finally, the implementation of the increased resistance is described.

4.3.1. Approach

A crucial step in this research was the parameterization of turbines in the Delft3D model. The chosen approach was calibration of porous plates based on simulations of the three-dimensional STAR-CCM+ model of one gate opening (Roompot 8) with turbines. Figure 4.9 shows the set-up of both models and how the Delft3D and STAR-CCM+ model are coupled.

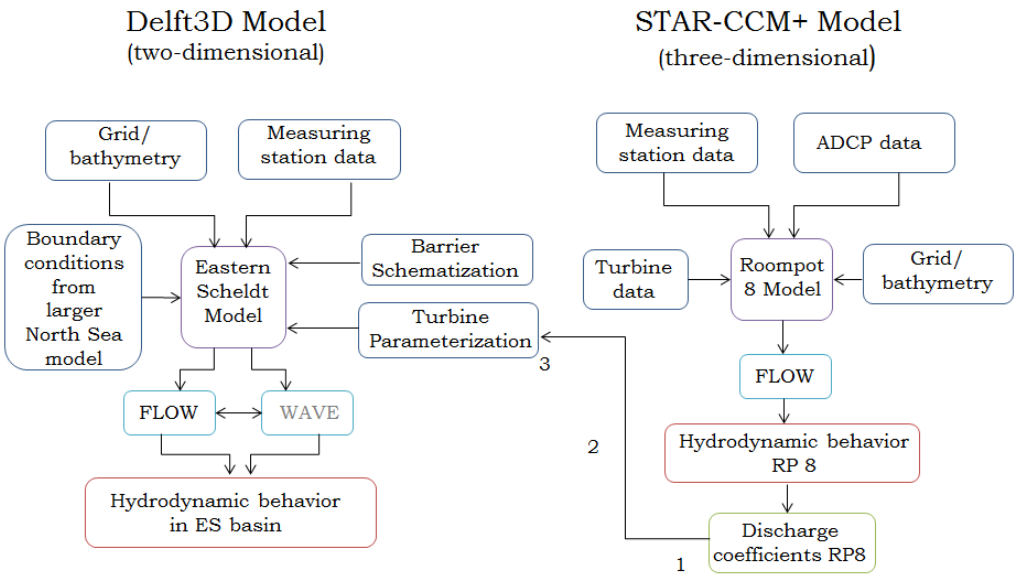

Figure 4.9: Parameterization approach: Schematization of model set-ups of Delft3D and STAR-CCM+ models and coupling of models

The turbine parameterization consisted of three steps:

1. Derivation of the discharge coefficients for Roompot 8 from the STAR-CCM+ model simulations.
2. Coupling of the STAR-CCM+ model output to the Delft3D model.
3. Implementation of the discharge coefficients in Delft3D.

These steps are described in the next subsections.

4.3.2. Discharge Coefficients Derived from STAR-CCM+ (1)

A brief explanation of the STAR-CCM+ model is provided, and hereafter the derivation of discharge coefficients from this model.

STAR-CCM+ Model

The STAR-CCM+ model was a representation of Roompot 8 and half a gate on each side of Roompot 8 (so two gate openings in total), see Figure 4.10, the total width of the domain was 90 meters. The total length of the STAR-CCM+ model domain was 420 m. The STAR-CCM+ model was not created or used by the author, simulations results were provided by Deltares.

Figure 4.10: Snap-shots of STAR-CCM+ model domain during a simulation with turbines, top- and side-view

The STAR-CCM+ model was semi-stationary, which entailed that each simulation had a fixed head difference over the domain during the simulation. The STAR-CCM+ model had the limitation that at the moment that this research was being performed, only simulation results were available for the simulations indicated in Table 4.3. Each simulation had a head difference of 0.2 m.

Table 4.3: Simulations STAR-CCM+ model

Ebb	No Turbines	Head difference 0.2m
	Turbines	Head difference 0.2m
Flood	No turbines	Head difference 0.2m
	Turbines	Head difference 0.2m

Derivation Discharge Coefficients
For each simulation from table 4.3, discharge coefficients were derived. These were derived through Equation 4.2. In this equation μ is the discharge coefficient, A_g is the wet flow through area of the gate opening, Q_g is the discharge through the gate opening g is the gravitational acceleration, ζ_u is the upstream water level and ζ_d is the downstream water level. For the cross-sectional flow through area of the gate, the downstream water level was used. Figure 4.11 shows the locations where the discharge and water levels were extracted. This downstream water level changed during the tidal cycle; during flood, the ES side was downstream and during ebb the NS was downstream.

$$\mu = \frac{Q_g}{A_g \sqrt{2g|\zeta_u - \zeta_d|}} \tag{4.2}$$

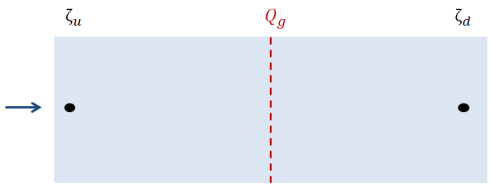

Figure 4.11: Locations of parameters in STAR-CCM+ for calculation discharge coefficients, flood situation

The results of this computation are found in Table 4.4, a detailed explanation of the calculation is provided in Appendix C. The relationship between a gate with (μ_{b+t}) and without (μ_b) turbines was formulated in the following manner, see Equation 4.3. Table 4.4 shows all three components of the equation.

$$\mu_{b+t} = X\mu_b \tag{4.3}$$

Table 4.4: Discharge coefficients derived from STAR-CCM+ model

	μ_b	X	μ_{b+t}
Ebb	1.06	**0.84**	0.89
Flood	0.95	**0.88**	0.83

For the resistance due to tidal energy extraction in the Delft3D model, this X factor was used.

4.3.3. Coupling of the Models (2)

The big difference between the two models, was that the STAR-CCM+ model was stationary, and the Delft3D model included tidal variations. The constant head difference of 0.2 m occurred between the ends of the domain of the STAR-CCM+ model, this was approximately 200 m upstream and downstream from the barrier. In reality, this 0.2 m head loss over the barrier occurs twice during flood and twice during ebb, indicated in Figures 4.12 and 4.13. The color blue indicates flood and red ebb. Roompot binnen ('inside') is a location 200 m landward of the basin and Roompot buiten ('outside') is a location 200 m seaward of the barrier. The Delft3D model simulates the entire tidal cycle, including all head differences, while the STAR-CCM+ model was considered to be an average of the two points in the tidal cycle where a difference of 0.2m occurs.

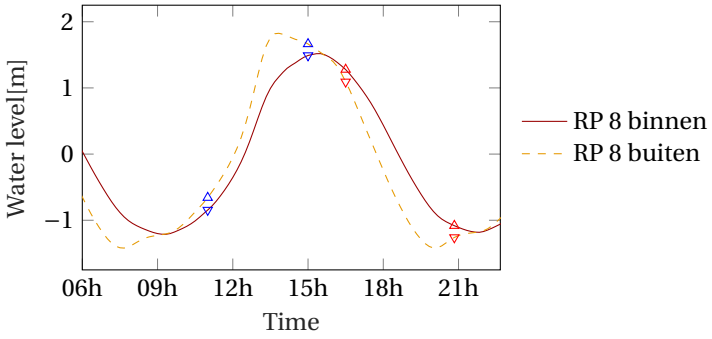

Figure 4.12: Water levels at RP 8 binnen (inside) and RP 8 buiten (outside), blue arrows indicate head difference of 0.2 m during flood, red arrows indicate head difference of 0.2 m during ebb

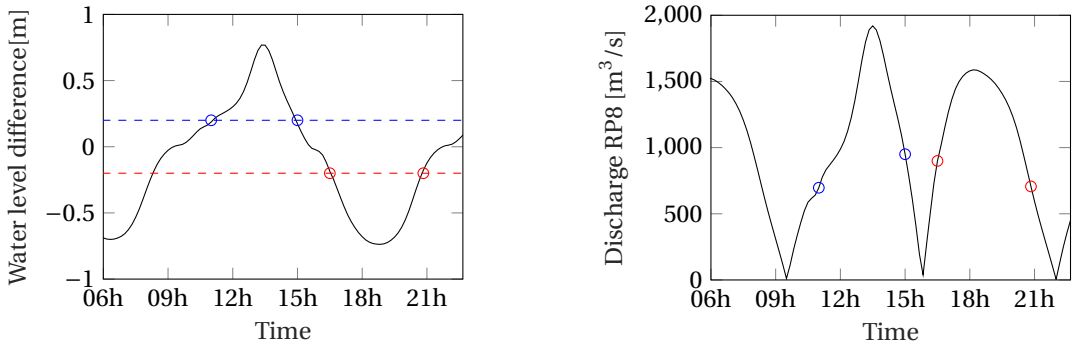

Figure 4.13: Water level difference between RP 8 binnen and RP 8 buiten and corresponding discharge magnitude through gate opening Roompot 8, blue circles indicate head difference of 0.2 m during flood, red circles indicate head difference of 0.2 m during ebb

Water levels at Roompot 8 binnen and Roompot 8 buiten were analyzed in a Delft3D simulation over the spring neap cycle (June 15 til 30) for the same gate opening as in the STAR-CCM+ model; Roompot 8, see Figure D.1 in Appendix D. Average discharge coefficients were calculated from all the time steps in which the head difference of 0.2 occurred for flood and ebb using Equation 4.2. The magnitude of the depth averaged discharge was determined at the time-step in which the head difference occurred, see Figure D.2 in Appendix D. The magnitude of the depth averaged discharge (Q_g) was taken over the sill of Roompot 8. The upstream and downstream water levels (Roompot 8 binnen and buiten) were taken at 4 grid cells (approximately 200 m) from the barrier for both te ES and NS side. The cross-sectional wet area was computed as the 'real life' cross section; the width is 39.5 m and the depth is the sill depth (9.5 m) plus the downstream water level.

The X factor determined in the previous section was applied to the average of the discharge coefficients from these snap-shots of 0.2 m head difference.

4.3.4. Implementation and Calibration Discharge Coefficients Turbines Delft3D (3)

The last step in the calibration was applying the X factor. The X factor was applied to the discharge coefficient present in the Delft3D model at the Roompot 8 gate opening for the head differences of 0.2m.

Reference Case

The reductions in discharges (coefficients) through a gate opening in the STAR-CCM+ model for ebb and flood respectively were -16 % (X factor 0.84) and -12% (X factor 0.88) compared to the case without turbines. In order to achieve this reduction in discharge for the same gate opening in the Delft3D model, the loss coefficient of the porous plates was increased such that this same reduction in discharge (coefficient) was reached. Through an iterative procedure (changing the c_{loss} value of the porous plates), these discharges (coefficients) were reached at c_{loss} values of 0.11 for the porous plates at Roompot 8.

Limitations Calibration

STAR-CCM+ Model

Some limitations to the calibration step were present. The results of the STAR-CCM+ model were not validated yet at the time that this research was performed, and therefore using this method was not completely reliable. Moreover, only the simulations with 0.2 m head difference were available, in order to verify if the chosen loss coefficient is appropriate for all head losses, more simulations should be evaluated.

Other Gate Openings
For the simulations that would be performed, other gate openings also need turbine parameterizations. Other gate openings have different sill heights, which could result in different coefficients if the same turbines are used, however for future installations different size turbines could also be installed. The choice is made to use the same c_{loss} value for other gate openings. Since other gate openings have different cross-sectional areas, the application of the loss coefficient will result in more or less overall resistance. This could be interpreted as larger turbines in larger openings and smaller turbines in smaller openings. This assumption may not hold true in reality, but will be used in the remainder of this work.

Sensitivity Range
To take these limitations into consideration as well as the simplified method for representing the turbines, the choice was made to use a sensitivity range for the simulations. This sensitivity range is the reference X factor + 5%, the reference X factor - 5% and the reference X factor -10%, see Table D.1 in Appendix D. The + and - are opposite for the resistance terminology (+ 5% is the - lower case), as an increase in percentage means less resistance and vice versa. The porous plates of Roompot 8 were again iteratively calibrated until the desired X factors were reached. Table 4.5 shows the resulting values of the porous plates and the applied X factors to the discharge coefficients for the Roompot 8 gate opening.

Table 4.5: Sensitivity range of discharge coefficients tidal energy extraction

	c_{loss}	X_{ebb}	X_{flood}
Base case	0.01	1	1
- lower	0.07	0.89	0.93
reference	0.11	0.84	0.88
+ upper	0.15	0.79	0.83
++ upper	0.20	0.74	0.78

This sensitivity range is based on expert judgment as well as other research in which similar factors were derived (De Kleermaeker, 2013). The results of that research were factors between 0.85 and 0.82 for flood and between 0.91 and 0.89 for ebb. A more detailed explanation of that research is provided in Appendix D.

4.4. Simulation Scenarios

In this section, the simulation scenarios are defined. These scenarios are based on the different hypotheses from Chapter 3. They are not necessarily realistic scenarios, but are defined in order to understand how different upscaling scenarios may affect the hydrodynamics in the ES.

4.4.1. Near-future Scenario

At the time of this research, one gate opening (Roompot 8) was equipped with turbines. Licensing had been granted for Roomot 10, and turbines were expected to be installed here in the near-future. Therefore, the Near-future scenario considers gate openings Roompot 8 and 10 equipped with turbines. In figure 4.14 (a) the Near-future scenario is shown; the red squares indicate the location of gates with increased resistance.

4.4.2. Maximum Roll-out Scenario

The amount of tidal energy extraction was expected to affect the hydrodynamics in the entire basin. The Maximum Roll-out scenario assesses the maximum impact of tidal energy extraction. The most realistic and optimistic (taking into account practical and safety issues) roll-out scenario was indicated to be 1 out of 3 gate openings equipped with turbines, and avoiding the shallower openings near the shores. This scenario consists of four openings equipped with turbines in Hammen section (3,6,9 and 12) four openings in Schaar section (4,7,10 and 13) and nine in Roompot section (5,8,10,13,16,19,22,25,28), thus a total of 17 barrier openings filled with turbines. This configuration is shown in figure 4.14 (b). In Appendix B the gate openings which

are equipped with turbines are indicated in bold.

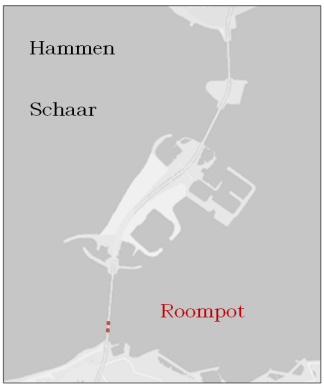

(a) Near-future scenario

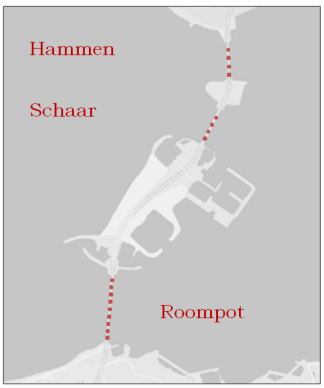

(b) Maximum Roll-out scenario

Figure 4.14: Near-future and Maximum Roll-out scenarios, gate openings equipped with turbines indicated with red squares

4.4.3. Partial Roll-out Scenarios

Three Partial Roll-out scenarios were defined, which are illustrated in figure 4.15. The three scenarios consist op the same gate openings as in the Maximum Roll-out scenario, but each a different section individually. These scenarios were created to test the length-scale of the disturbance in case such asymmetric positioning is realized.

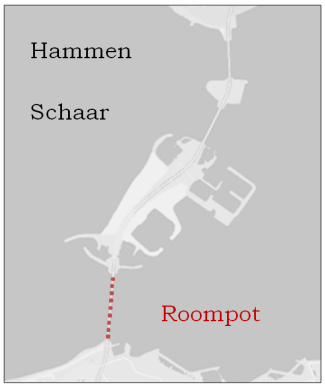

(a) Roompot Filled

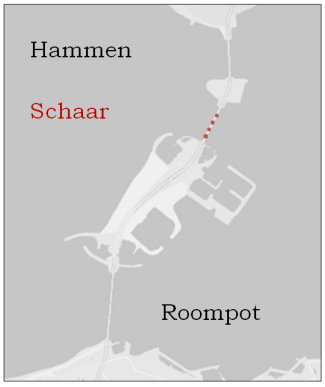

(b) Schaar Filled

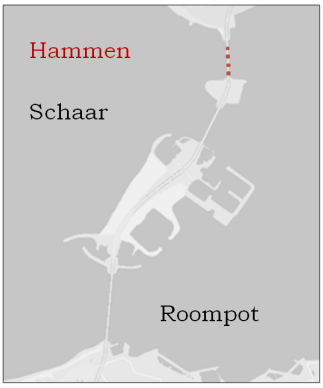

(c) Hammen Filled

Figure 4.15: Partial Roll-out scenarios, gate openings equipped with turbines indicated with red squares

4.4.4. Simulations

Table 4.6 shows the simulations that were performed. Each simulations ran for the chosen spring-neap cycle. For the Near-future scenario Maximum Roll-out scenario it was relevant to test the sensitivity range in order to take into account uncertainties. For the Partial Roll-out scenarios, effects of the asymmetry were especially relevant and not necessarily differences in the amount of extraction, therefore only the reference case was simulated for these scenarios.

Table 4.6: Simulations performed for each scenario

	Sensitivity range			
	- lower	reference	+ upper	++ upper
Near-future	•	•	•	•
Maximum	•	•	•	•
Partial - Roompot		•		
Partial - Schaar		•		
Partial - Hammen		•		

4.5. Simulation Monitoring

For each simulation, water levels and the tidal volume in the basin are monitored. In the channels discharges are monitored. These were considered as key hydrodynamic indicators. The measurement locations for monitoring these indicators are presented in this section.

4.5.1. Basin

The observation points and cross sections where information was monitored in the model for tidal ranges and volume in the basin are illustrated in figure 4.16.

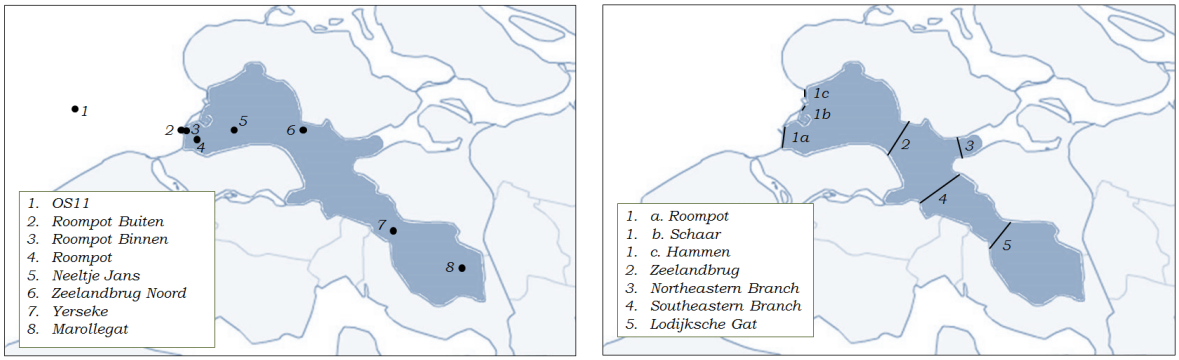

(a) Observation points

(b) Cross sections

Figure 4.16: Locations and cross-sections basin for monitoring of tidal range and volume during simulations

At the observation points, water levels and thus tidal ranges were monitored for each scenario. The tidal volume was monitored at the cross sections. These aspects were monitored as these were identified as important hydrodynamic indicators. Locations were chosen along the basin in order to determine how the local disturbance at the barrier propagated through the basin. Moreover, some of the observation points in the model are also actual measuring stations, and therefore results could be compared in the future.

Changes in tidal volume led to changes in tidal range and velocities during barrier construction. Tidal volume relates to the morphological equilibrium for the basin. Therefore, changes in the tidal volume indicate how much the sediment deficit of the channels is enhanced. The average volume was taken for ebb and flood during the spring-neap cycle, since differences in ebb and flood were expected to be the same and effects of variations in spring and neap even out over the spring-neap cycle.

The tidal range determines the emergence time of different height intervals of the tidal flats. The average tidal range over the spring-neap cycle was taken, to account for both the spring and neap tide. The effect of variations in amplitude was expected to even out over the spring-neap cycle.

4.5.2. Channels

In the channels, discharges were monitored. The locations where the discharges were monitored are indicated in Figure 4.17.

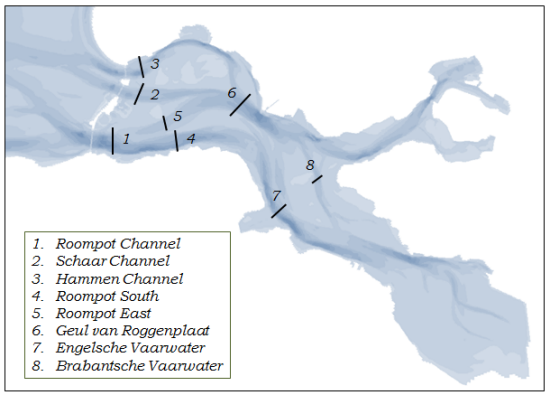

Figure 4.17: Cross-sections channels for monitoring discharges during simulations

The discharges were investigated at these cross sections to see how flow was affected in channels due to blockage of different barrier sections and to see how far the disturbance would propagate. The discharges in channels are an important hydrodynamic indicator for shoal building. Moreover, phase differences in channels surrounding tidal flats determine the water level gradient and therefore flow over the tidal flat due to the tide. The peak discharges were determined for both flood and ebb, but averaged over the spring-neap cycle. This is because sediment in the ES is sensitive to variations in local asymmetry of maximum velocities (assumed to be proportional to discharge). The effect of variations in amplitude of the peaks was expected to even out over the spring-neap cycle.

4.6. Key Points

An available two-dimensional Delft3D model (Pezij, 2015) covers relevant hydrodynamics and morphodynamic processes (tidal flow, wind, waves and sediment transport) of the basin with barrier, channels and tidal flats. This model was set-up for a spring-neap cycle simulation period. The barrier schematization was changed, by including sill heights of gate openings in the bathymetry. The Delft3D model was validated for water levels in the basin for the chosen spring-neap cycle (without turbines), compared to measured data. The validation showed a good representation of water levels in the basin (a RMSE around 7 cm compared to an average tidal range of 3 m).

This model was modified to account for tidal energy extraction. The tidal turbines were parameterized through a local momentum sink approach that increased the flow resistance locally. The increased flow resistance was modeled by porous plates for the barrier openings including turbines. The additional resistance due to the turbines was calibrated using output data from a semi-stationary three-dimensional STAR-CCM+ model of one opening with turbines. To evaluate variations in resistance, a simple sensitivity range (-5 to +10%) was defined as input to the numerical simulations. This sensitivity range ensured that the results would account for uncertainties regarding calibration data and limitations due to simplified turbine representation.

Hypothetical upscaling scenarios were defined, denoted 'Near-future', 'Partial Roll-out' and 'Maximum Roll-out', in which different sections of the barrier were outfitted with tidal turbines:

- Near-future: 2 barrier openings with turbines in Roompot section
- Maximum Roll-out: 17 barrier openings with turbines, regularly placed in all barrier sections
- Partial Roll-out: same 17 openings, but limited to one of the sections equipped with turbines at one time, creating 3 sub-scenarios from south to north: Roompot (9), Schaar, (4), or Hammen (4) respectively

For each simulation the results were monitored in the following manner; water levels were monitored at various observation points to determine the tidal ranges, the tidal volume was monitored at various cross sections and discharges were monitored in various cross sections in relevant channels. The results are presented in the next chapter.

5

Simulation Results Basin Hydrodynamics

In this chapter results of simulations of different scenarios are presented. For each scenario (Near-future, Maximum Roll-out and Partial Roll-out) changes in water levels and tidal volume in the basin are shown. Additionally, changes in peak discharges in channels are presented. Finally an analysis is performed on the hydrodynamic results from all scenarios.

5.1. Near-future Scenario

In the Near-future scenario two gate openings had an increased resistance in the model.

5.1.1. Basin

Water Levels

For the Near-future scenario, the water levels in the channels of the basin were analyzed, as explained in Chapter 4. The exact magnitude and percentage of the deviations of these water levels from the base case are presented in Tables E.1 and E.2 in Appendix E. The results are summarized in Figure 5.1. The figure shows the deviation of the mean high and low water levels as well as the mean tidal range within the chosen spring-neap cycle with respect to the base case where no turbines were present. The figures include the observation points OS11 (-14km), Roompot Buiten (-0.5km), Roompot Binnen (0.5 km), Roompot (2km), Neeltje Jans (6km), Zeelandbrug Noord (15km), Yerseke (32km) and Marollegat (43km), where 0km is the barrier, and positive indicates landward direction.

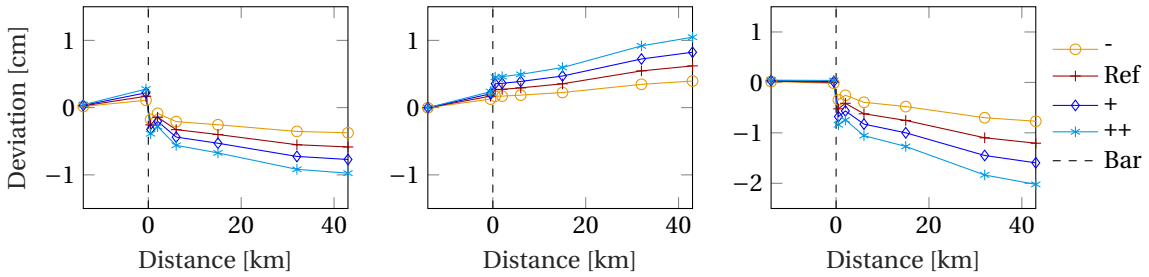

(a) Mean high water (b) Mean low water (c) Mean tidal range

Figure 5.1: Deviations in (a) mean high water, (b) mean low water and (c) mean tidal range w.r.t. base case along basin, Near-future scenario. Sensitivity range of simulations is included (- lower, reference, + upper and ++ upper). 0km is the barrier, and positive indicates landward direction.

Table 5.1 shows the average deviations in tidal range for the sensitivity range. The average is taken between Roompot Binnen and Marollegat observation points (so the deviation that occurs about mid-basin). For the reference case (red line with cross in the figure), the average deviation in mean tidal range was 0.9 cm. This was a 0.3 % decrease from the mean tidal range without turbines. The deviation increased in landward direction in both magnitude and percentage.

Table 5.1: Average deviation in tidal range, Near-future scenario

- lower	reference	+ upper	++ upper	
0.6	0.9	1.1	1.4	[cm]
0.2	0.3	0.4	0.4	[%]

Tidal Volume
The tidal volume accumulated through various cross sections throughout the basin were investigated. In Tables E.3 and E.4 in Appendix E the decrease in tidal volume is shown for the various cross sections described in Chapter 4 (Barrier opening, Zeelandbrug, Northeastern Branch, Southeastern Branch and Lodijksche gat) for the resistance sensitivity range. The percentage decrease in tidal volume was found to be relatively constant and in the same order of magnitude to the reduction in tidal range (0.3%). This corresponded to a decrease of 2.8 million cubic meters near to the barrier opening for the reference case.

Summary
Figure 5.2 shows the decrease in percentage for the tidal range and the tidal volume for the reference case for various locations and cross sections throughout the basin. A general reduction of 0.3% was found for both the local tidal range and tidal volume accumulated through certain cross-sections.

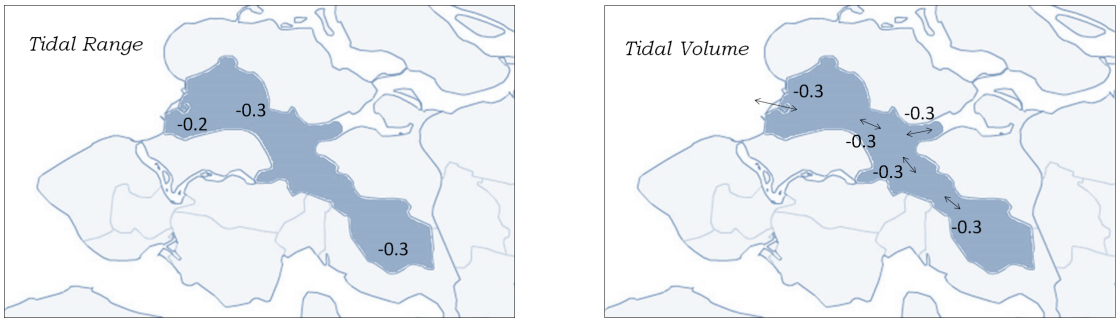

Figure 5.2: Overview of basin showing reduction tidal range and tidal volume expressed as %, Near-future scenario

5.1.2. Channels
In the channels, changes in both peak ebb and flood discharges were investigated. Table E.5 in appendix E shows the exact values of the decrease in flood and ebb discharges with respect to the base case for the reference scenario. Figure 5.3 summarizes the average change in peak discharges at various cross sections described in Chapter 4 (Roompot Channel, Schaar Channel, Hammen Channel, Roompot South, Roompot East, Geul van Roggenplaat, Engelsche Vaarwater and Brabantsche Vaarwater).

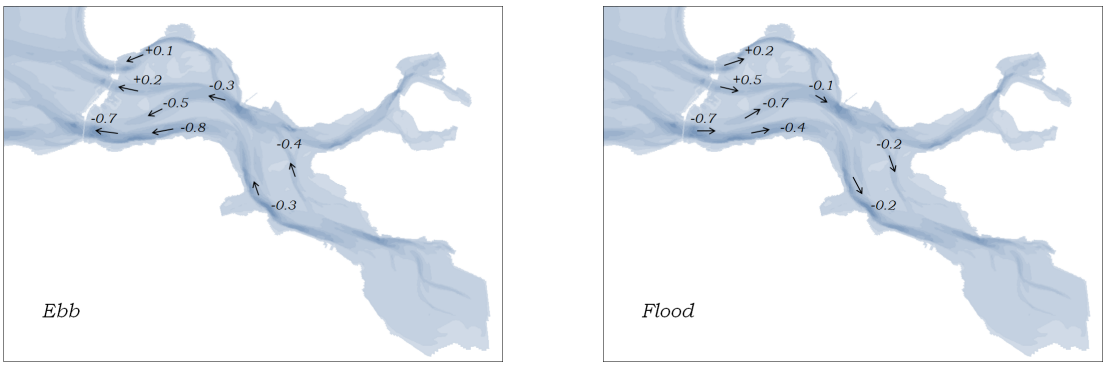

Figure 5.3: Overview of basin showing reduction in peak discharge expressed as %, Near-future scenario

Peak discharges decreased in the Roompot Channel directly behind the barrier, but increased in the Schaar and Hammen Channels for both ebb and flood. In the far-field discharges also decreased for both ebb and flood.

5.2. Maximum Roll-out Scenario

In the Maximum Roll-out scenario, 17 gate openings had an increased resistance in the model.

5.2.1. Basin

Water Levels
For the Maximum Roll-out, the water levels in the channels of the basin were analyzed. The exact values of the deviations and the percentage of the original tidal range for the are presented in Tables E.6 and E.7 in Appendix E. Figure 5.4 summarizes the results of deviations in the mean high and low water levels and mean tidal range within the chosen spring-neap cycle with respect to the base case where no turbines were present.

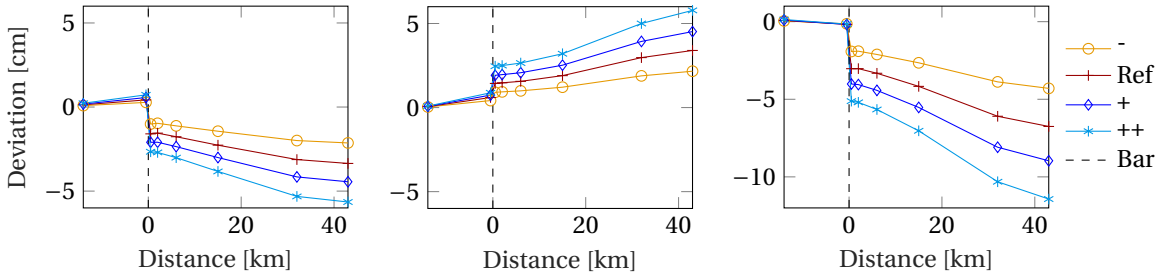

(a) Mean high water (b) Mean low water (c) Mean tidal range

Figure 5.4: Deviations in (a) mean high water, (b) mean low water and (c) mean tidal range w.r.t. base case along basin, Maximum Roll-out scenario. Sensitivity range of simulations is included (- lower, reference, + upper and ++ upper). 0km is the barrier, and positive indicates landward direction

Table 5.2 shows the average deviation in tidal range for the sensitivity range. The deviations increased in landward direction, just as the near future scenario, but the deviation was larger. The decrease in mean tidal range for the reference case was 4.9 cm, which corresponded to a decrease of 1.5%.

Table 5.2: Average deviation in tidal range, Maximum Roll-out scenario

- lower	reference	+ upper	++ upper	
3.1	4.9	6.5	8.3	[cm]
1.0	1.5	2.0	2.6	[%]

Tidal Volume
In Tables E.8 and E.9 in Appendix E the deviation in tidal volume for all cases are shown for the various cross sections. The reduction in accumulated tidal volume at the entrance of the basin was 15 million cubic meters for the reference case. This corresponded to a decrease of about 1.7% compared to the original tidal volume entering and leaving this part of the basin.

Summary
Figure 5.5 shows the decrease in percentage for the tidal range at certain locations and the tidal volume accumulated through certain parts of the basin for the reference case. In general a decrease of 1.7% was found for both the tidal range and tidal volume compared to the original situation.

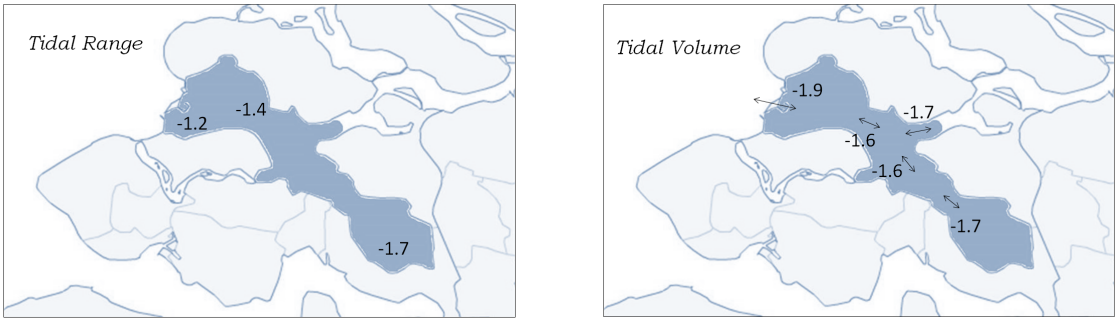

Figure 5.5: Overview of basin showing reduction tidal range and tidal volume expressed as %, Maximum Roll-out scenario

5.2.2. Channels

Discharges
The discharges through various cross-sections were investigated. Table E.10 in Appendix E shows the decrease in average peak flood and ebb discharges with respect to the base case for the reference scenario. Figure 5.6 summarizes the reductions in average peak discharges.

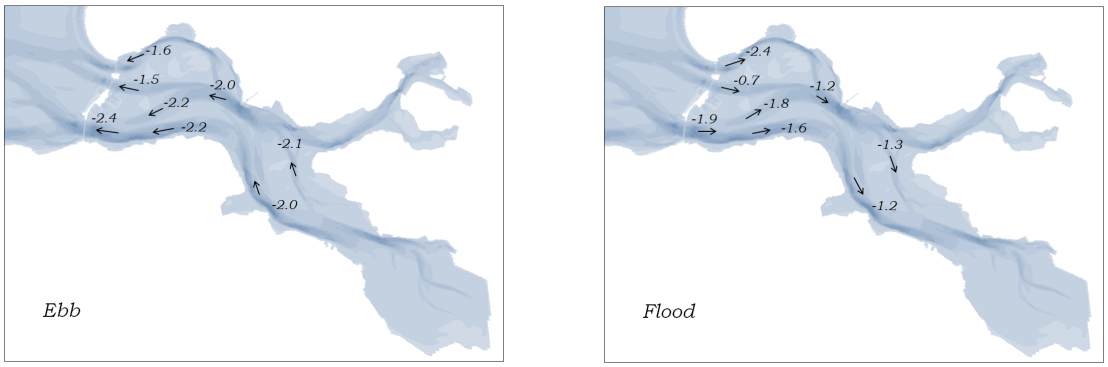

Figure 5.6: Overview of basin showing reduction average peak discharges expressed as %, Maximum Roll-out scenario

The peak discharges decreased everywhere in the basin, and to a larger degree than in the Near-future scenario.

5.3. Partial Roll-out Scenarios

For the Partial Roll-out scenarios, either 4 (Schaar or Hammen Filled) or 9 gate openings (Roompot Filled) had increased resistance.

5.3.1. Channels

Water Levels
For the Partial Roll-out scenarios, the water levels in the channels of the basin were analyzed. The exact values of the deviations and the percentage of the original tidal range are presented in Tables E.11 and E.12 in Appendix E. Figure 5.7 summarizes the results of the deviations in the mean high and low water levels and the mean tidal range with respect to the base case where no turbines were present.

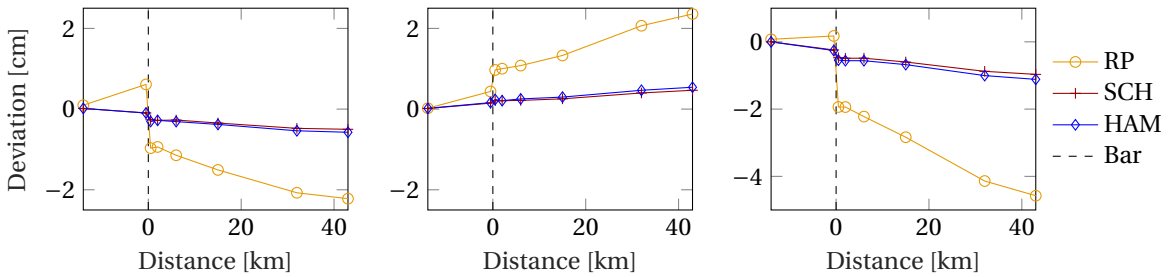

(a) Mean high water (b) Mean low water (c) Mean tidal range

Figure 5.7: Deviations in (a) mean high water, (b) mean low water and (c) mean tidal ranges w.r.t. base case along basin, Partial Roll-out scenarios. Partial Roompot (RP) 9 gate openings with turbines, Partial Schaar (SCH) and Hammen (HAM) 4 gate openings. 0km is the barrier, and positive indicates landward direction

Table 5.3 shows the average deviation in mean tidal range. Roompot Filled had higher deviations, because there were more gates with increased resistance. The scenario in which Roompot had turbines, resulted in deviations of water levels 3.3 cm, which was a deviation of 1.0% for the reference case. For Schaar Filled with turbines this was 0.7 cm (0.2%) and for Hammen Filled 0.8 cm (0.3%). The results are summarized in Figure 5.8 for the whole basin.

Table 5.3: Average deviation in tidal range, Partial Roll-out scenarios

Roompot Filled	Schaar Filled	Hammen Filled	
3.3	0.7	0.8	[cm]
1.0	0.2	0.3	[%]

Figure 5.8 shows the reduction in tidal range for all three Partial Roll-out scenarios at various locations in the tidal basin.

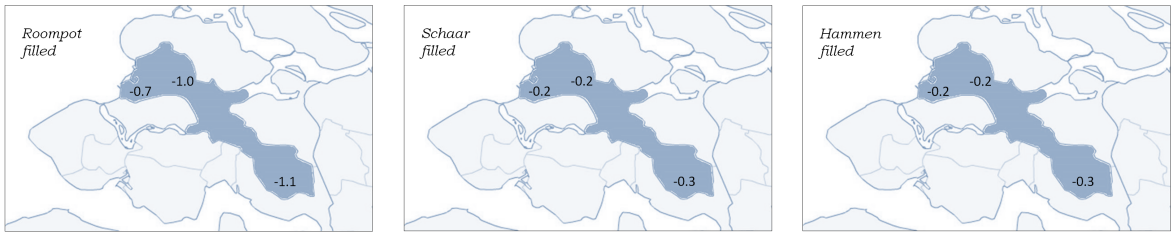

Figure 5.8: Overview of basin showing reduction in tidal range in %, Partial Roll-out scenarios

Tidal Volume

The changes in accumulated tidal volume over a tidal cycle were investigated for the Partial roll-out scenarios. In Table E.13 in Appendix E the decrease in tidal volume is shown for the various cross sections. The results are summarized in Figure 5.9.

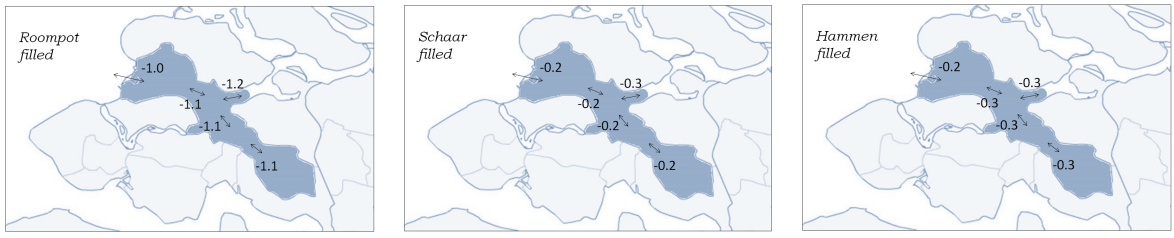

Figure 5.9: Overview of basin showing changes in tidal volume in %, Partial Roll-out scenarios

The reduction in tidal volume accumulated through the entrance of the basin was 10.4 million cubic meters for the Roompot Filled scenario. This was a deviation of about 1.1% from the original tidal volume.

For Schaar Filled the decrease was 2.0 cubic meters through the entrance and in percentage around 0.2%. For Hammen Filled the decrease was 2.3 million cubic meters at the entrance, in percentage around 0.3%.

5.3.2. Channels

Discharges
In Table E.15 in Appendix E the deviations in peak discharges are presented for each Partial Roll-out scenario.

Roompot Filled
In Figure 5.10 the results of the average peak discharges are summarized for the Roompot Filled scenario. The figure shows a decrease in discharge through the Roompot Channel and increases in the Schaar and Hammen Channels, similarly as the Near-future scenario. In the far-field discharges decreased.

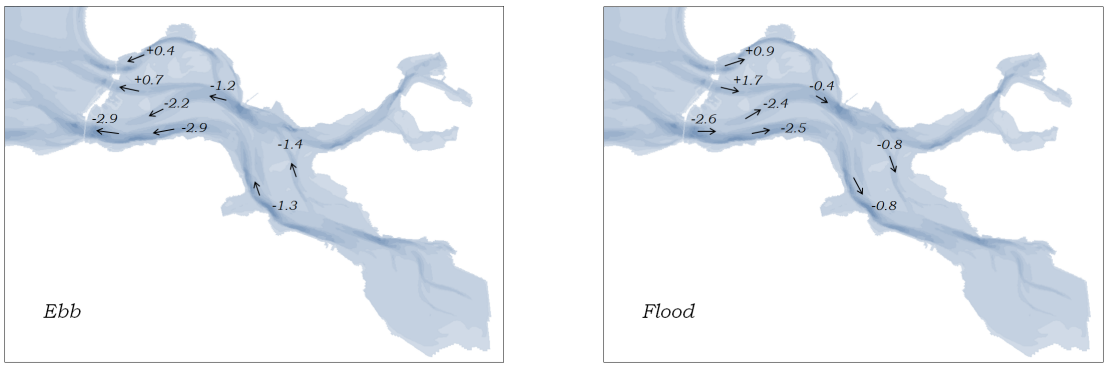

Figure 5.10: Overview of reduction average peak discharges expressed as %, Roompot Filled Partial Roll-out scenario

Schaar Filled
In Figure 5.11 the results of average peak discharges are summarized for the Schaar Filled scenario. The figure shows a reduction in discharge in the Schaar Channel directly behind the barrier. In the far-field there is also a reduction in discharges. The discharges increased in the Roompot Channel directly behind the barrier. In the Hammen Channel, the ebb velocities decreased, but the flood discharges increased.

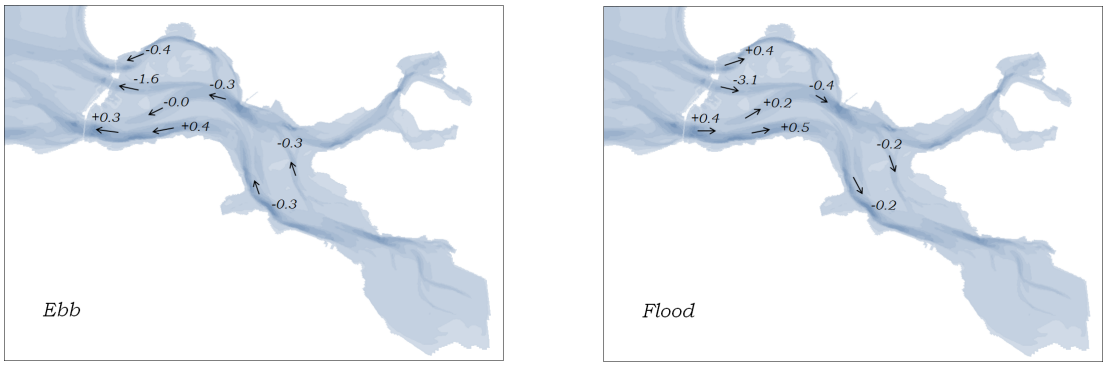

Figure 5.11: Overview of basin showing reduction average peak discharges expressed as %, Schaar Filled Partial Roll-out scenario

Hammen Filled
In Figure 5.12 the results of the average peak discharges are summarized for the Hammen Filled scenario. The figure shows a reduction in discharge directly behind the barrier in the Hammen Channel as well ass in the far-field. An increased discharge is seen in the Roompot channels. In the Schaar Channel, the ebb velocities decreased, while the flood velocities increased.

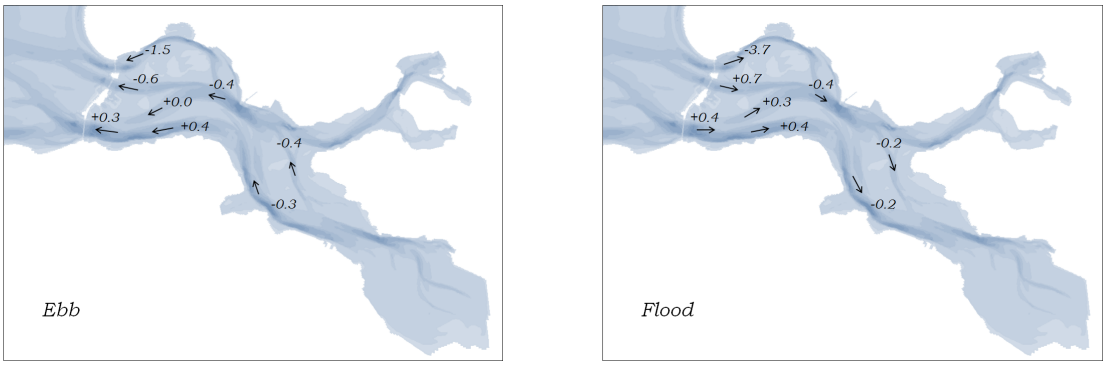

Figure 5.12: Overview of basin showing reduction average peak discharges expressed as %, Hammen Filled Partial Roll-out scenario

5.4. Analysis of Hydrodynamic Changes

This section analyzes the results described in the preceding sections. The results are analyzed in terms of the water levels, tidal volume and discharges.

5.4.1. Water Levels

The impact on the mean tidal range of all scenarios is summarized in Figure 5.13 for the reference case. This Figure includes all the scenarios; Near-future (2 gates), Partial Hammen and Schaar Filled (4 gates), Partial Roompot Filled (9 gates) and the Maximum Roll-out (17 gates).

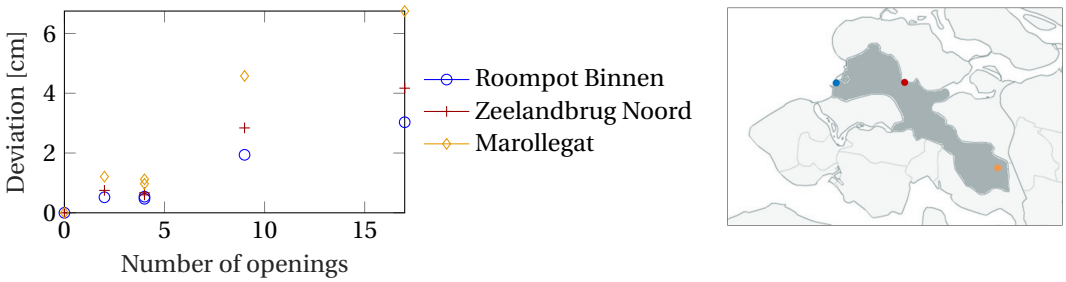

Figure 5.13: Deviation in tidal range as a function of gate openings equipped with turbines for three locations indicated on the map, reference case deviations for all scenarios. Near-future roll-out is 2 gate openings, Hammen and Schaar Partial Filled are 4 gate openings, Roompot Partial Filled is 9 gate openings, Maximum roll-out is 17 gate openings

The deviation in tidal range increases in landward direction. There is near-linear relationship between the deviation in tidal range and the number of gate openings with turbines. The figure shows that the Near-future scenario has a larger impact on the tidal range than the Hammen and Schaar Filled scenarios. Moreover, the Roompot Filled scenario has a relatively larger impact on the tidal range and the impact wa relatively smaller for the Maximum Roll-out scenario. Most likely, this was due to the multiplication factor that was used, which accounted for more resistance in larger openings than in smaller openings. The Roompot barrier section has larger gate openings. Consequently, this indicates that more energy is extracted and produced when placing the turbines in the Roompot section.

Results from the Delft3D model are compared in Table 5.4 to results from the IMPLIC model (De Kleermaeker, 2013), since both models ran simulations for two gate openings with turbines (Near-future scenario). The table shows deviations in mean tidal range from simulation results, the mean deviation in tidal range was taken as an average between the deviations in tidal range at Roompot Binnen and Marollegat from both model results. Resulting deviations in water levels from the IMPLIC model for both drag coefficients are in between the lower case (-) and reference case results of the resistance sensitivity range of the Delft3D model.

Table 5.4: Deviation in mean tidal range for Near-future scenario for Delft3D and IMPLIC

		deviation MTR [cm]
Delft3D	- lower case	0.6
	reference case	0.9
	+ upper case	1.1
	++ upper case	1.4
IMPLIC	c_d0.7	0.7
	c_d0.9	0.8

This comparison shows that the results are in the same order of magnitude. It also indicates that the upper values of the sensitivity range might be over-estimating the resistance due to tidal energy extraction.

5.4.2. Tidal Volume

The impact on the mean tidal volume of all scenarios is summarized in Figure 5.14.

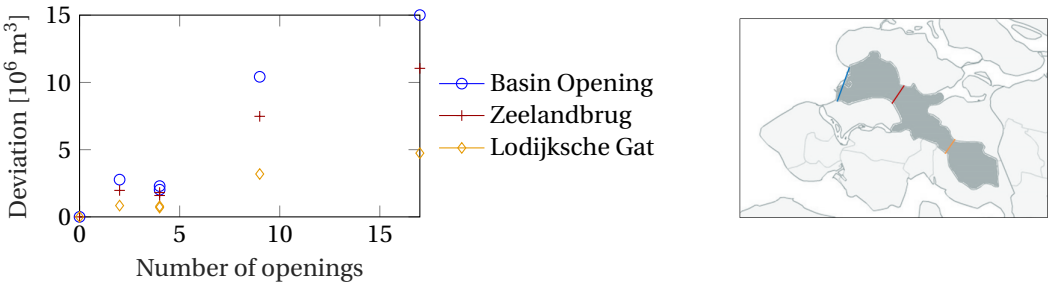

Figure 5.14: Deviation in tidal volume as a function of gate openings equipped with turbines for three cross-sections indicated on the map, reference case deviations for all scenarios. Near-future roll-out is 2 gate openings, Hammen and Schaar Partial Filled are 4 gate openings, Roompot Partial Filled is 9 gate openings, Maximum roll-out is 17 gate openings

The reduction in tidal volume reduces in landward direction, but in relative sense the same per scenario. The same (near-linear) pattern is seen as with the tidal range; the Near-future scenario (2 gate openings) and the Roompot filled scenario (9 gate openings) have a higher impact on the tidal volume than the Schaar and Hammen filled (4 gate openings) scenarios, since there is relatively more resistance due to the larger gate openings.

5.4.3. Discharges

The analysis of discharges is split in two; firstly the deviations in the far-field (defined in Section 3.3) are discussed and secondly the changes in the mid-field are analyzed.

Far-field

In all cases the discharges reduced in the two far-field channels; the Engelsche Vaarwater and the Brabantsche Vaarwater. In Figure 5.15 the reductions in peak ebb discharge in the far-field for all scenarios are shown. The reductions were relatively and absolutely seen, larger in the ebb-phase than in the flood-phase. This could be due to a larger part of the water traveling over the flat rather than through the channel in which the cross-section was placed. The Maximum Roll-out scenario had the largest effect, followed by the Roompot Filled scenario. The Near-future and Hammen and Schaar Filled scenarios had a similar effect, in line with the conclusions drawn from the tidal range and tidal volume results. This confirms the hypothesis that asymmetric positioning of turbines does not affect the discharges in the far field, but only the amount of energy extraction.

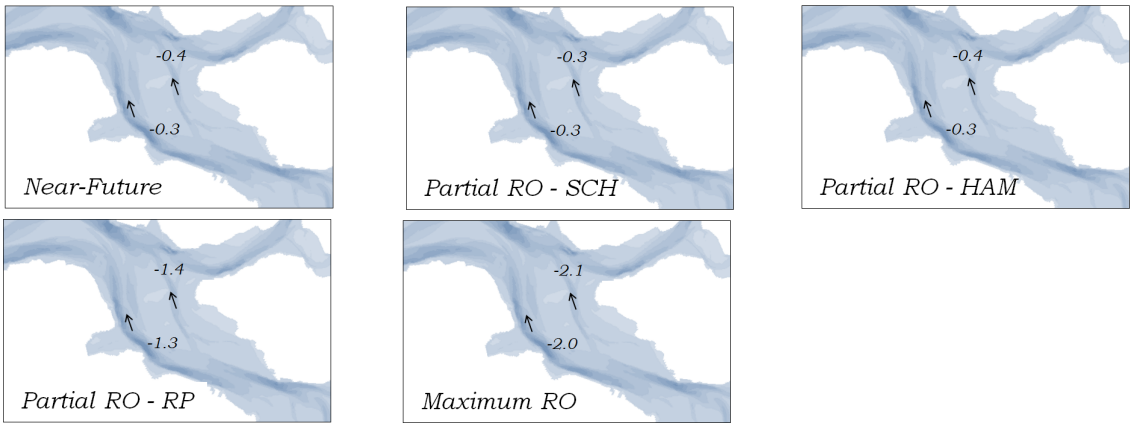

Figure 5.15: Overview of far-field channels (Brabantsche Vaarwater and Engelsche Vaarwater) showing reduction average peak ebb discharges in far-field, expressed as % , for all upscaling scenarios; Near-future (2 gate openings with turbines), Partial Roll-out Schaar Filled (4 gate openings), Partial Roll-out Hammen Filled (4 gate openings), Partial Roll-out Roompot Filled (9 gate openings), Maximum Roll-out (17 gate openings)

Mid-field

In the symmetrical scenario, namely the Maximum Roll-out scenario, reductions were found everywhere in the mid-field. For all three (asymmetric) Partial Roll-out scenarios, the reduction in discharge in the channel behind that barrier section was more severe than for the Maximum Roll-out scenario for both ebb and flood. The larger reduction could indicate that more energy is extracted from the system if no turbines are present in the other sections.

For the two scenarios in which the Roompot section had increased resistance (Near-future and Partial Roompot Filled) reductions were found in the Roompot channel and increased discharges in the Schaar and Hammen channels during both ebb and flood, see Figure 5.16. These increases in discharge might be beneficial for sedimentation on the Roggenplaat since the sediment capacity of the flow is dependent on the velocity magnitude.

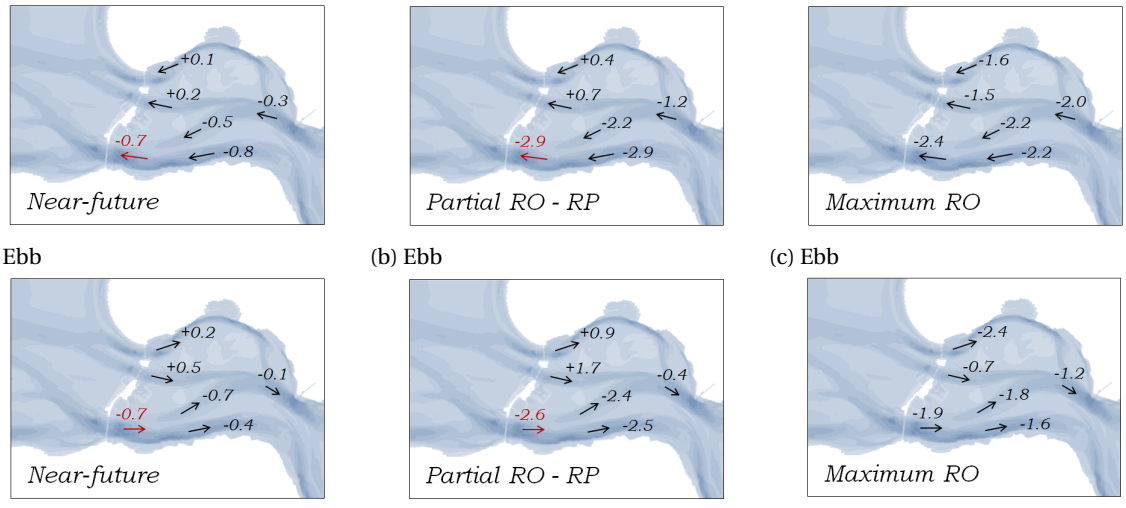

(a) Ebb (b) Ebb (c) Ebb

(d) Flood (e) Flood (f) Flood

Figure 5.16: Overviews of mid-field of basin showing reduction average peak discharges in mid-field, expressed as %, Near-future, Partial Roompot Filled and Maximum Roll-out scenarios. Red arrow indicates barrier section with turbines (except with Maximum Roll-out since all barrier sections are equipped with turbines)

In the Partial Schaar and Hammen Filled scenarios the discharges decreased in the channels behind the barrier section were turbines were situated. In both scenarios, the discharge increased during ebb and flood in the Roompot channels. This might be beneficial for sedimentation of Neeltje Jans on the southern side. However in both cases, the north side experiences decreases in discharge. Both scenarios showed reductions

in discharge for both the north and south side of the Roggenplaat. Moreover, in both cases during flood, one of the channels has increased discharge while the other has decreased discharge. This may influence the water level gradient over the flat and therefore the sediment transport gradient. This requires further investigation.

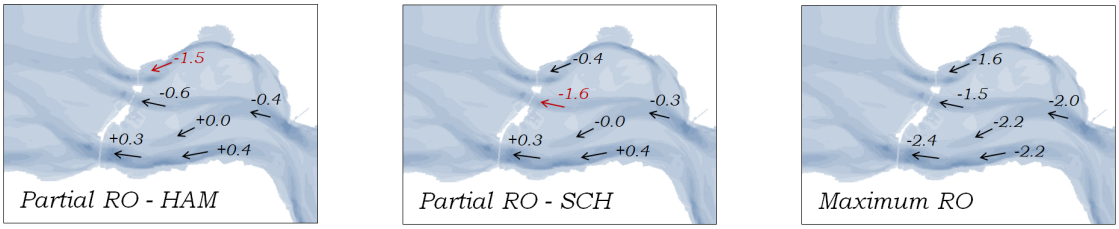

(a) Ebb (b) Ebb (c) Ebb

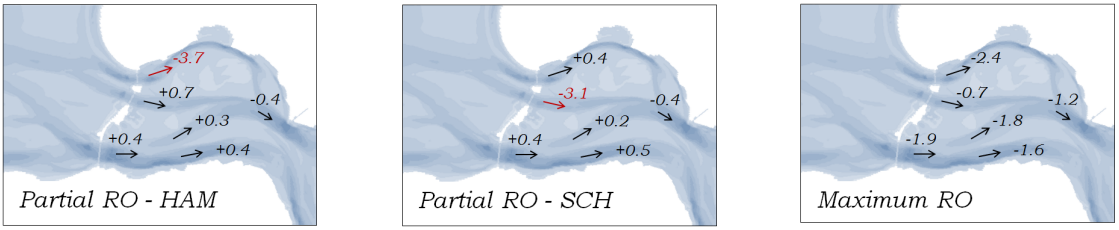

(d) Flood (e) Flood (f) Flood

Figure 5.17: Overview of mid-field basin showing changes in average peak discharges in mid-field, expressed as %, Partial Hammen and Schaar Filled and Maximum Roll-out scenarios. Red arrow indicates barrier section with turbines (except with Maximum Roll-out since all barrier sections are equipped with turbines)

5.5. Key Points

Numerical simulations lasting one spring-neap cycle were performed for the scenarios (Near-future, Maximum Roll-out and Partial Roll-out). The results for tidal range and volume are as follows:

- Near-future: reduction in average mean tidal range for the whole basin for the resistance sensitivity range, was between 0.6 and 1.4 cm, or on average 0.2 to 0.5% of the tidal range for barrier without turbines, with the same result tidal volume (0.2 to 0.5 %) deviation throughout the basin.
- Maximum Roll-out: reduction in average mean tidal range for the whole basin was between 3 and 8 cm, or on average 1 to 2.6% of the tidal range for barrier without turbines, with a similar result for tidal volume (1.1 to 2.8%) deviation throughout the basin.
- Partial Roll-out: reduction in average tidal range around for the 3 sub-scenarios are in between results for Near-future and Maximum Roll-out scenarios; tidal volumes for Roompot, Schaar and Hammen section installations are reduced by 1.1, 0.2 and 0.3% respectively compared to the situation without turbines.

The reduction in tidal range and volume appeared to be near-linearly increasing with the number of turbines installed. Moreover, the deviation in tidal range increases in landward direction for all scenarios. Figure 5.18 summarizes the deviations in tidal range at the basin opening (Roompot Binnen) and in the far end of the basin at Marollegat for the Near-future and Maximum Roll-out scenarios. The deviations for the Partial Roll-out scenario are in between.

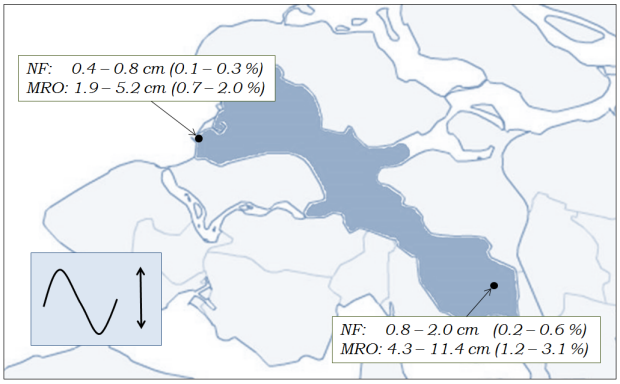

Figure 5.18: Overview of basin showing deviation in tidal range near mouth of basin (Roompot Binnen) and far end of basin (Marollegat) for Near-future (NF) and Maximum Roll-out (MRO) scenarios

In the mid-field (from barrier to mid-basin), peak discharges decreased in the channels directly behind the barrier section with turbines, and increased in the channels behind sections with no turbines. In the far-field (from mid to end-basin), results were not affected by the positioning of turbines, only the number of turbines/amount of energy extraction.

6

Analysis of Tidal Flat Morphology

This chapter provides an analysis of the impact on the tidal flat morphology due to the change in hydrodynamics caused by tidal energy extraction. First, the change in emergence times of the flats are investigated. Hereafter, a reflection on the impact on erosion rates is reported.

6.1. Emergence Time

The results from Chapter 5 showed that the mean low water level would increase for the various scenarios. This section investigates the effect of the rise in of low water level on the emergence time of tidal flats. Three tidal flats are investigated; Roggenplaat, Neeltje Jans and Galgenplaat, see Figure 6.1. The three tidal flats have an area of around 1500 hectare, 250 hectare and 950 hectare respectively.

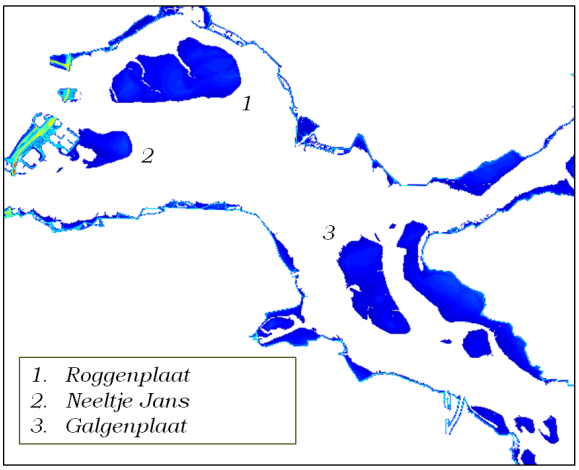

Figure 6.1: Overview of basin and the three largest tidal flats; Roggenplaat, Neeltje Jans and Galgenplaat

Hypsometric curves were constructed using data from the Light Detection and Ranging (LiDAR) measurement campaign from 2013. This data had a resolution of 2 meters, which was much smaller than the grid size from the Delft3D model. Hypsometric curves of the three flats are shown in Figure 6.2. The curves show the surface area (A(z)) as a function of water level (z). The distribution is shown within the tidal range for each flat. They were constructed in the following manner (De Vet et al., 2017b):

- Selection made of grid cells for each tidal flat of area between MLW and MHW (inter-tidal area)
- Hypsometric function A(z) = A(Z>z) - A(Z > MHW) acquired by multiplying the surface area per grid cell with the number of grid cells of which the bed level is larger than z but smaller than MHW.

Per tidal flat, a local estimate of the tidal range is used since it varies throughout the basin.

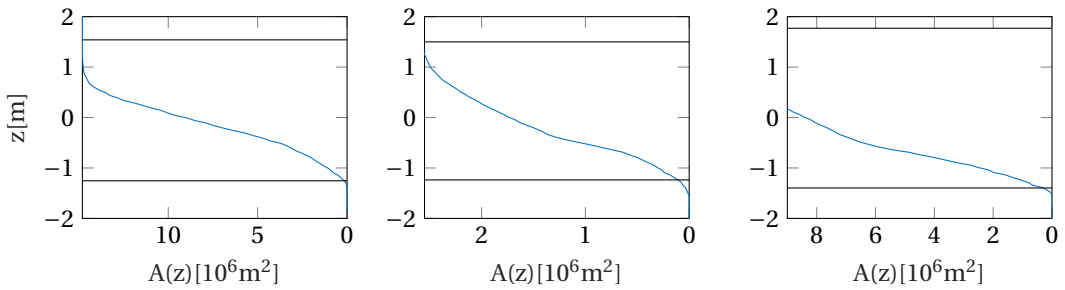

(a) Roggenplaat (b) Neeltje Jans (c) Galgenplaat

Figure 6.2: Hypsometric curves of tidal flats (a) Roggenplaat, (b) Neeltje Jans and (c) Galgenplaat between local MLW and MHW, constructed using LiDAR data from 2013. Water level z with respect to N.A.P.

For each scenario, the change in low water level on the increased emerged acreage was determined as shown in Figure 6.3. The difference between the base case MLW and the MLW from the scenario results shows the loss in emerged acreage.

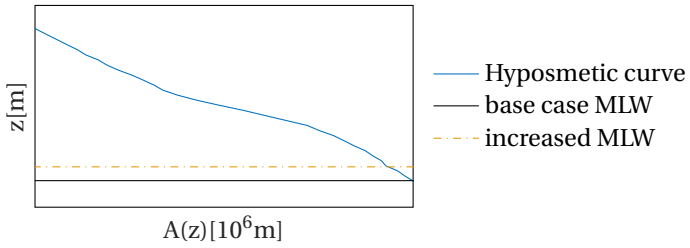

Figure 6.3: Example of determination loss in acreage due to increase in water level of the base case without turbines, and an arbitrary case of increased water level due to tidal energy extraction

6.1.1. Near-future Scenario

In Table 6.1 the change in water level and corresponding decrease in emerged area is shown for the Near-future scenario.

Table 6.1: Increase in MLW and corresponding loss in emerged area for Near-future scenario

	MLW rise [cm]	Area loss [ha]	Area loss [%]
Roggenplaat	0.3	1.0	0.1
Neeltje Jans	0.3	0.2	0.1
Galgenplaat	0.4	1.3	0.1
All		2.5	0.1

6.1.2. Maximum Roll-out Scenario

In Table 6.2 the change in water level and corresponding decrease in emerged area is shown for the Maximum Roll-out scenario.

Table 6.2: Increase in MLW and corresponding loss in emerged area for Maximum Roll-out scenario

	MLW rise [cm]	Area loss [ha]	Area loss [%]
Roggenplaat	1.6	5.2	0.4
Neeltje Jans	1.6	1.3	0.5
Galgenplaat	2.3	13.1	1.4
All		19.5	0.7

6.1.3. Partial Roll-out Scenarios

In Tables 6.3, 6.4 and 6.5 the change in water levels and corresponding decrease in emerged area is shown for the Partial Roll-out scenarios.

Table 6.3: Increase in MLW and corresponding loss in emerged area for Partial Roompot Roll-out scenario

	MLW rise [cm]	Area loss [ha]	Area loss [%]
Roggenplaat	1.1	3.6	0.3
Neeltje Jans	1.1	0.9	0.4
Galgenplaat	1.6	8.6	0.9
All		13.1	0.5

Table 6.4: Increase in MLW and corresponding loss in emerged area for Partial Schaar Roll-out scenario

	MLW rise [cm]	Area loss [ha]	Area loss [%]
Roggenplaat	0.2	0.7	0.1
Neeltje Jans	0.2	0.2	0.1
Galgenplaat	0.3	0.9	0.1
All		1.8	0.1

Table 6.5: Increase in MLW and corresponding loss in emerged area for Partial Hammen Roll-out scenario

	MLW rise [cm]	Area loss [ha]	Area loss [%]
Roggenplaat	0.3	0.8	0.1
Neeltje Jans	0.3	0.2	0.1
Galgenplaat	0.4	1.1	0.2
All		2.1	0.1

6.1.4. Analysis

Figure 6.4 summarizes the results from this section. The figure shows the loss in emerged area as a function of gate openings equipped with turbines per tidal flat. For a comparison, approximately 15 ha of the three tidal flats combined is lost annually due to erosion and sea-level rise.

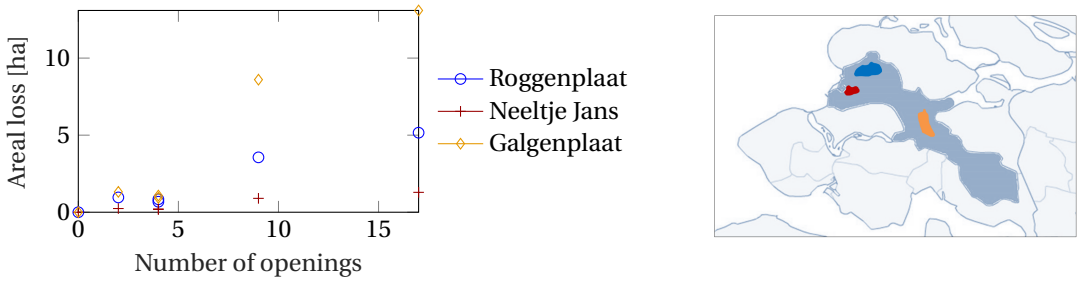

Figure 6.4: Deviation in emerged area of tidal flats as a function of gates openings equipped with turbines for the reference case and overview of basin with locations of tidal flats. All scenarios included; Near-future (2 gate openings with turbines), Partial Schaar and Hammen (4 gate openings each), Partial Roompot (9 gate openings) and Maximum Roll-out (17 gate openings)

The relationships are near-linear. This is in line with the results from the previous chapter, since more resistance is present in the openings of the Roompot section due to their respective sizes. The Galgenplaat, where the water level increases most, also has the largest loss in acreage. Neeltje Jans, where the water level increases the least, loses the least too.

The tidal energy extraction scenarios can be compared to sea-level rise. De Ronde et al. (2013) defines three sea-level rise scenarios based on KNMI (Royal Dutch Meteorological Institute) data:

- Scenario Low: 2.5 mm/year from 1990 - 2050 and 4 mm/year from 2050 - 2100.
- Scenario Middle: 4.17 mm/year from 1990 - 2050 and 7 mm/year from 2050 - 2100.
- Scenario High: 5.83 mm/year from 1990 - 2050 and 10 mm/year from 2050 - 2100.

The sea-level rise rate of of 4.17 mm per year is used for the comparison in this work (Scenario Middle 1990-2050). It should be noted that this is a specific prediction which could change over the course of time.

The decrease in low water is taken as an average between the deviations of Roompot Binnen and Marollegat. The results are shown in Table 6.6.

Table 6.6: Rise in MLW and Sea-level rise equivalence for all tidal energy extraction scenarios

	MLW rise [cm]	SLR [years]
Near-Future	0.5	1.1
Maximum roll-out	2.4	5.8
Partial roll-out Roompot filled	1.7	4.0
Partial roll-out Schaar filled	0.3	0.8
Partial roll-out Hammen filled	0.4	0.9

The sea-level rise equivalence is between 1 and 6 years. This could be interpreted as a reduction of the life-time of the tidal flats by as many years, considering they will diminish in time anyways.

6.2. Erosion

The results have shown that the tidal range and discharges (assumed to be proportional to velocities) change as a result of tidal energy extraction. This is expected to influence the rate of erosion of tidal flats. This is however not investigated in this work. A conceptual statement is provided.

The decrease in tidal range will change the inundation frequency in different height zones of the tidal flat; and therefore a resulting increased impact of wind and waves is expected. Additionally, the changes in discharge may lead to even larger reductions in sedimentation on tidal flats. Furthermore, water level gradients may change over the flats in the mid-field due to the relative differences in discharges in the surrounding channels because of (asymmetric) tidal energy extraction. This should be quantified and confirmed by further work regarding erosion rates.

6.3. Key Points

The increase in low water level due to tidal energy extraction scenarios leads to a decreased emergence of the tidal flats. The reduction in acreage was estimated for the three largest tidal flats (Galgenplaat, Neeltje Jans and Galgenplaat) based on hypsometric curves of these tidal flats. Moreover, the increase in MLW for each scenario was compared to equivalence in sea-level rise years. The results for acreage lost and sea-level rise equivalence are as follows:

- Near-future: Loss in acreage for the three tidal flats combined is 2.5 ha, 0.1% of the current acreage. The increase in MLW is equivalent to 1.1 sea-level rise year.
- Maximum Roll-out: Loss in acreage for the three tidal flats combined is 19.5 ha, 0.7% of the current acreage. The increase in MLW is equivalent to 5.8 sea-level rise years.
- Partial Roll-out: Loss in acreage and sea-level rise years in between Near-future and Maximum Rol-out.

The rate of erosion is speculated to increase somewhat due to the changes in tidal range and discharges throughout the basin induced by tidal energy extraction. Further work is required to make a prediction on the magnitude of these rates of erosion.

7 Discussion

In this chapter the results are interpreted and the limitations are discussed.

7.1. Interpretation of Results

In this section the results are discussed in terms of validity, expectations and new insights and the results are interpreted from a socio-environmental perspective.

7.1.1. Validity of Results

In this work an existing two-dimensional Delft3D model was adapted to include tidal energy extraction in order to predict hydrodynamic changes due to various scenarios of upscaling of tidal energy extraction within the Eastern Scheldt (ES) barrier. Water level predictions from model simulations (without turbines) matched actual measurements in the basin well and therefore the model was considered a good tool for analysis of basin hydrodynamics for the purpose of this work.

A comparison between water level measurements in the basin and predictions from model simulations for the upscaling scenarios was not possible, since those turbines were not installed. However, the additional resistance due to turbines in gate openings was calibrated using a state-of-the-art three-dimensional model of the gate opening with turbines installed currently (Roompot 8). Additionally, water level predictions from this work match with predictions from previous work with a one-dimensional model.

Therefore, the model and parameterization that were used provide a sufficient first indication on changes in basin hydrodynamics due to upscaling of tidal energy extraction, which should be interpreted as such.

7.1.2. Expectation

The hydrodynamic results showed deviations in tidal range, volume and discharges throughout the basin due to tidal energy extraction at the barrier. This was expected since similar changes in hydrodynamics occurred due to the construction of the barrier. The tidal range and volume decreased throughout the basin with increasing tidal energy extraction. Between the barrier and mid-basin, peak discharges decreased in channels directly behind the barrier section with turbines and increased in channels behind sections with no turbines. The former was expected, the latter not, but the explanation is simply that when one section is causing a resistance to the flow, it will seek an 'easier' path in the other sections. From mid- to end-basin, discharges are not affected by positioning of turbines, only the amount of energy extraction, which was also expected.

7.1.3. New Insights

A number of insights are derived from this work in terms of the modeling approach, the model results, and the analysis of the results. Previous research (De Kleermaeker, 2013) shows the influence of two gate openings with turbines on water levels in the ES basin using a one-dimensional model and a theoretically derived turbine parameterization. In this work, a two-dimensional model has been developed which includes all relevant processes for basin hydrodynamics and tidal flat morphodynamics. It has been used to evaluate not only the tidal range (as was done with the one-dimensional model) but also allowed for an evaluation of the distribution of tidal volume and discharges throughout the basin. The model allows for evaluation of the contribution of tidal energy extraction to the ongoing erosion of the tidal flats due to the possibility of

wind and wave modules as well as sediment transport, although they have not been used in this work. The parameterization approach allowed for a successful implementation of tidal turbines in a storm surge barrier by coupling the two-dimensional model to a state-of-the-art three-dimensional model of one gate opening with turbines.

This work has shown the impact of tidal energy extraction on basin hydrodynamics of not only the near-future installation, but has also shown the effect of various upscaling scenarios. Moreover, the analysis of the increase in low water level due to tidal energy extraction allowed for an insightful comparison with sea-level rise years and an estimation of the loss in acreage using hypsometric curves of the tidal flats.

7.1.4. Socio-environmental Perspective

The socio-environmental dilemma with respect to turbine installation is whether the benefits of renewable energy outweigh the negative impact on the ecological value of the basin. The tidal flats are important areas for birds and animal life. However, the sediment deficit and consequent erosion of tidal flats induced by the construction of the barrier is already causing a serious autonomous negative trend. The tidal flats are expected to diminish completely if no interventions are taken within the next 100 to 200 years, according to predictions of De Ronde et al. (2013).

Tidal energy extraction is expected to enhance this trend, although the changes in hydrodynamics are smaller than those induced by the construction of the barrier. In Table 7.1, average deviations in tidal volume and range are shown either resulting from the installed barrier (as measured) or resulting from tidal energy extraction (as predicted). Note that changes are shown either relative to the situation without barrier (for the impact of the installed barrier) or relative to situation with installed barrier (for the impact of tidal energy extraction). Relative changes resulting from tidal energy extraction would of course be even smaller when compared to the situation without barrier. These deviations are an average of the whole basin; deviations in tidal range near the barrier are smaller and deviations in tidal range in more landward direction are larger.

Table 7.1: Comparison of average reduction in tidal volume and range due to barrier construction and tidal energy extraction in %

	Barrier Construction	Near-future	Maximum Roll-out	Partial Roll-out
Reference	No barrier	Barrier	Barrier	Barrier
Tidal Volume	-30	-0.2 to -0.5	-1.1 to -2.8	-0.2 to -1.1
Tidal Range	-12	-0.2 to -0.5	-1.0 to -2.6	-0.3 to -1.0

The ES basin is already completely out of equilibrium and the small changes in hydrodynamics from tidal energy extraction could enhance this disequilibrium slightly. Whether this increase in rate of deterioration of the tidal flats is significant, should be considered in terms of social acceptance and overall environmental impact. Is renewable energy or the ecological value of the tidal flats more important in terms of the environment? What should be considered is how much energy is ultimately produced and what the impact of the reduction in acreage of tidal flats is on animal and bird life, which is not quantified in this work.

To preserve the tidal flats, several mitigation measures have already been considered such as nourishments and erosion-reduction measures (Van Zanten and Adriaanse, 2008). If nourishments of the tidal flats are planned periodically, it could counter-act the effects of tidal energy extraction. This would need further investigation, however.

7.2. Limitations of the Work

A number of limitations to this work are presented.

7.2.1. Morphological Modeling

The model simulations of this work do not account for crucial processes of tidal flat morphodynamics. The model simulations did not include wind and waves, or sediment transport - although this is possible with the model - and therefore conclusions cannot be drawn about the impact on erosion rates of tidal flats. The exclusion of these processes does not affect the outcome of the hydrodynamic results. For further analysis on tidal flat morphodynamics, however, these are essential to include. This is expected to be done by the larger research project which will continue after completion of this thesis.

7.2.2. Turbine Parameterization

The turbine implementation in this work simplifies the actual momentum extraction due to tidal turbines. The turbine parameterization was implemented through a momentum sink approach; porous plates accounted for the additional resistance in a gate opening due to tidal turbines. Porous plates have a constant coefficient over time which accounts for momentum extraction. In reality, the momentum extraction by turbines on local flow is velocity dependent and in the ES case, variable for ebb and flood. Moreover, the turbines in the ES are extracted from the water when the head difference over the barrier reaches a certain limit. By implementing the constant coefficient in the model, loss is overestimated for high and low flow velocities, since the turbines are less efficient and operational windows are not accounted for.

In the work of Mungar (2014) an option including a velocity dependent loss coefficient has been explored, and (Sandia Laboratories) is working on an implementation of tidal turbines in Delft3D. However, this was not used in this research, as it was assumed that using one coefficient that takes an average of the loss, provides accurate enough results for a first estimation of tidal energy extraction on large-scale hydrodynamics. For more accurate results, this should be taken into account.

7.2.3. STAR-CCM+ Model

The data used for calibrating the increase in resistance came from a three-dimensional STAR-CCM+ model which was still work-in-progress and only representative for one specific gate opening. This three-dimensional model was not fully validated at the time of this thesis. Moreover, only limited simulations results were available. To account for this a sensitivity range was included, which was quite large. The Delft3D model should be re-calibrated when the STAR-CCM+ model is completed.

Additionally, the STAR-CCM+ model only represented turbines installed in Roompot 8. A crucial assumption that was made in the implementation of turbines in other gate openings in the model was that each gate opening had an increased resistance proportional to its cross-sectional area. This should be interpreted as larger turbines in larger openings and smaller turbines in smaller openings. This assumption can only be tested once it is known what kind of turbines will be installed in other gate openings, and possible three-dimensional computations are performed for those openings.

In conclusion, there are a number of shortcomings to the model and turbine parameterization, which need attention if more accurate results are desired. However, as a first estimation of tidal energy extraction on large-scale hydrodynamics the method used provides meaningful results.

8

Conclusions and Recommendations

The research presented in this thesis provided insight into the impact of tidal energy extraction on the hydrodynamics and morphology in the Eastern Scheldt (ES) tidal basin. Hydrodynamic predictions could be made of not only the current installation, but also various upscaling scenarios, using a two-dimensional model covering relevant basin hydrodynamics. Tidal turbines were parametrized in this model by using data from a state-of-the-art three-dimensional model of one gate opening with turbines. The hydrodynamic results allowed for an evaluation of the impact on tidal flat morphology. Resulting conclusions and recommendations are summarized below.

8.1. Conclusions

Q1: *How can relevant hydro- and morphodynamic processes of a tidal basin in combination with tidal energy extraction in a storm surge barrier at its inlet be modeled?*

Relevant hydro- and morphodynamic processes (tidal flow, wind, waves and sediment transport) of the basin with barrier, channels and tidal flats are covered by an available two-dimensional Delft3D model (Pezij, 2015). Tidal energy extraction in the barrier is accounted for by modification of this model by using a local momentum sink (porous plates) that increases flow resistance for barrier openings with turbines. The additional resistance due to turbines is calibrated using output data from a three-dimensional STAR-CCM+ model of one opening with turbines.

Q2: *How are basin hydrodynamics affected by upscaling of tidal energy extraction?*

Numerical simulations over one spring-neap cycle were performed for various upscaling scenarios. The results show small deviations in tidal range, volume and discharges throughout the basin due to tidal energy extraction, compared to changes that have occurred as a result of the installation of the barrier. Reductions in tidal range and volume appear to be near-linearly increasing with the number of turbines installed. Deviations in tidal range increase in landward direction. Between the barrier and mid-basin, peak discharges decrease in channels directly behind the barrier section with turbines and increase in channels behind sections with no turbines. From mid- to end-basin, discharges are not affected by positioning of turbines, only the amount of energy extraction.

Q3: *How does upscaling of tidal energy extraction contribute to the ongoing morphological changes of tidal flats?*

Simulation results indicate that the emergence time of tidal flats decreases due to tidal energy extraction as a result of an increase in mean low water level throughout the basin. The increase in low water level due to tidal energy extraction would only be a fraction of the increase in water level due to sea-level rise in coming years. Additionally, the reduction in acreage of these flats due to the rise in mean low water level resulting from tidal energy extraction is relatively small compared to the ongoing loss in acreage due to both sea-level rise and erosion induced by the sediment deficit resulting from the barrier construction.

In summary, meaningful hydrodynamic predictions could be developed by modifying an available two-dimensional Delft3D model of the ES to include tidal energy extraction, and this permitted a first evaluation of the impact on tidal flat morphology from upscaling tidal energy extraction. Further work is however required to optimize basin and turbine modeling and evaluate long-term morphodynamics (sediment transport).

8.2. Recommendations

To evaluate the relative impact of tidal energy extraction on the ongoing morphological changes of tidal flats more accurately, it is necessary to include wind, waves and sediment transport processes explicitly in the Delft3D model.

For more precise results, turbine parameterization in the model can be improved. At the completion of this thesis work, the three-dimensional STAR-CCM+ model used as input for the turbine parameterization was still work-in-progress. When this model has been completed and validated, turbine modeling and parameterization should be re-examined. In case large scale deployment is planned, then further STAR-CCM+ modeling is required accounting for individual opening sill height and turbine characteristics. Moreover, for more accurate representation of momentum extraction by turbines, it would be beneficial to implement velocity dependent resistance in the Delft3D model which is variable for ebb and flood, such as in the work done by Mungar (2014) and Sandia Laboratories. This term should also account for operational windows of the turbines.

A comprehensive socio-environmental evaluation is ultimately required, but needs more specific and details regarding the (negative) impact of tidal energy extraction on the autonomous negative trend of the tidal flats. This evaluation should compare benefits from (renewable) tidal energy extraction to the (incremental) ecological impact resulting from further reduction in acreage of tidal flats that support animal and bird life.

Bibliography

S. Baston, S. Waldman, and J. Side. Modelling energy extraction in tidal flows. *TeraWatt position paper*, pages 1–39, 2015. doi: 10.13140/RG.2.1.4620.2481.

A. Betz. *Introduction to the theory of flow machines*. Pergamon Press, Oxford, 1966.

F. Biesboer. De Oosterschelde bracht het keerpunt, 2011. URL https://www.deingenieur.nl/artikel/de-oosterschelde-bracht-het-keerpunt.

J. Bosboom and J.F. Stive. *Coastal Dynamics 1 - Lecture notes CIE4305*. Delft University of Technology. VSSD, 2015.

I. Das. *Morphodynamic modelling of the Galgeplaat*. Msc thesis, Delft University of Technology, 2010.

R.A. De Bruijn. *The future of the Oosterschelde with a new inlet channel*. Msc thesis, Delft University of Technology, 2012.

S. De Kleermaeker. Herberekeningen getij-reductie in de Oosterschelde door vertikale getij-turbines in de Oosterscheldekering. Technical report, Deltares rapport 1208867-000-ZKS-0003, 2013.

P. De Pater. *Effect of removal of the Oosterschelde storm surge barrier*. Msc thesis, Delft University of Technology, 2012.

J.G. De Ronde, J.P.M. Mulder, L.A. Van Duren, and T.J.W. Ysebaert. Eindadvies ANT Oosterschelde. Technical report, Deltares rapport 1207722-000-ZKS-0010, 2013.

P.L.M. De Vet, B.C. Van Prooijen, R. Schrijvershof, J.J. Van Der Werf, T. Ysebaert, and Z.B. Wang. Processes driving the flow and morphology of a complex shaped intertidal flat : the Roggenplaat. pages 1–19, 2017a.

P.L.M. De Vet, B.C. Van Prooijen, and Z.B. Wang. The differences in morphological development between the intertidal flats of the Eastern and Western Scheldt. *Geomorphology*, 281:31–42, 2017b. ISSN 0169555X. doi: 10.1016/j.geomorph.2016.12.031. URL http://dx.doi.org/10.1016/j.geomorph.2016.12.031.

Delft Hydraulics and Rijkswaterstaat. The Storm Surge Barrier Eastern Scheldt - Evaluation of water movement studies for design and construction of the barrier. Technical report, WL-code:Z88; RWS code: PEGESS-N-89011, 1989.

Deltares Systems. Delft3D-FLOW, User Manual. pages 1–684, 2014. URL www.deltaressystems.nl.

DMEC. Within one day €850.000 for tidal energy power station Oosterschelde. URL http://www.dutchmarineenergy.com.

J. Dronkers. Tidal asymmetry and estuarine morphology. *Netherlands Journal of Sea Research*, 20:117–131, 1986.

E-Overheid. Zandhonger Oosterschelde. URL https://zoek.officielebekendmakingen.nl/stcrt-2011-18645.html.

M. Eelkema. *Eastern Scheldt inlet morphodynamics*. Phd thesis, Delft University of Technology, 2013.

C.T. Friedrichs. *Tidal Flat Morphodynamics: A Synthesis*, volume 3. Elsevier Inc., 2012. ISBN 9780080878850. doi: 10.1016/B978-0-12-374711-2.00307-7. URL http://dx.doi.org/10.1016/B978-0-12-374711-2.00307-7.

V. M. Gatto, B.C. Van Prooijen, and Z.B. Wang. Net sediment transport in tidal basins : quantifying the tidal barotropic mechanisms in a unified framework. *Ocean Dynamics(2017)*, 67:1385–1406, 2017. doi: 10.1007/s10236-017-1099-3.

M.O. Green and G. Coco. Reviews of wave-driven sediment resuspension and transport in estuaries. *Review of Geophysics*, (55):77–117, 2013. doi: 10.1002/2013RG000437.

L. Hoogduin. *Sediment transport through the Eastern Scheldt storm surge barrier*. Msc thesis, Delft University of Technology, 2009.

L.H.M. Kohsiek, J.P.M. Mulder, and T. Louters. De Oosterschelde naar een nieuw onderwaterlandschap. Technical report, RWS Dienst Getijdewateren, 1987.

T. Louters, J.H. Van Den Berg, and J.P.M. Mulder. Geomorphological changes of the Oosterschelde tidal system during and after the implementation of the delta project. *Journal of Coastal Research*, 14(3):1134–1151, 1998. ISSN 07490208.

J.P.M. Mulder and T. Louters. Changes in basin geomorphology after implementation of the Oosterschelde Estuary project. *Hydrobiologia*, 282-283:29–39, 1994. ISSN 0018-8158. doi: 10.1007/BF00024619.

S. Mungar. *Hydrodynamics of horizontal-axis tidal current turbines - A modelling approach based on Delft3D*. Msc thesis, Delft University of Technology, 2014.

M. Pezij. *Understanding the morphological development of the Oesterdam nourishment*. Msc thesis, University of Twente, 2015.

Rijkswaterstaat. Waterinfo. URL `https://waterinfo.rws.nl/`.

Rijkswaterstaat Directie Sluizen en Stuwen. ZLDK-1987-05005 Stormvloedkering Oosterschelde Overzicht pijler en elementen maatvoering Bestek S.S.1216 Blad 3 OS-50-603, 1987.

RVO. 's Werelds grootste commerciële getijdeninstallatie. URL `http://www.rvo.nl/actueel/praktijkverhalen/'s-werelds-grootste-commerci{ë}le-getijdeninstallatie`.

Sandia Laboratories. SNL-Delft3D-CEC. URL `http://energy.sandia.gov/energy/renewable-energy/water-power/market-acceleration-deployment/snl-delft3d-cec/`.

Tocardo. Tidal Power Plant in Dutch Delta Works. URL `http://www.tocardo.com/Project/oosterschelde/`.

D. V. Val, L. Chernin, and D. V. Yurchenko. Reliability analysis of rotor blades of tidal stream turbines. *Reliability Engineering and System Safety*, 121:26–33, 2014. ISSN 0951-8320. doi: 10.1016/j.ress.2013.07.011. URL `http://dx.doi.org/10.1016/j.ress.2013.07.011`.

E. Van Zanten and L.A. Adriaanse. Verminderd getij - Verkenning naar mogelijke maatregelen om het verlies van platen, slikken en schorren in de Oosterschelde te beperken. Technical report, Rijkswaterstaat, 2008.

M.C. Verbeek, R.J. Labeur, W.S.J. Uijttewaal, and P. De Haas. The near-wake of horizontal axis turbines in a storm surge barrier. 2017.

J. Vroon. Hydrodynamic characteristics of the Oosterschelde in recent decades. *Hydrobiologia*, 282-283(1): 17–27, 1994. ISSN 00188158. doi: 10.1007/BF00024618.

D. Walstra. CT 4309 Coastal Dynamics II - Lecture slides Coastal Modelling 4, 2017.

Z.B. Wang, J. Vroom, B.C. Van Prooijen, R.J. Labeur, and M.J.F. Stive. Movement of tidal watersheds in the Wadden Sea and its consequences on the morphological development. *International Journal of Sediment Research*, 28(2):162–171, 2014. ISSN 1001-6279. doi: 10.1016/S1001-6279(13)60028-1. URL `http://dx.doi.org/10.1016/S1001-6279(13)60028-1`.

J.I. Whelan, J.M.R. Graham, and J. Peiro. A free-surface and blockage correction for tidal turbines. *Journal of Fluid Mechanics*, 624:281–291, 2009. doi: 10.1017/S0022112009005916.

F. Zijl, M. Verlaan, and H. Gerritsen. Improved water-level forecasting for the Northwest European Shelf and North Sea through direct modelling of tide , surge and non-linear interaction. *Ocean Dynamics*, 63(July): 823–847, 2013. doi: 10.1007/s10236-013-0624-2.

Appendices

A

Consequences of the Delta Works

This appendix provides an overview of the hydrodynamic changes and resulting morphological changes that have occurred, and are still occurring, due to the various construction works in the ES basin since 1958.

A.1. Historical Background on Interventions

Due to the construction works in the ES, the hydrodynamics in the basin have changed significantly. The most influential intervention was the ES barrier, due to the reduction of cross-sectional area available for water flowing into and out of the basin. Figure A.1 shows the basin as it was in 1990 and various works completed before 1990. The construction works can be divided into the following phases (Vroon, 1994):

- 1958 - 1964: The Delta project was initiated and construction work started. In 1964 the Grevelingendam was completed, cutting off the Eastern Scheldt from its northern neighbor.
- 1964-1969: The Volkerak dam was constructed in 1969, which included sluices to regulate river flow (not included in the Figure, just outside Figure A.1 to the northeast).
- 1969-mid 1985: Preparations for the ES Project including some minor construction works near the mouth of the estuary.
- mid 1985 to 1987: Completion of the ES project. This included the storm surge barrier and two compartmentalization dams (Oesterdam and Philipsdam) in the north- and southeastern branches of the basin.

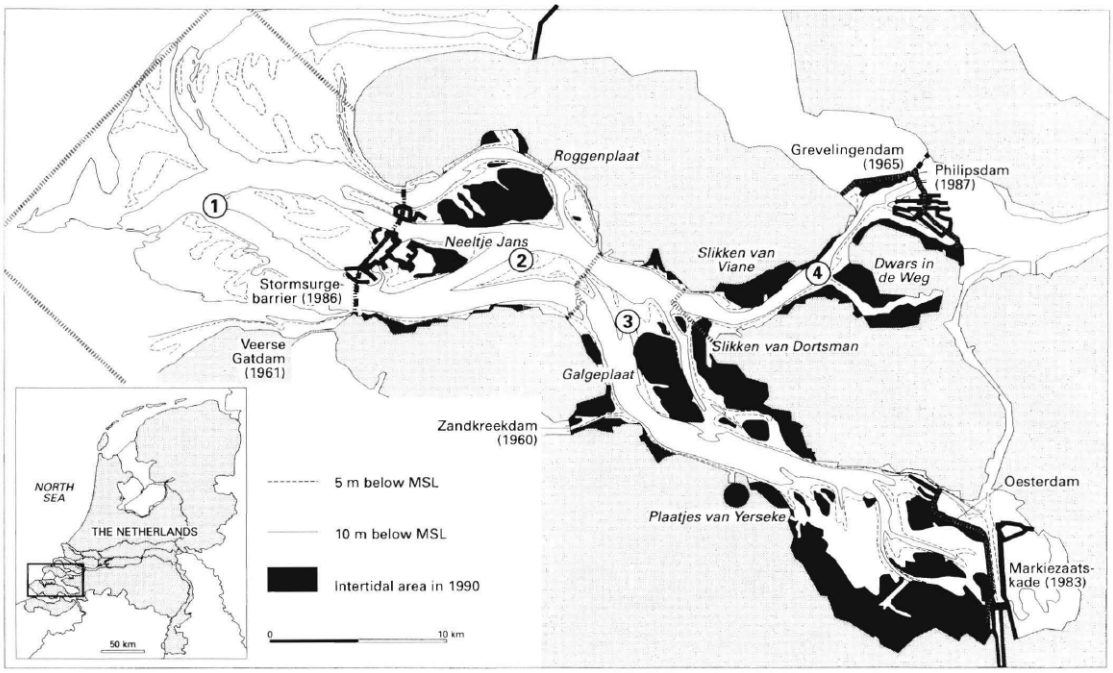

Figure A.1: Overview ES and construction works (Louters et al., 1998)

A.2. Changes in Hydrodynamics

The construction works have resulted in a reduction of the tidal range, volume and velocities within the basin. The tidal volume has decreased by approximately 30%, the current velocities have decreased 20-40% in the western and central parts of the basin and up to 80-100% close to the barrier and in the eastern parts of the basin. The average tidal range has decreased by 12%(Louters et al., 1998).

A.2.1. Tidal Volume and Range

The closure of the Grevelingen and Volkerak resulted in an increase of the flood volume, but due to the construction works of the barrier, the flood volume decreased, as shown in Figure A.2. A linear relationship has been observed between the reduction of cross sectional area and loss in tidal volume (Louters et al., 1998), confirming that this drop in tidal volume is a direct consequence of the barrier.

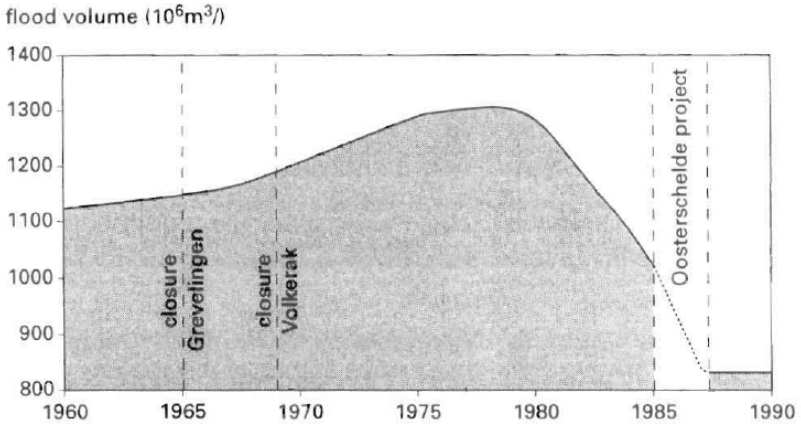

Figure A.2: Evolution of flood tidal volume at the mouth of the ES basin since 1960 (Louters et al., 1998)

The reduction in tidal range is on average 12% (about half a meter) with respect to the situation before the works, as is seen in Figure A.3. Vroon (1994) states that the reduced tidal range has led to a lower inundation

frequency in the higher zones of the basin, having an impact on ecology. Moreover, there is an increased period that the tidal flats are exposed to wave energy. This is discussed later on in this Chapter.

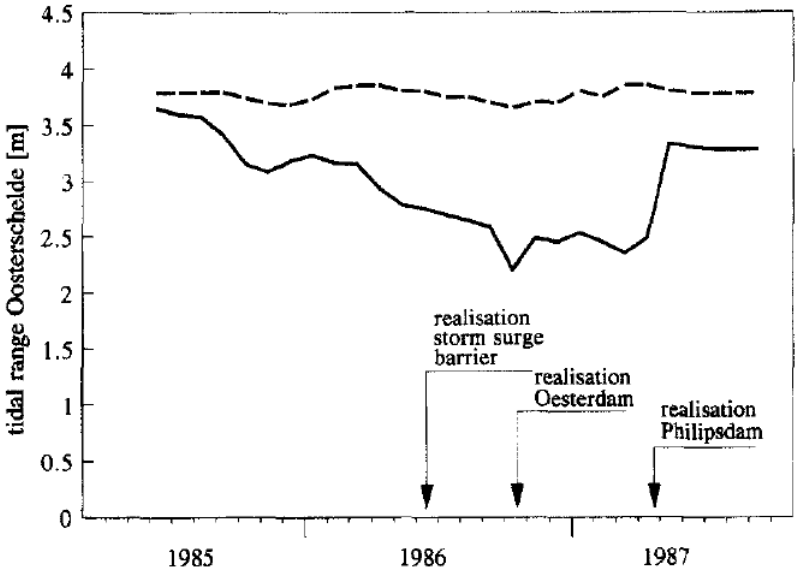

Figure A.3: Hydrodynamic consequences of a phased planning schedule, actual tidal range (solid line) and theoretical tidal range without works (broken line) (Vroon, 1994)

A.2.2. Tidal Flow Velocities

The construction works led to a reduction in flow velocities, proportional to the decrease in discharge. Differences were observed between these reductions in northern and southern parts of the basin and between ebb and flood. An example of differences in ebb and flood velocities, as compared to the situation before the construction works is shown in figure A.4 for a location near the Galgenplaat(middle of the basin). At this location flood velocities have decreased significantly, while ebb velocities have remained relatively similar. The reduction in flood velocities has dramatically decreased sediment transport in the flood phase, see the solid line in figure A.4.

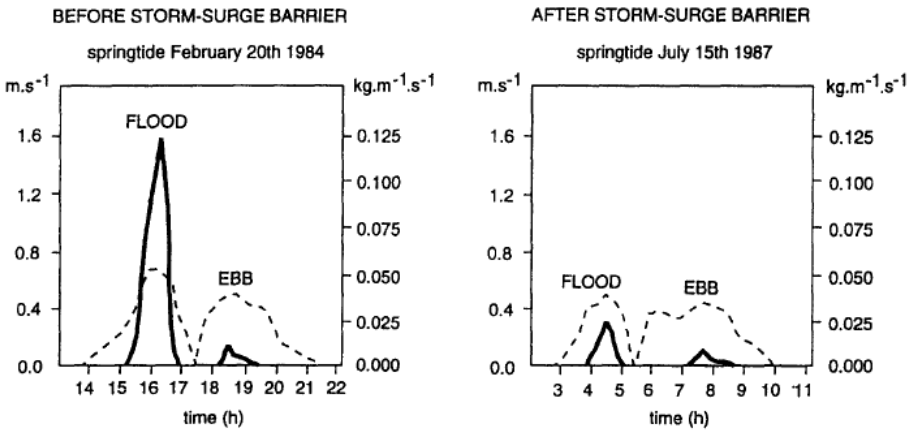

Figure A.4: Current velocities (interrupted line) and sand transport(solid line) in 1984 and 1987 observed near Galgenplaat (Mulder and Louters, 1994)

A.3. Morphological Development

A.3.1. Sediment Deficit

The construction of the Delta Works started around 1958, and interventions starting in 1964 began influencing the ES basin. Before this period, the ES basin was exporting sediment, indicating that the estuary had not yet reached a morphological equilibrium. The increase in tidal prism caused by the Grevelingen and Volkerak

dams, resulted in an even larger export of sediment. Eelkema (2013) states that this led to increased flow velocities, scouring the channels and slightly increasing the height of the tidal flats. The eventual closure led to a decrease in tidal prism, and therefore a corresponding decrease in the channel volume had to follow, which is the effect that is noticed at present (i.e. sedimentation in the channels and scouring of the tidal flats). This is explained by the empirical formula in equation A.1; the tidal prism(P) of an inlet and the cross-sectional area(A_e) of its entrance show a linear relationship (a and b are coefficients), which applies for both the inlet of a basin, as for channels. Figure A.5 illustrated this equilibrium relationship for various inlets.

$$P = a * A_e + b \tag{A.1}$$

Sediment providing channels with a decreased volume must be coming from tidal flats, as the barrier blocks import of sediment. This is known as the sediment deficit of the ES. According to Louters et al. (1998), an import of 400-600 million m^3 of sediment is necessary to reach a new dynamic equilibrium between hydrodynamic conditions and morphology.

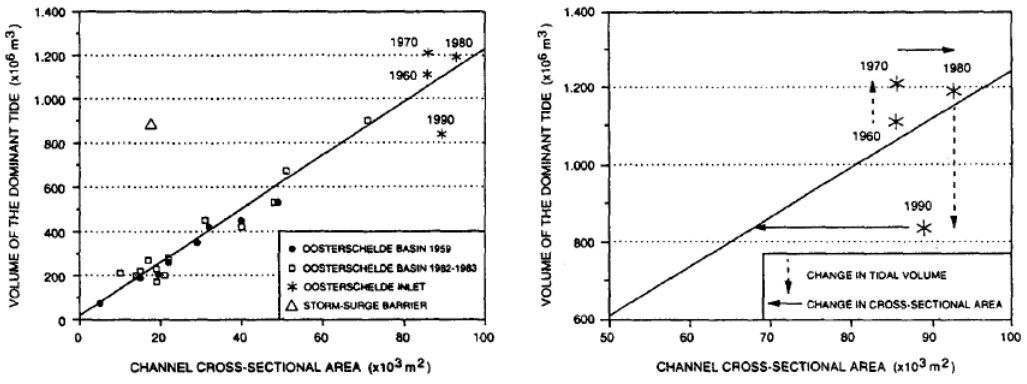

Figure A.5: Morphodynamic equilibrium relation between tidal volume and cross sectional area for different tidal inlets. Channel erosion is observed between 1965 and 1970. Since 1985, the decreased cross section at the inlet induced scour holes and the decreased tidal volume induced scouring of the channels. (Mulder and Louters, 1994)

According to De Vet et al. (2017b), tidal flats in the ES basin were in dynamic equilibrium, or even slightly increasing in height, before the construction of the storm surge barrier, which matches Eelkema's findings. After the construction works, tidal flats have been eroding strongly. This change in trend is most likely due to the change in hydrodynamics imposed by the barrier (De Vet et al., 2017b). Figure A.6 shows the decline in height, area and volume of tidal flats in the ES.

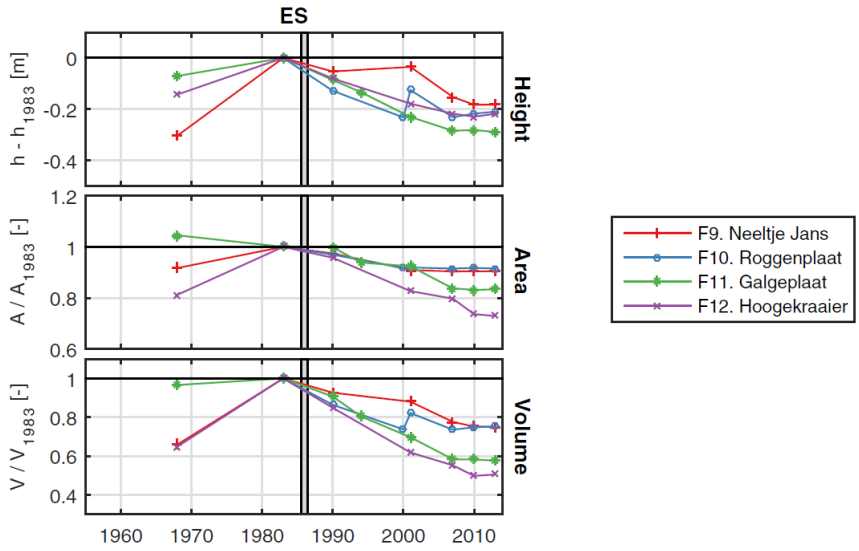

Figure A.6: Long term changes of the average height, area and volume of flats in the ES. The vertical gray box indicates the completion of the storm surge barrierDe Vet et al. (2017b)

A.3.2. Autonomous Negative Trend

The sediment deficit of the channels is leading to erosion of tidal flats, and sea-level rise (SLR) is leading to decreased emergence of these areas. Due to the combination of these effects, all tidal flats combined are decreasing in area by approximately 60 ha per year. Since the construction of the barrier, about 1300 hectares(10%) have been lost due to erosion and sea-level rise.

In Figure A.7 a prediction of the reduction in emerged area between 2010-2100 is shown for all tidal flats combined, and for different emergence time intervals (0-20%, 20-40%, 40-60%, 60-80% and 80-100%) of all tidal flats (i.e. 80-100% indicates the total area which is emerged for 9.80-12.25 hours during a tidal cycle). For birds in the ES the most important zone corresponds to the interval 40-80% (De Ronde et al., 2013).

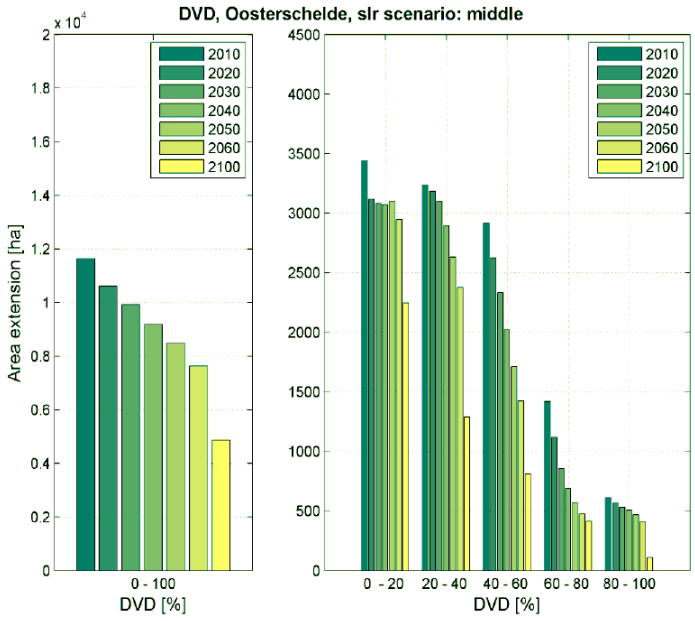

Figure A.7: (a) decrease in emerging area for all tidal flats in the ES over time and (b) decrease in emerging area per emergence time interval for the scenario 'middle' (De Ronde et al., 2013)

Figure A.7 shows the results for a 'middle' scenario, a 'low' and 'high' scenario are also defined by De Ronde et al. (2013). The three different sea-level rise scenarios correspond to a sea-level rise of 12, 24 and

33 cm respectively for the period between 2010 and 2060. This corresponds to 2.5 to 4 mm/year, 4.17 to 7 mm/year and 5.83 to 10 mm/year for the three scenarios. Figure A.8 shows the areal decline for the tidal flats in the ES per sea-level rise scenario.

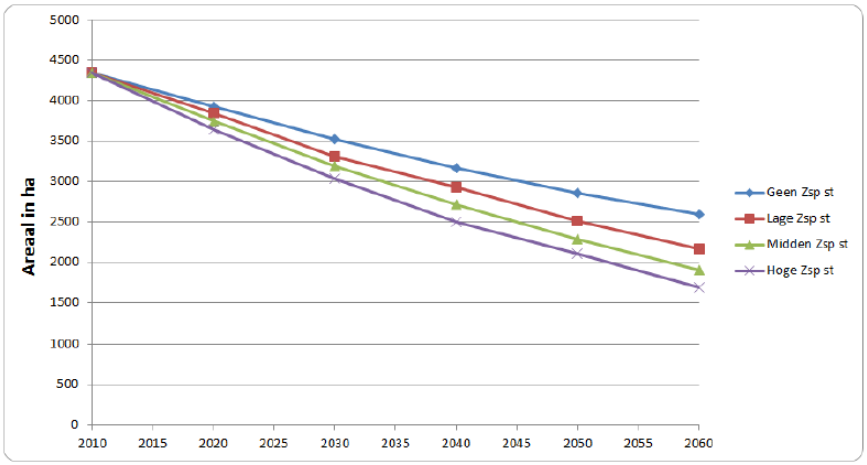

Figure A.8: Decrease in acreage of tidal flats in the ES as a result of different sea-level rise scenarios over time (De Ronde et al., 2013). (Geen Zsp st = No SLR, Lage ZSp st = Low SLR, Midden Zsp = Middle SLR, Hoge Zsp st = High SLR)

B

Sill Heights Eastern Scheldt Barrier

This appendix shows the sill heights of each gate opening, and in which gate openings turbines are implemented in the model (indicated in bold in the tables).

Tables B.1, B.2 and B.3 give the sill heights of Hammen, Schaar and Roompot respectively. The sill heights have been obtained from the technical drawings of Rijkswaterstaat Directie Sluizen en Stuwen (1987).

Table B.1: Sill heights Hammen

Gate	Sill height w.r.t NAP [m]
H1	4.7
H2	4.7
H3	5.7
H4	6.7
H5	7.7
H6	8.7
H7	8.7
H8	8.7
H9	7.7
H10	6.7
H11	5.7
H12	4.7
H13	4.7
H14	4.7
H15	4.7

Table B.2: Sill heights Schaar

Gate	Sill height w.r.t NAP [m]
S1	4.3
S2	4.5
S3	4.5
S4	5.5
S5	6.5
S6	7.5
S7	7.5
S8	7.5
S9	7.5
S10	6.5
S11	6.5
S12	5.5
S13	4.5
S14	4.5
S15	4.5
S16	4.5

Table B.3: Sill heights Roompot

Gate	Sill height w.r.t NAP [m]
R1	4.5
R2	5.5
R3	6.5
R4	6.5
R5	7.5
R6	8.5
R7	9.5
R8	9.5
R9	9.5
R10	10.5
R11	10.5
R12	10.5
R13	10.5
R14	10.5
R15	10.5
R16	10.5
R17	9.5
R18	9.5
R19	9.5
R20	9.5
R21	9.5
R22	9.5
R23	9.5
R24	9.5
R25	8.5
R26	8.5
R27	7.5
R28	7.5
R29	6.5
R30	5.5
R31	4.5

C

Discharge Coefficients STAR-CCM+ Model

This appendix shows the computation of discharge coefficients from STAR-CCM+ model output.

The water level difference, wetted area and discharge are provided from the STAR-CCM+ model for both flood and ebb simulations, and with and without turbines. This model was not used by the author, data was provided by Deltares in July 2017. Table C.1 shows the values which are provided by the STAR-CCM+ model and the calculated discharge coefficients for the situation without turbines.

Table C.1: Discharge coefficients for ebb and flood derived from STAR-CCM+ model for situation with only barrier

		Flood	Ebb	
Mass flow barrier opening	Q_b	651	862	m^3/s
Water level difference	$\|\zeta_u - \zeta_d\|$	0.2	0.2	m
Gravitational acceleration	g	9.81	9.81	m/s^2
Water depth above sill	H	8.7	10.4	m
Wetted width	y	39.5	39.5	m
Discharge coefficient barrier	μ_b	0.95	1.06	-

For the situation with turbines, the discharge coefficient μ is computed again. The head difference, gravitational acceleration, mean water depth above the sill and the wetted width remain the same. However, the discharge through the barrier has changed. The resulting values are presented in table C.2. The discharge coefficients have decreased in value compared to those of the barrier with no turbines in table C.1.

Table C.2: Discharge coefficients for ebb and flood derived from STAR-CCM+ model for situation with barrier and turbines

		Flood	Ebb	
Discharge with turbines	Q_t	570	722	m^3/s
Discharge coefficient with turbines	μ_{b+t}	0.83	0.89	-

D

Turbine Parameterization

This appendix provides additional information regarding the turbine parameterization.

D.1. Model Coupling

These head losses were analyzed over the spring neap cycle (June 15 til 30), see Figures D.1 and D.2. The time-steps in which a head difference of +0.2 m (within a range of 2 cm) occurred, were the flood discharges and are indicated with the blue circles. The time-steps with a -0.2m head difference were the ebb discharges and are indicated in red. The average discharge coefficient was calculated from all the time steps in which the head loss of 0.2 occurred for flood and ebb.

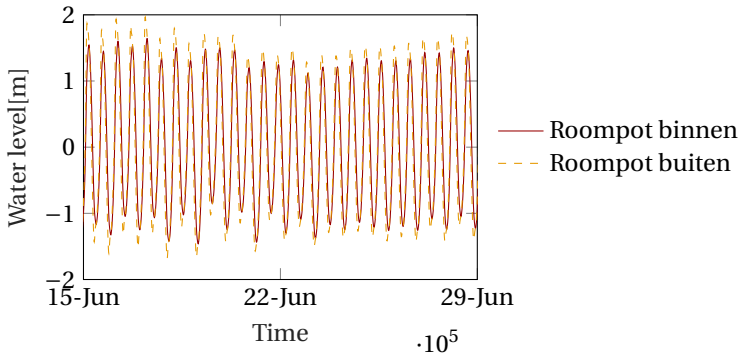

Figure D.1: Water levels Roompot binnen(inside) and buiten(outside)

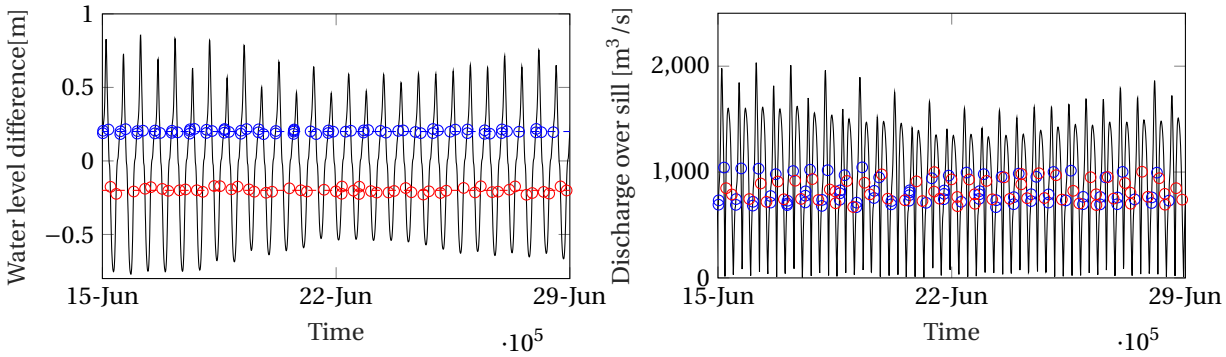

Figure D.2: Water level difference and corresponding discharge over sill

D.2. Discharge Coefficients

Table D.1 shows the range that is used for calibration of the discharge.

Table D.1: Discharge coefficients for calibration of range

		Ebb	Flood
Barrier	μ_b	1.15	1.12
Barrier with turbines, reference case	μ_{b+t}	0.97	0.99
	$factor$	0.84	0.88
Barrier with turbines, -5% case	μ_{b+t}	1.02	1.04
	$factor$	0.89	0.93
Barrier with turbines, +5% case	μ_{b+t}	0.91	0.93
	$factor$	0.79	0.83
Barrier with turbines, +10% case	μ_{b+t}	0.85	0.87
	$factor$	0.74	0.78

D.3. Discharge Coefficients Previous Research

Research by De Kleermaeker (2013) was performed to give predictions on changes in water levels in the ES basin due to tidal turbines using the one-dimensional IMPLIC model. This research used a discharge formula together with a thrust formulation for turbines and iteratively derived coefficients for ebb and flood to use in the IMPLIC model. Discharge coefficients were calculated for barrier including turbines for two different drag coefficients (C_d); 0.7 and 0.9.

The results of the research were factors of 0.85 and 0.91 for flood and ebb respectively for a C_d of 0.7 and factors of 0.82 (flood) and 0.89 (ebb) for a C_d of 0.9. Apart from the different drag coefficients, slightly different values were used for the water depth, global water level difference and swept area of the turbines than in this work. These coefficients were multiplied by the barrier discharge coefficient. In the IMPLIC model, the discharge coefficients for gate openings without turbines were 0.93 for flood and 1.03 for ebb. By multiplying the derived coefficients of the turbines with those of the barrier, the discharge coefficients in table D.2 are found.

Table D.2: Discharge coefficients IMPLIC model

		Flood	Ebb
Discharge coefficient for gate opening	μ_b	0.93	1.03
Discharge coefficient for gate opening including turbines with $C_d = 0.7$	μ_{b+t}	0.79	0.94
Discharge coefficient for gate opening including turbines with $C_d = 0.9$	μ_{b+t}	0.76	0.92

E

Simulation Results

This appendix provides additional information for the simulation results.

E.1. Near-future Scenario

E.1.1. Basin

Water Levels

Table E.1: Deviation mean water levels and mean tidal ranges channels at various observation points, near-future scenario

		-lower [cm]	reference [cm]	+upper [cm]	++upper [cm]
OS11	MHW	0.02	0.03	0.03	0.04
	MLW	0.00	0.00	0.00	0.00
	MTR	0.02	0.03	0.04	0.04
Roompot Buiten	MHW	0.11	0.17	0.22	0.28
	MLW	0.13	0.17	0.21	0.24
	MTR	-0.02	0.00	0.01	0.04
Roompot Binnen	MHW	-0.18	-0.26	-0.32	-0.39
	MLW	0.17	0.27	0.36	0.45
	MTR	-0.35	-0.52	-0.68	-0.84
Roompot	MHW	-0.09	-0.14	-0.20	-0.28
	MLW	0.17	0.27	0.36	0.46
	MTR	-0.26	-0.41	-0.57	-0.74
Neeltje Jans	MHW	-0.21	-0.33	-0.44	-0.56
	MLW	0.19	0.29	0.39	0.49
	MTR	-0.39	-0.62	-0.83	-1.06
Zeelandbrug Noord	MHW	-0.25	-0.40	-0.53	-0.67
	MLW	0.22	0.35	0.47	0.60
	MTR	-0.48	-0.75	-1.00	-1.27
Yerseke	MHW	-0.35	-0.55	-0.73	-0.92
	MLW	0.35	0.55	0.72	0.92
	MTR	-0.70	-1.10	-1.45	-1.84
Marollegat	MHW	-0.37	-0.58	-0.77	-0.98
	MLW	0.40	0.62	0.82	1.05
	MTR	-0.77	-1.21	-1.59	-2.02

Table E.2: Percentage of deviation mean tidal ranges channels at various observation points, near-future scenario

		lower [%]	reference [%]	upper [%]	upper [%]
OS11	MTR	0.01	0.01	0.01	0.01
Roompot Buiten	MTR	-0.01	0.00	0.00	0.01
Roompot Binnen	MTR	-0.13	-0.20	-0.26	-0.32
Roompot	MTR	-0.10	-0.16	-0.22	-0.28
Neeltje Jans	MTR	-0.14	-0.23	-0.30	-0.39
Zeelandbrug Noord	MTR	-0.16	-0.25	-0.34	-0.43
Yerseke	MTR	-0.20	-0.32	-0.42	-0.53
Marollegat	MTR	-0.21	-0.33	-0.44	-0.55

Tidal Volume

Table E.3: Deviation mean tidal volume at various cross sections, near-future scenario

Location	-lower $[m^3 * 10^6]$	reference $[m^3 * 10^6]$	+ upper $[m^3 * 10^6]$	++ upper $[m^3 * 10^6]$
Barrier Opening	−1.76	−2.77	−3.67	−4.66
Zeelandbrug	−1.26	−1.97	−2.61	−3.31
Northeast Branch	−0.22	−0.34	−0.45	−0.56
Southeast Branch	−0.79	−1.23	−1.63	−2.06
Lodijksche Gat	−0.53	−0.84	−1.11	−1.41

Table E.4: Percentage of deviation mean tidal volume at various cross sections, near-future scenario

Location	-lower [%]	reference [%]	+ upper [%]	++ upper [%]
Barrier Opening	−0.17	−0.27	−0.36	−0.41
Zeelandbrug	−0.18	−0.28	−0.37	−0.47
Northeast Branch	−0.19	−0.30	−0.40	−0.51
Southeast Branch	−0.18	−0.29	−0.38	−0.48
Lodijksche Gat	−0.19	−0.29	−0.39	−0.49

E.1.2. Channels

Discharges

Table E.5: Percentage of deviation peak ebb end flood discharge at various cross-sections, near-future scenario

Location	Ebb $[m^3/s * 10^2]$	[%]	Flood $[m^3/s * 10^2]$	[%]
Roompot Channel	−2.84	−0.73	−3.06	−0.66
Schaar Channel	+0.21	+0.15	+0.76	+0.45
Hammen Channel	+0.08	+0.07	+0.37	+0.22
Roompot South	−0.78	−0.80	−0.43	−0.44
Roompot East	−1.29	−0.53	−2.10	−0.66
Geul van Roggenplaat	−0.84	−0.32	−0.32	−0.11
Engelsche Vaarwater	−0.71	−0.34	−0.54	−0.21
Brabantsche Vaarwater	−0.30	−0.40	−0.18	−0.20

E.2. Maximum Roll-out Scenario

E.2.1. Basin

Water Levels

Table E.6: Deviation mean water levels and mean tidal ranges channels at various observation points, maximum roll-out scenario

		lower [cm]	reference [cm]	upper [cm]	upper [cm]
OS11	MHW	0.08	0.13	0.18	0.23
	MLW	0.04	0.06	0.07	0.09
	MTR	0.05	0.08	0.11	0.14
Roompot Buiten	MHW	0.28	0.42	0.56	0.72
	MLW	0.42	0.60	0.74	0.88
	MTR	-0.14	-0.17	-0.18	-0.15
Roompot Binnen	MHW	-1.01	-1.60	-2.10	-2.66
	MLW	0.91	1.43	1.92	2.46
	MTR	-1.92	-3.03	-4.01	-5.12
Roompot	MHW	-0.97	-1.55	-2.09	-2.70
	MLW	0.93	1.47	1.96	2.50
	MTR	-1.90	-3.03	-4.05	-5.20
Neeltje Jans	MHW	-1.12	-1.77	-2.35	-3.01
	MLW	0.99	1.56	2.07	2.65
	MTR	-2.11	-3.33	-4.43	-5.66
Zeelandbrug Noord	MHW	-1.44	-2.27	-3.00	-3.83
	MLW	1.21	1.90	2.52	3.20
	MTR	-2.65	-4.17	-5.53	-7.03
Yerseke	MHW	-1.99	-3.12	-4.16	-5.32
	MLW	1.89	2.97	3.93	5.00
	MTR	-3.88	-6.10	-8.09	-10.31
Marollegat	MHW	-2.14	-3.35	-4.44	-5.65
	MLW	2.16	3.40	4.52	5.78
	MTR	-4.30	-6.75	-8.96	-11.43

Table E.7: Percentage of deviation mean tidal ranges channels at various observation points, maximum roll-out scenario

		lower [%]	reference [%]	upper [%]	upper [%]
OS11	MTR	0.02	0.03	0.03	0.05
Roompot Buiten	MTR	-0.05	-0.06	-0.06	-0.05
Roompot Binnen	MTR	-0.73	-1.16	-1.54	-1.96
Roompot	MTR	-0.72	-1.15	-1.54	-1.98
Neeltje Jans	MTR	-0.77	-1.22	-1.62	-2.07
Zeelandbrug Noord	MTR	-0.89	-1.40	-1.85	-2.36
Yerseke	MTR	-1.12	-1.75	-2.33	-2.97
Marollegat	MTR	-1.18	-1.85	-2.45	-3.13

Tidal Volume

Table E.8: Deviation mean tidal volume at various cross sections, maximum roll-out scenario

Location	-lower $[m^3 * 10^6]$	reference $[m^3 * 10^6]$	+ upper $[m^3 * 10^6]$	++ upper $[m^3 * 10^6]$
Barrier Opening	−9.53	−15.01	−19.92	−25.41
Zeelandbrug	−7.03	−11.05	−14.66	−18.70
Northeast Branch	−1.20	−1.87	−2.47	−3.11
Southeast Branch	−4.41	−6.95	−9.24	−11.80
Lodijksche Gat	−3.01	−4.74	−6.30	−8.04

Table E.9: Percentage of deviation mean tidal volume at various cross sections, maximum roll-out scenario

Location	-lower [%]	reference [%]	+ upper [%]	++ upper [%]
Barrier Opening	−0.94	−1.92	−2.41	−2.96
Zeelandbrug	−0.99	−1.56	−2.07	−2.63
Northeast Branch	−1.08	−1.70	−2.23	−2.82
Southeast Branch	−1.03	−1.62	−2.16	−2.76
Lodijksche Gat	−1.05	−1.66	−2.21	−2.82

E.2.2. Channels

Discharges

Table E.10: Percentage of deviation peak ebb end flood discharge and asymmetry at various cross-sections, maximum roll-out scenario

Location	Ebb $[m^3/s * 10^2]$	[%]	Flood $[m^3/s * 10^2]$	[%]
Roompot Channel	−9.26	−2.37	−8.68	−1.88
Schaar Channel	−1.94	−1.47	−1.14	−0.67
Hammen Channel	−1.83	−1.58	−3.91	−2.41
Roompot South	−2.17	−2.21	−1.56	−1.63
Roompot East	−5.43	−2.24	−5.85	−1.83
Geul van Roggenplaat	−5.17	−1.97	−3.77	−1.23
Engelsche Vaarwater	−4.18	−2.01	−3.22	−1.23
Brabantsche Vaarwater	−1.57	−2.10	−1.16	−1.27

E.3. Partial Roll-out Scenarios

E.3.1. Basin

Water Levels

Table E.11: Deviation mean water levels and mean tidal ranges at various observation points, partial roll-out scenarios

		Roompot Filled [cm]	Schaar Filled [cm]	Hammen Filled [cm]
OS11	MHW	0.10	0.02	0.02
	MLW	0.02	0.02	0.02
	MTR	0.07	0.00	0.00
Roompot Buiten	MHW	0.61	-0.09	-0.10
	MLW	0.44	0.15	0.16
	MTR	0.17	-0.24	-0.26
Roompot Binnen	MHW	-0.97	-0.26	-0.31
	MLW	0.97	0.21	0.24
	MTR	-1.94	-0.47	-0.54
Roompot	MHW	-0.94	-0.28	-0.28
	MLW	1.00	0.21	0.21
	MTR	-1.94	-0.49	-0.56
Neeltje Jans	MHW	-1.14	-0.27	-0.31
	MLW	1.08	0.22	0.25
	MTR	-2.22	-0.49	-0.56
Zeelandbrug Noord	MHW	-1.51	-0.35	-0.38
	MLW	1.33	0.25	0.30
	MTR	-2.84	-0.60	-0.68
Yerseke	MHW	-2.07	-0.48	-0.54
	MLW	2.07	0.40	0.47
	MTR	-4.14	-0.88	-1.00
Marollegat	MHW	-2.22	-0.50	-0.57
	MLW	2.36	0.47	0.54
	MTR	-4.58	-0.97	-1.12

Table E.12: Deviation in percentage mean tidal ranges at various observation points, partial roll-out scenarios

		Roompot Filled [%]	Schaar Filled [%]	Hammen Filled [%]
OS11	MTR	0.02	0.00	0.00
Roompot Buiten	MTR	0.06	-0.08	-0.09
Roompot Binnen	MTR	-0.74	-0.18	-0.21
Roompot	MTR	-0.74	-0.19	-0.21
Neeltje Jans	MTR	-0.81	-0.18	-0.21
Zeelandbrug Noord	MTR	-0.95	-0.20	-0.23
Yerseke	MTR	-1.19	-0.25	-0.29
Marollegat	MTR	-1.25	-0.26	-0.31

Tidal Volume

Table E.13: Deviation mean tidal volume at various cross sections, partial roll-out scenario

Location	Roompot		Schaar		Hammen	
	$[m^3 * 10^6]$	[%]	$[m^3 * 10^6]$	[%]	$[m^3 * 10^6]$	[%]
Barrier Opening	−10.42	−1.03	−2.02	−0.20	−2.29	−0.23
Zeelandbrug	−7.48	−1.06	−1.59	−0.22	−1.81	−0.26
Northeast Branch	−1.28	−1.16	−0.27	−0.25	−0.31	−0.28
Southeast Branch	−4.68	−1.10	−1.00	−0.24	−1.15	−0.27
Lodijksche Gat	−3.19	−1.12	−0.69	−0.24	−0.79	−0.28

E.3.2. Channels

Discharges

Table E.14: Deviation peak ebb end flood discharge and asymmetry at various cross-sections, partial roll-out scenario

	Roompot Filled		Schaar Filled		Hammen Filled	
	Ebb $[m^3/s * 10^2]$	Flood $[m^3/s * 10^2]$	Ebb $[m^3/s * 10^2]$	Flood $[m^3/s * 10^2]$	Ebb $[m^3/s * 10^2]$	Flood $[m^3/s * 10^2]$
Roompot Channel	-11.37	-11.83	1.10	1.63	1.07	1.61
Schaar Channel	0.98	2.90	-2.18	-5.17	-0.76	1.13
Hammen Channel	0.46	1.44	-0.43	0.58	-1.78	-5.96
Roompot South	-2.87	-2.43	0.34	0.49	0.38	0.37
Roompot East	-5.34	-7.67	-0.08	0.80	0.05	1.03
Geul van Roggenplaat	-3.18	-1.33	-0.85	-1.13	-1.09	-1.22
Engelsche Vaarwater	-2.79	-2.09	-0.64	-0.51	-0.72	-0.54
Brabantsche Vaarwater	-1.05	-0.71	-0.25	-0.20	-0.27	-0.22

Table E.15: Percentage of deviation peak ebb end flood discharge and asymmetry at various cross-sections, partial roll-out scenario

Location	Roompot		Schaar		Hammen	
	Ebb [%]	Flood [%]	Ebb [%]	Flood [%]	Ebb [%]	Flood [%]
Roompot Channel	−2.91	−2.57	+0.28	+0.36	+0.27	+0.35
Schaar Channel	+0.74	+1.72	−1.64	−3.08	−0.57	+0.67
Hammen Channel	+0.39	+0.89	−0.38	+0.35	−1.54	−3.68
Roompot South	−2.92	−2.54	+0.35	+0.52	+0.39	+0.39
Roompot East	−2.21	−2.40	−0.03	+0.24	+0.02	+0.32
Geul van Roggenplaat	−1.21	−0.44	−0.32	−0.37	−0.42	−0.39
Engelsche Vaarwater	−1.33	−0.80	−0.30	−0.19	−0.34	−0.21
Brabantsche Vaarwater	−1.41	−0.77	−0.33	−0.22	−0.36	−0.24

www.deltares.nl

Deltares